

Expo Report

A Nanoparticle Reactor Instrumentation and Measurement System

L. Flannigan, B. McCrindle, H. McPhee, P. Pastolero

McMaster University

ENGPHYS 4A06

April 2, 2019



Problem Statement	3
Demo Specifications	5
Engineered Solution	9
Operating Instructions	11
Assembly Instructions	13
Mathematical Modelling	23
Fluid Containment and Transport	23
Image Processing	31
Environment and Process Control	36
Optical Characterization	46
Fan Control and Load Cell	55
Beaker Lid Design	58
Beaker Lid	59
Latch	63
Seal	65
GUI	66
Optimization Demo Performance	66
Time Taken to Complete Process	66
Reliability of Characterization	67
Accuracy of Size Produced	67
Standard Deviation of Distribution	67
Integration Demo Performance and Testing Plans	68
Time Taken to Complete Process	68
Reliability of Characterization	68
Accuracy of Size Produced	73
Standard Deviation of Distribution	74
Module Demo Performance	76
Fluid Transport	76
Image Processing	78
Sensor Alignment	79
Optical Testing Plan	82
Environment and Process Control	85
GUI Testing	90



EHS Code Considerations	90
Electrical Safety	90
Working with Chemicals	90
Power Supply Safety	91
MSDS Considerations	92
References	94



Problem Statement

Nanotechnology research has grown quickly over time, partly due to the rapid development of engineered nanoparticles. These nanoparticles have found a variety of uses in both industry and research, with gold nanoparticles as one of the more versatile types. Biomedical research in particular has discovered a wide range of applications for gold nanoparticles, ranging from photodynamic therapy for treating skin diseases, photothermal therapy for cancer treatment, X-ray imaging, drug delivery systems, and biological/chemical sensing. Biomedical researchers are always seeking ways to optimize existing methods and develop novel applications for these useful particles [1]. As a result, there needs to be a reliable and efficient method for synthesizing gold nanoparticles in small batches in order for research groups to be able to study their properties in a controlled setting. However, as we will see, current small batch synthesis methods require human supervision and are labor intensive and error-prone. Through extensive online research, we can see that there is currently no solution on the market that automates the preparation, synthesis, and characterization procedures for gold nanoparticles.

When reaching out to Dr. Soleymani at McMaster University, a professor that currently supervises a laboratory that frequently synthesizes gold nanoparticles for their research, she emphasized the impact that an all-in-one device could have within her group, and many others. The current procedure for synthesizing 12 nm gold nanoparticles followed within her lab is described below.

1. *Clean Erlenmeyer flask and magnetic stirring rod with HCl*
2. *Create a 1 mM AuCl₃ solution (300 mL DI + 207.6 uL AuCl₃ solution)*
3. *Heat solution to 100 °C on a hotplate and stir at 1200 rpm*
4. *Add 0.5 g trisodium citrate dihydrate to 30 mL of DI water*
5. *Wait for AuCl₃ solution to reach 100 °C*
6. *Add 30 mL trisodium citrate solution, continue mixing at 1200 rpm for 10 min*
7. *Take off heat (cool with ice) and mix for additional 15 min*
8. *Verify absorbance peak of 520 nm wavelength*

There are several sources of error in the procedure provided above. According to Dr. Soleymani's graduate students, the process for determining when the gold nanoparticles are ready to move on to the next stage of synthesis is "looking for a particular shade of color". As one can imagine, this is a subjective and poorly defined parameter for recognizing when the chemical reaction is finished, leading to particles that are the wrong size or concentration. Knowing this, *nanoRIMS* seeks to standardize this process.

The gold nanoparticle production process can be split into three distinct steps:

1. Chemical Preparation



2. Chemical Reduction (Synthesis)
3. Nanoparticle Characterization

We initiated research into potential market competitors that already accomplish any combination of these steps. The main solution that appeared in our search is Syrris [2], a company that manufactures micro-reactors for scalable chemical solutions. Their micro-reactors offer accurate performance over a thermal range of -40 °C to +200 °C, and they can handle automated mixing of chemicals as well. These devices can scale their output from 50 mL to 5 L and will pump chemicals into the reaction as necessary. This device clearly handles step 2, synthesis, and it is unlikely we would be able to outperform Syrris in this regard.

Further research shows that the Syrris devices still require the researchers to prepare the solutions involved in the reactions beforehand, which corresponds to step 1 and is one of the largest sources of errors in the current method. Researchers also have to manually input and modify the synthesis procedures if they want to change the nanoparticles being made. Since our device will be optimized for synthesizing gold nanoparticles, the user would be able to directly change the desired size (between 10 nm and 50 nm) by a simple option on screen, rather than developing a whole new programmed procedure. Additionally, while Syrris' microreactor is capable of synthesizing gold nanoparticles, it has no method of characterizing the nanoparticles within the system. This means Syrris cannot accomplish step 3, and the researcher will have to use SEM, TEM, or optical characterization methods themselves. As a result, we believe our device can automate and outperform Syrris in regards to the chemical preparation and nanoparticle characterization steps, as they currently provide no solution for these problems.



Demo Specifications

The testing methods used to verify these specifications are described in the “Performance and Testing” section of this report.

Module Demo Specifications		
Metric	%	Performance
Temperature Control	25%	-Hold temperature of 300 mL of water to within +/- 10 °C, between 25 and 100 °C -Cool 300 mL from 100 °C to 25 °C within 90 minutes -Heat 300 mL to 100 °C from 25 °C within 60 minutes
	50%	-Hold temperature of 300 mL of water to within +/- 5 °C, between 25 and 100 °C -Cool 300 mL from 100 °C to 25 °C within 60 minutes -Heat 300 mL to 100 °C from 25 °C within 45 minutes
	75%	-Hold temperature of 300 mL of water to within +/- 2 °C -Cool 300 mL from 100 °C to 25 °C within 50 minutes -Heat 300 mL to 100 °C from 25 °C within 37.5 minutes
	100%	-Hold temperature of 300 mL water to within +/- 0.5 °C -Cool 300 mL from 100 °C to 25°C within 20 min -Heat 300 mL to 100 °C from 25 °C within 30 min
Mixing Control	25%	-Stir solution within +/- 60 rpm of set rotation speed, between 750 and 2000 RPM.
	50%	-Stir solution within +/- 45 rpm of set rotation speed, between 750 and 2000 RPM.
	75%	-Stir solution within +/- 30 rpm of set rotation speed, between 750 and 2000 RPM.
	100%	-Stir solution within +/- 15 rpm of set rotation speed, between 750 and 2000 RPM.
Fluid Transport	25%	-Transport at least 300 mL of water from one container to another



	50%	-Transport fluid volumes >10 mL to within +/- 10% -Image droplets of at least 7 mm in diameter, no measurement of volume -Provide adequate seal to stock containers in device
	75%	-Transport fluid volumes >10 mL to within +/- 5% -Have user enter amount of fluid in reservoir -Image droplets of at least 5 mm in diameter, measure its volume within 15%
	100%	-Transport fluid volumes >10 mL to within +/- 1% -Have user enter amount of fluid in reservoir -Track how much of stock solutions has been used -Image droplets of at least 3 mm in diameter, measure its volume within 3%
Optical Characterization	25%	-Be able to record intensity measurement using light source and detector using diffraction grating, within a 500 nm to 600 nm wavelength range
	50%	-Be able to distinguish wavelength of light for intensity measurement +/- 5 nm using diffraction grating setup, within 500 nm to 600 nm
	75%	-Be able to distinguish wavelength of light for intensity measurement +/- 1 nm using diffraction grating, within 500 nm to 600 nm
	100%	-Be able to distinguish wavelength of light for intensity measurement +/- 0.2 nm using diffraction grating, within 400 nm to 600 nm
Sensor Integration	25%	-Identify presence of object on the scale and measures them to within +/- 10 g
	50%	-Identify presence of object on the scale and measures them to within +/- 5 g -Measure temperature to within +/- 1.5 °C
	75%	-Identify presence of object on the scale and measures them to within +/- 2 g -Measure temperature to within +/-1.0 °C



	100%	-Identify presence of object on the scale and measures them to within +/- <1 g -Measure temperature to within 0.5 °C
User Interface	25%	-Display characterization results to a user on a touch screen -Allow user to start procedure
	50%	-Display characterization and temperature results to the user on a touch screen -Allow user to start procedure and select desired size
	75%	-Display temperature and characterization results to user after procedure on touch screen as a graph over time -Allow user to start procedure and select desired size
	100%	-Display temperature and characterization results to user after procedure on touch screen as a graph over time -Allow user to start procedure and select desired size

Integration Demo Specifications		
Metric	%	Performance
Time to complete process	25	1 day
	50	12 hours
	75	8 hours
	100	6 hours
Reliability of characterization <i>Success is a measurement within 25% of TEM size and DLS distribution measurements</i>	25	Successful characterization 1/20 runs
	50	Successful characterization 1/15 runs
	75	Successful characterization 1/10 runs
	100	Successful characterization 1/5 runs



Accuracy of size produced	25	Distribution peak within 6 nm of desired size
	50	Distribution peak within 5 nm of desired size
	75	Distribution peak within 4 nm of desired size
	100	Distribution peak within 3 nm of desired size
Standard Deviation (σ) of Distribution	25	1σ of at most 70 nm
	50	1σ of at most 60 nm
	75	1σ of at most 50 nm
	100	1σ of at most 40 nm

Note: “completing the process” indicates that nanoparticles, regardless of quality, have been synthesized and the characterization process has been completed. The number of successful completions vs. failures in the testing process will also be reported in the results.

Optimization Demo		
Metric	%	Performance
Time to complete process	25	6 hours
	50	4 hours
	75	3 hours
	100	2 hours
Reliability of Characterization. <i>Success is a measurement within 10% of TEM size and</i>	25	Successful characterization for 2/5 runs.
	50	Successful characterization 3/5 runs
	75	Successful characterization 4/5 runs
	100	Successful characterization 5/5 runs



DLS distribution measurements		
Accuracy of size produced	25	Within 3 nm of desired size
	50	Within 2 nm of desired size
	75	Within 1 nm of desired size
	100	Within 0.5 nm of desired size
Standard Deviation (σ) of Distribution	25	1σ of at most 40 nm
	50	1σ of at most 30 nm
	75	1σ of at most 20 nm
	100	1σ of at most 15 nm

Engineered Solution

It is the need for a system that can reliably synthesize and characterize gold nanoparticles that lead to the idea for our device, *nanoRIMS*. Our device is intended to fully automate the process of preparing, synthesizing, and characterizing gold nanoparticles in small batches for research laboratories and other low scale operations, such as a biosensor startup. It is meant to replace the current method in many research laboratories, which is manual synthesis supervised by graduate students. Automating this process saves graduate students approximately 1 hour of synthesis time, every week. For the purposes of integration, the system will target 12 nm gold nanoparticles specifically. The final design of the system is as such:

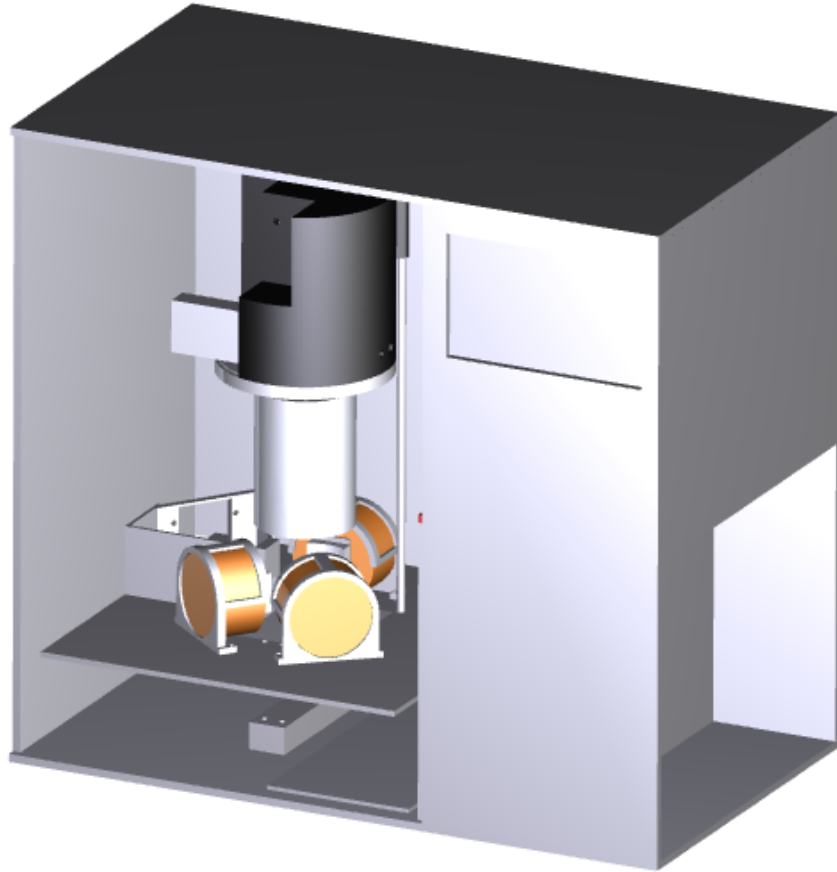


Figure 1: Front face of the proposed design. The main containment area holds the beaker, lid, and all optical and heating/cooling components. Below these components is the load cell and drawer holding electronic components. The open, far right bottom compartment holds the solution containers. The middle section holds the peristaltic pumps and the power supply.

The system will be able to be placed on a lab bench connected to the 120 V_{AC} supply provided by all Canadian power outlets. Power will be distributed to the internal electronics through a EVGA 400 W 80+ certified ATX supply. As previously stated, the system will be able to accurately and precisely prepare the correct chemical solution held in the main beaker, synthesize the gold nanoparticles, and characterize the final solution using an optical based method. The process flow for the system follows the block diagram illustrated below.

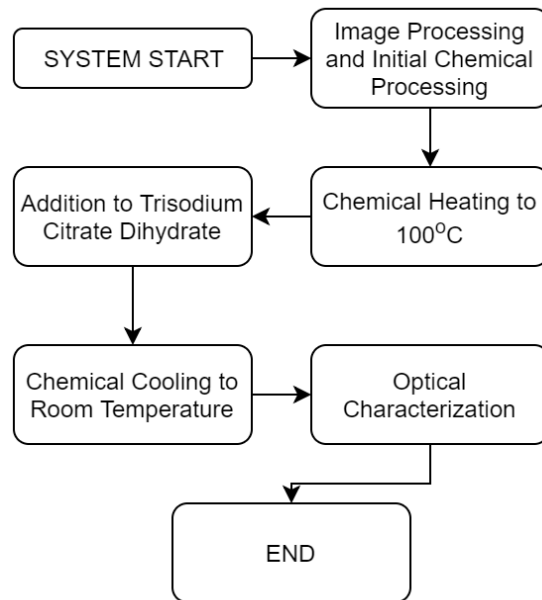


Figure 2: System Process Flow Diagram

Individual flowcharts describing the sub-routines completed during the process are placed within their relevant sections in the report.

Operating Instructions

Power Budget:

Part	Voltage Supplied	Maximum Power (W)
XLT2422-01LS Peltier	12V	50
White LED	12V	0.013
TCD1304 CCD Array	5V	0.1
DFR0198 Thermocouple	5V	Self powered
San Ace 60 9GA Fan	12V	3.12
G8015-G Fan	12V	1.56
HX711 24-bit ADC	5V	0.075



Thermaltake A1178 Heatsink x 3	12V	5.76
Load Cell	5V	0.5
A4988 Stepper Motor Driver x 3	12V	144
SickleFlow 120mm Fan	12V	4.2
Arduino Uno	5V	0.4
MG996R High Torque Servo Motor	5V	4.5
Raspberry Pi 3B+	5V	2
Total Power (Maximum)	216W	

The total allowable output of the chosen EVGA 430 power supply shared between the +5V and +12V supply is 430W, giving us significant overhead for temporary power spikes or adding additional components at a later time.

In order to properly run *nanoRIMS* for gold nanoparticle synthesis, the user should follow the following steps:

- 1) Check the reservoir bottle labelled “TCD Solution”, found on the open right side of the system. If the liquid level in this bottle is below the marked line, refill it with a solution of trisodium citrate dihydrate in deionized (DI) water in a 0.5 g : 30 mL ratio. Confirm the pump tubing is in the bottle.
- 2) Check the bottle labelled “DI”. If the liquid level in this bottle is below the marked line, refill with DI water. Confirm the pump tubing is in the bottle.
- 3) Ensure that the main beaker (a standard 400 mL beaker) is dry and clean from all chemical residue. Rinse with DI water. Open the door of the reactor and place the beaker in the centre of the reactor, held by the peltier element assembly. Close the reactor door. NB: When placing the beaker into its slot, confirm that the markings on the beaker are **not blocking the optical path of the broadband source**. This will cause severe degradation in optical characterization.
- 4) Ensure the EVGA 400W 80+ certified ATX supply is plugged into a standard 120 V AC power outlet, and turn on the power switch. You can turn off the power to the system at any point if needed.



- 5) On the nanoRIMS touchscreen, select the size of nanoparticle desired. Click “start” to begin the synthesis process. The system will monitor the temperature and stage in the process as it operates.
- 6) When the touch-screen indicates that the process is complete, check the characterized size to make sure it is correct.
- 7) Open the reactor door and carefully remove the beaker from the reactor.
- 8) Pour the gold nanoparticles into the desired storage containers, label them correctly, and store them in a lab refrigerator.

Assembly Instructions

In order to assemble nanoRIMS, the following instructions should be followed. Relevant code, engineering drawings and circuit diagrams are found in this report. Inventor part and assembly files, as well as PCB gerber files can be found in the following [Google Drive](#).

The bill of materials for nanoRIMS is outlined below.

Description of Part	Part Number	Quantity	Total Cost (\$CAD)	Legend
Visible Transmission Grating, 1200 Grooves/mm, 36.9° Groove Angle, 12.7 mm x 12.7 mm	GT13-12	1	87.191	Optical Components
Epoxy-Encased White Light LED, 13.0 mW, 7.5° Half Viewing Angle, Qty. of 5	LEDWE-15	1	12.194	Environment
SM05-Threaded Mount for TO-18, TO-39, TO-46, or T-1 3/4 LEDs	S05LEDM	1	42.432	Fluids
Ø12.5 mm N-BK7 Aspheric Lens, f=25 mm, NA=0.23, Uncoated	AL1225	1	216.008	Electronics/Control
SM05 Lens Tube Without External Threads, 1.5" Long	SM05M15	1	21.086	Full Enclosure
TCD1304DG(8Z,AW) Linear CCD Array	757-TCD1304DG8ZAW	1	34.2	



Peltier element, 50W max power	Marlow Industries / XLT2422-01 LS	3	88.2	
Digitized Thermocouple, Waterproof	DFRobot DFR0198	1	22.3	
Spinning fan, tach, PWM x1	1688-1571-ND	1	18.34	
Cooling fan x1	Mechatronics Fan Group / G8015L05B	1	15.29	
Small Round Neodymium Magnets	N/A	10	2.83	
Load cell amp x1	SparkFun Electronics / SEN-13230	1	13.94	
Heat Sink & Fan Unit	Thermaltake / A1178	3	30	
Beaker Load Sensor	MF01-N-221-A04	1	14.22	
A4988 Stepper Motor Driver	Longrunner	1	15.66	
A4988 Robojax Stepper Motor Driver	RoboJax	1	14.5	
3003 Aluminum Sheet, 0.032"	Metal Supermarkets	1	16.95	
Silpat Silicone/Fibreglass Baking Mat	Canadian Tire	1	29.99	
1/4 Inch 199-0 Black Acrylic: 300x500mm	CUTACO	2		
1/4 Inch 199-0 Black Acrylic: 312.7x550mm	CUTACO	2		
1/4 Inch 199-0 Black Acrylic: 260x300mm	CUTACO	1		
1/4 Inch 199-0 Black Acrylic: 200x300mm	CUTACO	1		



1/4 Inch 199-0 Black Acrylic: 233.65x300mm	CUTACO	1		
1/4 Inch 199-0 Black Acrylic: 120x290mm	CUTACO	1		
1/4 Inch 199-0 Black Acrylic: 350x500mm	CUTACO	2		
1/4 Inch 199-0 Black Acrylic: 200x500mm	CUTACO	2		
Acrylic Total Cost	P&A Plastics Hamilton		\$342.98	
10-32x3/4 Round Socket Head Machine Screws (17 Pack)	Home Depot	3	\$7.50	
10-32 Machine Nuts (13 Pack)	Home Depot	4	\$10	
Cooler Master SickleFlow 120	R4-L2R-20A C-GP	1	10	
Everbilt 1 Inch 25mm Corner Brackets (4 Pack)	773 637	8	10	
Hex Screws	Home Depot 3550, 3221, 4048, 4044	4,4,1,1	9.15	
3 Ft USB A to Mini-B	Amazon	2	2.67	
M4, M5, M6, M8 Screw Set	Echogear	1	18.99	
Uno R3	Elegoo	2	12.65	
Neodymium Cylinder Magnets	Whectin	3	14.79	
MOSFET + CCD PCB	JLCPCB	1	42.73	
5.0 mm Pitch 3-pin 3-pack Screw Terminal	Canada Robotix	3	3.99	
5.0 mm Pitch 2-pin 2-pack Screw Terminal	Canada Robotix	2	3.99	
1/4" Plated Steel Threaded Rod	Home Depot	2	6.02	
MG996R Servo Motor	Digikey	1	Components Shop	
SG90 Servo Motor	Digikey	1	Components Shop	



Welco Peristaltic Pump, WP11-P1/4BA2-P-B	Welco	1	180.7	
Welco Peristaltic Pump, WP10-P1/8BA2-P-B	Welco	1	180.7	
Welco Peristaltic Pump, WPM1-P1EA-NBP	Welco	1	130	
Wide Mouth Lab Sample Bottle	Dynalon	1	47.76	
Liquid Sample Collection Bottles	Jiuwu	1	10.19	
Vinyl Tubing, 1/8" ID, 1 ft	Home Hardware	1	0.29	
Vinyl Tubing, 1/4" ID, 4 ft	Home Hardware	1	1.52	
Polyethylene Tubing, 0.17" ID, 4 ft	Home Hardware	1	1.56	
Raspberry Pi 3B+		1	46.22	
Raspberry Pi 7' Touch Screen		1	89.98	
H-bridge controller	L298N	5	Peter (components shop)	
High current h-bridge	DROK 16A Dual Channel H-Bridge	1	18.99	
Arduino Uno	Rev3	1	46.22	
MOSFET Switches	irf540n	4	7.04	
Raspberry Pi Power Supply	Canakit/Am azon	1	11.99	
32 GB microSD Card	SanDisk Ultra	2	14.99	
Total Cost			1978.941	
Cost Per Person			494.73525	



See part and assembly drawings in appendix A, labelled as follows:

Appendix Label	Drawing Description
A	Exploded view of reactor assembly
B	Back wall of reactor--space for electronics drawer and power supply
C	Back of electronics drawer
D	Enclosure top and bottom
E	Far Right Wall
F	Front Door (left side) of Enclosure
G	Front Door (right side--with space for Pi touchscreen) of Enclosure
H	Far Left Wall (with hole for enclosure fan) of Enclosure
I	Middle Wall of Enclosure (with venting for power supply and gap for wiring)
J	Partition (between reservoir and pumps) of Enclosure
K	Shelf (space for pumps, tubing and wiring)
L	Reactor Assembly Exploded View
M	Bottom of the Beaker Lid
N	Beaker Lid Cover (outer casing)
O	Beaker Lid Top
P	Heater Film and Insulation



Q	Heat Sink Holder
R	Lid insulation
S	Peltier extension
T	Servo Motor Cover
U	Servo Motor Holder
V	Spring & Rail Holder for lid latching system
W	Servo motor latching system--Case and Arm
X	Bottom of Diffraction Grating Holder (includes slit)
Y	Top of diffraction grating holder
Z	LED and Lens enclosure (bottom)
AA	LED and Lens enclosure (top)
AB	Bottom of optical enclosure
AC	Top of optical enclosure
AD	Linear CCD Optical Enclosure
AE	Reactor plate

The manufacturing of all of these parts, according to the dimensions in the appendix drawings are done through a combination of 3D printing, laser cutting, and machining. The method of manufacturing for each part is summarized in the table below.

Method of Manufacturing	Parts
3D-Printing	M, N, O, Q, T, U, W, X, Y, Z, AA, AB, AC, AD
Laser cutting (from acrylic listed in BOM, above)	B, C, D (x2), E, F, G, H, I, J, K, V, AE
Mill from aluminum	S, P
Cut from silicon	P, R



These pieces are then assembled following the exploded assemblies found in A and L, or through the Inventor Assembly file titled “Enclosure.iam”. The acrylic pieces that make up the structural enclosure of nanoRIMS are assembled using the brackets and screws found in the bill of materials, and cemented using acrylic cementing solvent, “Acryweld”.

The peltier elements, heat sinks with fans and holders are mounted onto the reactor plate (part AE) using screws, and according to the dimensions found in the enclosure assembly file. The optical enclosure components (X, Y, Z, AA, AB, AC, AD) are slotted together and mounted on the plate. The diffraction grating, CCD and characterization LED and lens are placed in their respective holders, as labelled. The reactor plate is then mounted onto the load cell using the quarter inch threaded rods, located as indicated in the assembly file. The beaker lid, assembled according to the exploded diagram found in L (with screws used in the pre-printed holes), is also mounted on these rods. This includes the pump, seen in the assembly diagram. The image processing LED and the Pi cam are mounted in the openings in part O. Finally, the spring holder (part V) is mounted onto the top of the quarter inch rods, and the lid connected to the holder with the spring. The enclosure fan (found in the BOM) is mounted on the outer left wall (H) with M4 screws. The thermocouple is inserted through the hole in part M.

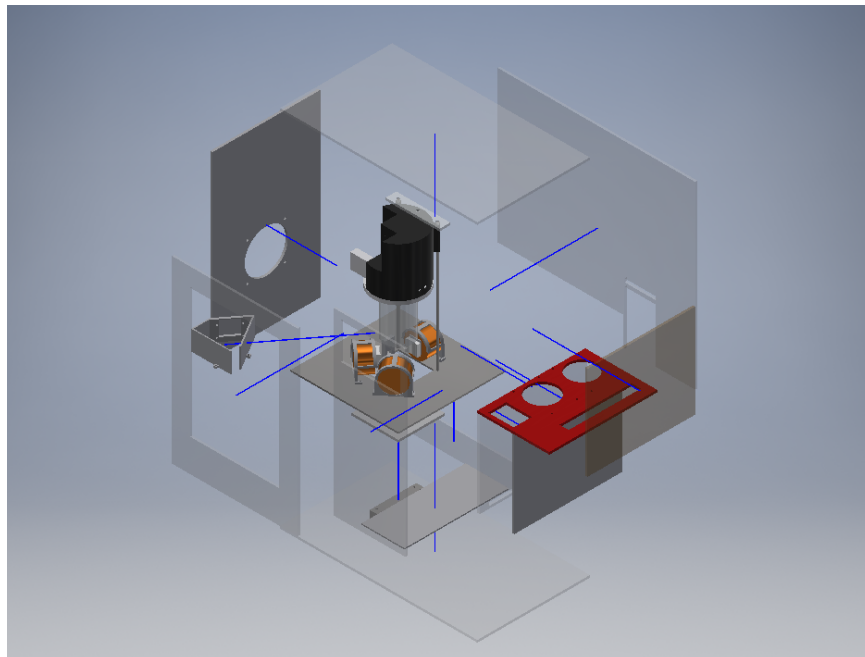


Figure 3: Exploded View of nanoRIMS Enclosure

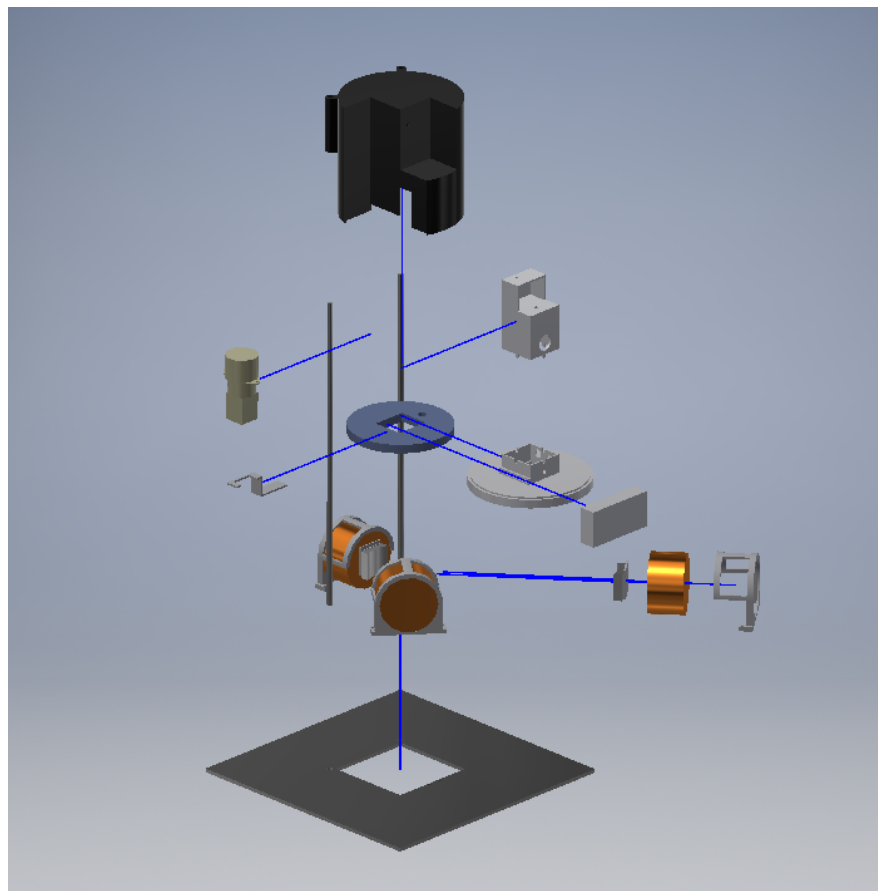


Figure 4: Exploded View of Reactor Plate and Lid Assembly

The next step in assembling nanoRIMS is completing the wiring and control systems. In order to operate nanoRIMS, two PCBs were designed and ordered. The Gerber files for both of these boards are found in the file drive. Images of both boards and their wiring instructions are included below.

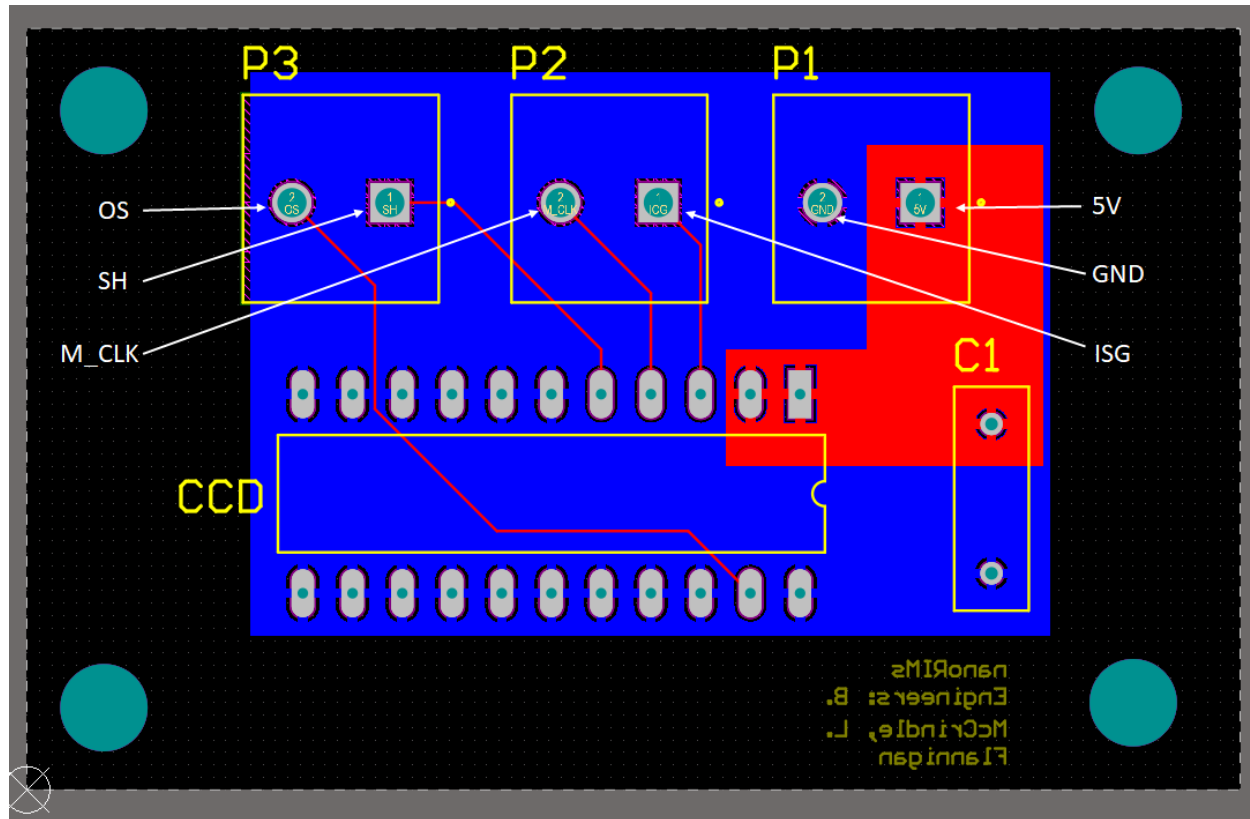


Figure 5: Frontside of the CCD PCB Schematic

PCB Pin	STM32 Pin
ISG (Integration Shift Gate)	PA1
M_CLK (Master Clock)	PB1
SH (Pixel Shift Gate)	PB10
OS (Output Signal)	PC0
GND	GND (STM or Power Supply Unit)
5V	5V (STM or Power Supply Unit)

The next board is used to control the enclosure fans, beaker spinner, characterization LED and image processing LED. It also connects the thermocouple to the main control system. This PCB is wired as described in the table below.

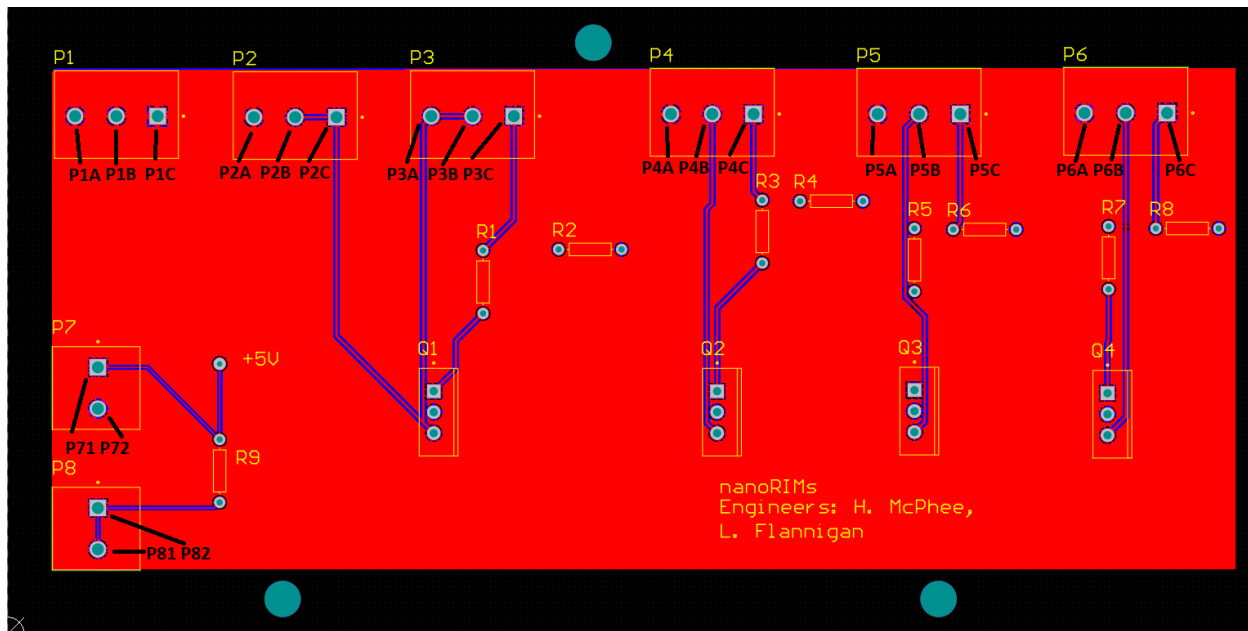


Figure 6: Reactor Control PCB Schematic

PCB Pin	Connection
P1A, P1B, P1C, P2A	Powered with 12V supply. Power line of heat sink fans and enclosure fan.
P2B, P2C, P3A, P3B	Grounds of heat sink fans and enclosure fan.
P3C	Control signal for fans from Arduino (see code for pin #)
P4A	Power line of spinner
P4B	Ground line of spinner
P4C	Control signal for spinner from Arduino (see code for pin #)
P5A	Power line of characterization LED
P5B	Ground line of characterization LED
P5C	Control signal for characterization LED from arduino (see code for pin #)
P6A	Power line of image processing LED
P6B	Ground line of image processing LED
P6C	Control signal for image processing LED from arduino (see code for pin #)
R1	4.5 kOhm resistor



R2	10 kOhm resistor
P71	Temperature data connect to Arduino (see code for pin #)
P72	Data line (blue) from thermocouple
P81	Ground line (orange) from thermocouple
P82	Power line (red) from thermocouple
Q1, Q2, Q3, Q4	Irf540n n-channel power MOSFET

The Peltier elements, heating film and all pumps are controlled using h-bridge motor controllers. The heater film is powered using the high current h-bridge, and powered with the 24V line from the power supply. The rest of the system is powered using LN298 drivers. All of these drivers are cooled using a fan during operation. Each driver has clearly labelled on, off and PWM pins. For the peltier elements, these signals are provided by the Arduino and the required pins are indicated in the control system code (found in Appendix B, code D). The pumps are controlled from the Raspberry Pi, and the on, off and PWM pins are clearly labelled within the master control code (also found in Appendix B, code F).

To run nanoRIMS, the user needs to download the following programs onto the Raspberry Pi:

- OpenCV
- Arduino IDE
- System Workbench for STM32

The user then downloads the code found in Appendix B. Arduino code is flashed to the Arduino (connected to the Pi with a USB connector), and the firmware for CCD microcontroller is loaded onto the board (also connected through a USB). Once this is done, and connections are made according to the above instructions, the system can be run from the Pi's touchscreen by utilizing the system code found in Appendix B.

Mathematical Modelling

Fluid Containment and Transport

To contain the Deionized Water (DI), Trisodium Citrate Dihydrate (TCD), and Gold Chloride (AuCl_3) solution, suitable sized containers and their material is critical for long-term storage. Typical materials for bottles include: polypropylene, high- or low-density polyethylene (HDPE or LDPE), polycarbonate, and fluoropolymers [1]. *nanoRIMS* does not require autoclaving, impact resistance, or significant chemical resistance to store DI or TCD. Thus, the cheapest option with excellent chemical compatibility for our purposes was chosen [2]; the result of the decision process being HDPE or LDPE.

To reduce maintenance and solution refill frequency for TCD (~30 mL dispensed/cycle), a large reservoir is required. The largest available reusable lab bottles for long term usage are 1 L. This would allow for ~30 cycles of nanoparticle synthesis. Wide-mouth bottles were then chosen over

narrow-mouth to allow for ease of modification and increased area for multiple holes (tubing and venting).

The reservoir for DI was set to be 1 L to increase simplicity and exchangeability in case of damage to either reservoir. The DI reservoir is not meant to store chemicals for periods greater than a day due to absorption of atmospheric gases causing degradation of the water [3]. To store a volume of AuCl_3 for a similar number of runs, 5 mL glass bottles were chosen. At 206.7 μL dispensed/cycle, the bottles would be ready for ~24 synthesis cycles. Glass was chosen as the material for its excellent chemical inertness, lack of leeching relative to PE, and availability in small containers.

In order to determine how quickly the 30 mL TCD solution must be pumped, nanoparticles were synthesized in Dr. Soleymani's lab using three different procedures: standard operating procedure (SOP), addition of TCD over 30 seconds, and addition of TCD over 10 seconds. The 10 second addition nanoparticles' peak size agreed with the SOP results within error. When the TCD solution was added to the solution over 30 seconds, the peak size of the nanoparticles shifted significantly from that of the standard operating procedure, and the growth of secondary nanoparticles increased significantly, as seen in the figures below. This is likely due to the fact that the synthesis reaction began before all of the TCD was added to the solution. The beginning of the synthesis reaction can be observed visually, in the form of a colour change. The time it takes from the initial addition of TCD to this colour change was measured and found to be 20 seconds, the time that sets our maximum pumping speed.

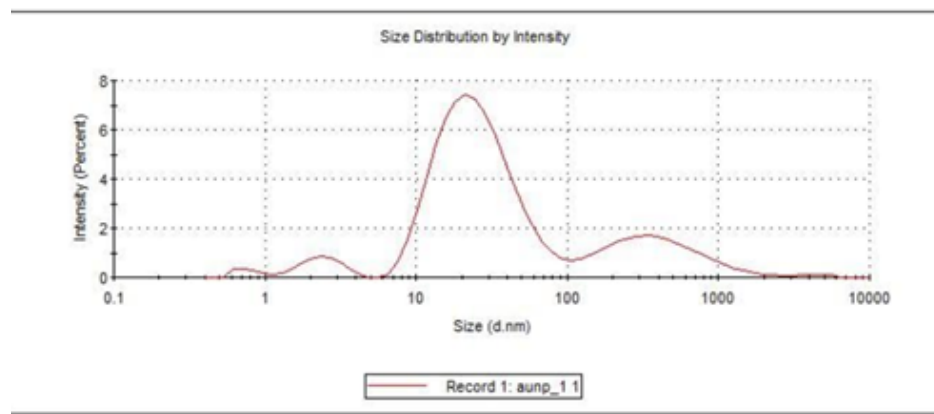


Figure 7: DLS, Standard procedure

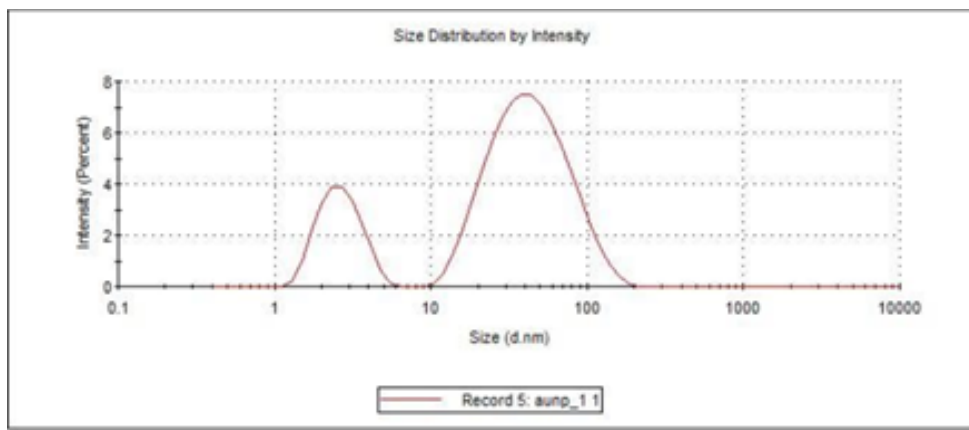


Figure 8: DLS, 30 second TCD addition

For the chemical reaction to produce the desired results, precise control of dispensed volumes must be achieved. For an accuracy of 1% for volumes greater than 10 mL, *nanoRIMS* implements a positive displacement technique similar to how pipettes are currently used.

Positive displacement technology allows for precise flow control as each actuation of the pump displaces a set volume so long as the pressure loss is below a maximum set point. Rather than supplying a certain pressure, this allows for a constant flow rate at a given drive speed. Using this, one can calculate the volume dispensed simply by integrating the constant flow rate over time. This also allows for the system to be independent of the reservoirs' hydrostatic pressures (i.e. volume).

As *nanoRIMS* is pumping solutions of TCD and AuCl_3 , the development of fouling or other matter due to precipitation may prove to be an issue for mechanical pumps whose driving mechanism is in contact with the fluid. This would cause performance degradation and/or failure reducing the lifetime of the device. Thus, to reduce maintenance costs and increase reliability, a pumping solution that never directly touches the fluid was chosen..

The common pumps used for *nanoRIMS*' design would be either (1) diaphragm or (2) peristaltic. Diaphragm pumps suffer from requiring a form of valve control, increasing complexity of the pumping system, or has check valves which will foul over time causing the pump's performance to degrade [4]. Peristaltic pumps do not suffer from these drawbacks and work well with a variety of chemical solutions. Furthermore, should a diaphragm pump fail due to fouling, the unit must be replaced whereas if a peristaltic unit fails due to tube issues, the tubing can be replaced separately. Given the desired properties, *nanoRIMS* pumps were set to be peristaltic.

To determine the pump parameters, certain desired system properties were set: (1) minimum elevation rise between the lowest and highest points, (2) chemical compatibility of tubing/piping with solutions, (3) minimum complexity of parts (i.e. valves, nozzles, diffusers, etc.), and (4) able to pump an overall tubing length of 1 m.

Given the 1 L reservoirs for TCD and DI, the elevation gain was measured to be 25 cm (with clearance for the tubing). Due to the non-corrosive nature of TCD, DI, and AuCl_3 , commonly

available vinyl tubing was chosen for its chemical compatibility [5], replaceability, and low cost. Depending on the outer diameter (OD) of the peristaltic pump tubing, tubes with a very similar inner diameter (ID) can be pressure-fit to produce a water tight seal (at near atmospheric pressures). The result of this procedure can be seen in Figure 9. The inlet and outlets do not require special entrances/exits and can be left as the end of a tube. Thus, no extra parts other than the tubing is required.



Figure 9: Pressure-fit vinyl tubing on peristaltic pump tubing (Pharma BPT).

To determine the pressure loss throughout the system, the following energy conservation energy was used [6]:

$$\Delta P = \left(f_D^L + \sum K \right) \frac{\rho U^2}{2} + \rho g \Delta h \quad (1)$$

As a conservative calculation, the worst-case scenario for the system was used. The following table outlines the parameters for the system:

Variable	Sym.	Value	Reason
Grav. Const.	g	9.81 m/s ²	Known constant
Density	ρ	998 kg/m ³	Fluid is approx. water at STP [6]
Dyn. Viscosity	μ	1.002x10 ⁻³ Pa·s	Fluid is approx. water at STP [6]
Length	L	1 m	System parameter
Diameter	D	1/8" = 3.175 mm	Set arbitrarily, conservatively small
Minor Loss	ΣK	3 u.l.	Sudden expan., contract., and inlet [6]
Flow Rate	Q	3 mL/s	System parameter
Velocity	U	0.379 m/s	Flow Rate/Area = Q/(πD ² /4)
Reynolds No.	Re	1200 u.l.	ρUD/μ (Laminar) [6]
Friction Factor	f	0.0533 u.l.	Vinyl tubing, smooth walls, circular tube, laminar flow [6]
Elevation Gain	Δh	25 cm	System parameter



The minor loss coefficient was conservatively set to be the sum of a sharp-edged inlet (0.5 u.l.), a sudden contraction (0.5 u.l.), and sudden expansion (2.0 u.l.). These values represent the inlet of the tube, the inlet to the pump, and the outlet of the pump, respectively. All values were retrieved or determined using formulas in [6]. The sharp-edged inlet's minor loss coefficient was retrieved as 0.5.

The sudden expansion loss coefficient was calculated using the following equation:

$$K_L = \alpha(1 - d^2/D^2)^2 \quad (2)$$

Where ' α ', ' d ', and ' D ' are the kinetic energy correction factor (2.0 for laminar flow [6]), smaller pipe diameter, and larger pipe diameter, respectively. At the worst case, $D \gg d$, thus:

$$K_L = \alpha = 2.0 \quad (3)$$

Using Table 14-4 in [6], the minor loss coefficient for sudden contraction was retrieved as 0.5, the maximum possible value mimicking a sharp-edged inlet. Thus, the sum of the minor losses ends up as 3 u.l.

The friction factor was calculated using the following equation for laminar flow in a circular tube [6]:

$$f = 64.00/Re \quad (4)$$

Given our Reynolds Number of 1200 u.l., the friction factor was calculated to be 0.533 u.l.

Therefore, our peristaltic pump requires a conservative maximum pressure supply of:

$$\Delta P = \left(f \frac{L}{D} + \sum K \right) \frac{\rho U^2}{2} + \rho g \Delta h = 3.687 kPa \quad (5)$$

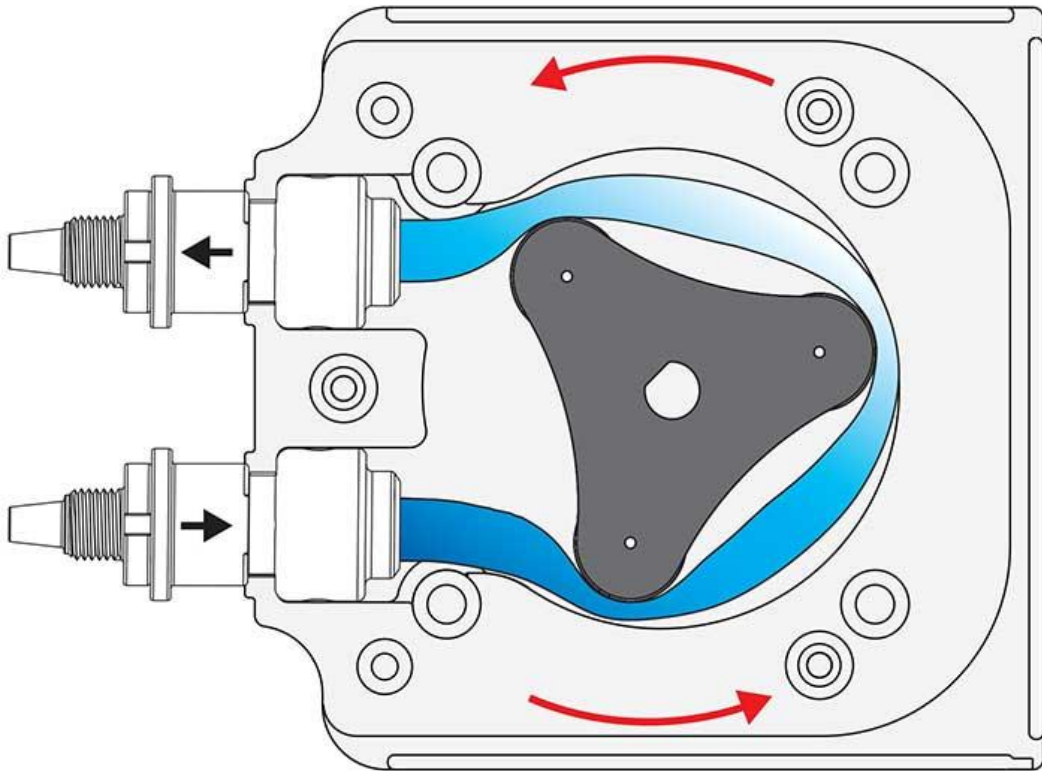


Figure 10: Positive Displacement 3-Rotor Peristaltic Pump Concept. [7]

The operating principle of peristaltic pumps can be seen in Figure 10, where a rotor squeezes on a tube to displace a certain volume of fluid. If the rotor can provide enough torque to overcome the tube system's pressure, it will move the fluid a distance 'x' in the tubing according to the following formula:

$$x = \text{Vol. Displaced} \div \text{Tube Cross section} \quad (6)$$

Given the system specification for dispensed volume accuracy (1% for volumes $>10 \text{ mL}$) of 0.1 mL , the sourced peristaltic pump must be able to accurately dispense volumes below this threshold (i.e. volume resolution $< 0.1 \text{ mL}$). Stepper motor driven pumps allow for precision control over all motor types due to the number of steps being able to be specified. Another advantage is the high pull-out torque over other motor types allowing for the pump to come to a stop immediately and thus not over-dispense. For the AuCl_3 solution, each step should also displace $< 1\%$ of the required volume. However, as this volume is on the order of 100's of μL , surface tension will prevent drops from being dispensed before a critical drop size. The Image Processing section goes over the method used to characterize these drops.

The sourced pumps were the following from Welco:



- 1) WP11-P3/16(200)BA4-H-BP
- 2) WP10-P1/8(200)BA4-H-BP
- 3) WPM1-P1EA-NBP

The important parameters are summarized below:

Pump Model	Vol. to Dispense (mL)	Vol. Disp. (mL/rot.)	Steps per Rot.	Vol. Disp. (uL/st.)	Vol. Disp. (m3/st.)	Speed (rpm)	Flow Rate (mL/min)
WP11	30	1.6	1600	1	1.00E-09	20 - 150	32 - 240
WP10	300	0.8	1600	0.5	5.00E-10	20 - 150	16 - 120
WPM	0.2067	0.04	2800	1.43E-02	1.43E-11	1 - 150	0.04 - 6

As shown in the Table above, the volume displaced per step is below the 1% threshold for all volumes to be dispensed. Furthermore, the WP11 that will pump the 30 mL can dispense it in 7.5 s, below our DLS results' maximum time to dispense. The maximum pump height is stated to be 2 m of water which is equivalent to 19.5 kPa, above the conservative value calculated above.

To dispense the target volumes to sufficient accuracy, our system uses a feedback loop where the load cell and pumps communicate. This is to overcome the limitation that our stepper motors will randomly skip steps depending on the environment and system parameters.

In part of the feedback loop shown in the flowchart below, the load cell serially communicates the actual dispensed mass (converted to volume using density) which the Raspberry Pi controlling the pumps uses to determine completion or the following volume to dispense. The 90% is to prevent any over-dispensing should no steps be skipped in a particular cycle. Overall, a second Raspberry Pi commands the pumping Pi through serial communication and the pumping Pi reports back the results of its task. The code for this process can be found in the Appendix.

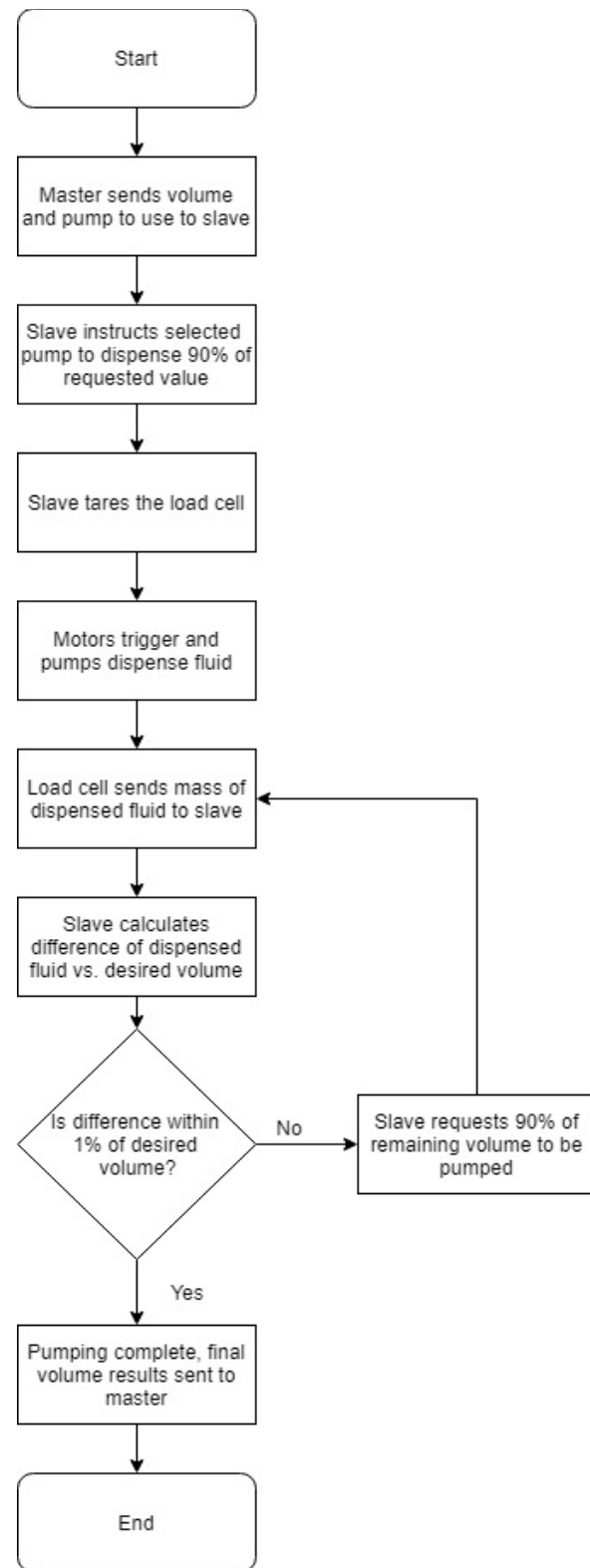


Figure 11: Process Control For Pumping

Image Processing

Along with being the first step that occurs during the synthesis process, it is by far the most sensitive step due to the amount of liquid that must be added into the beaker relative to the other two solutions. Since the amount of AuCl_3 that will be pumped into the beaker will be on the order of microliters, an image processing routine is employed to approximate the volume of each pumped drop. A control loop is implemented to check the volume of the drop during its build up on the nozzle. The amount of fluid that is pumped by the AuCl_3 peristaltic pump will change depending on the amount of fluid on the end of the nozzle. This is to ensure that the final image of the droplet is captured before the drop is forced to fall due to gravity. A flow chart outlining this process is shown below.

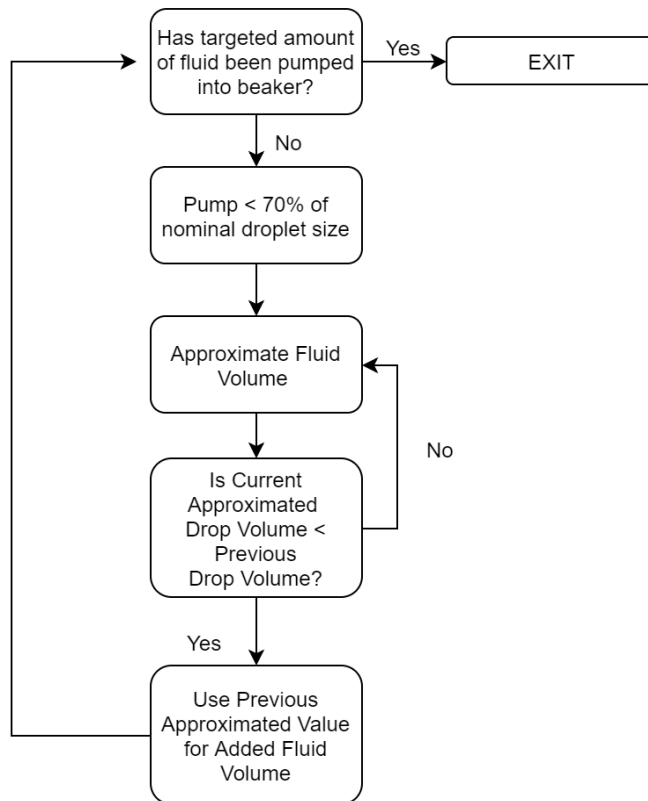


Figure 12: Droplet Pumping Process Flow

In order to determine the mass of a droplet of fluid released from the nozzle, a thresholded image separating the drop from the background is necessary. An image is taken of the drop right before it starts to fall towards the beaker while it is still stationary. The nozzle is placed at the focal plane of the Raspberry Pi Camera (PiCam) to capture the largest contrast

between the background and the drop itself. This contrast is of utmost importance since the edge of the droplet will be imperative for image thresholding.

Normally, if the contrast between the background the drop was large enough, a basic thresholding technique could be effective in creating the desired blob. Unfortunately, since the fluid used is clear and thus projecting objects and other sources of light that are directly behind it, there is a challenge when pursuing a basic thresholding method. Therefore, the steps used for isolating the drop are laid out in the block diagram below:

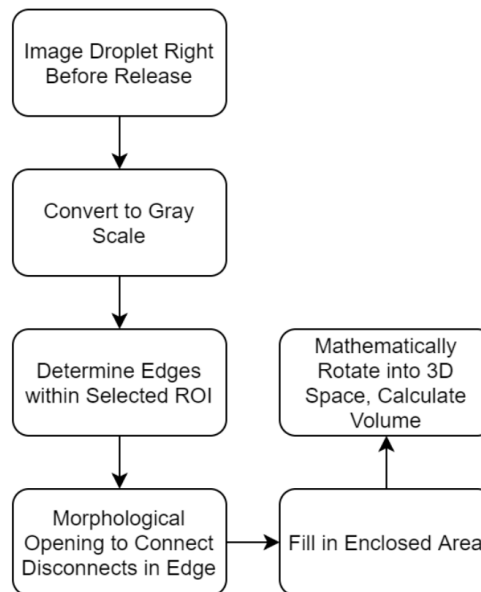


Figure 13: Thresholding flow chart for isolating a droplet

Through pumping calibrations, a single droplet is built on the end of the nozzle with a pre-programmed, static, region of interest to remove any background noise and increase computational efficiency. An example of an image captured using this method is shown below.

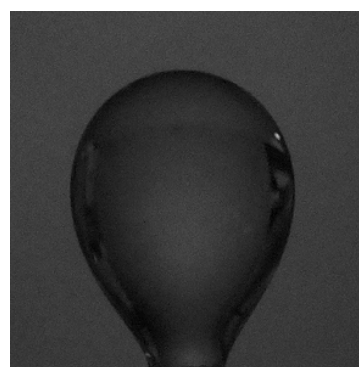


Figure 14: Imaged droplet with low exposure

From here, the image is converted into a grayscale image to remove the 3-channel RGB complexity. With the cropped image, the Canny edge detection algorithm is used to isolate the edges from the background. Implemented using OpenCV, the basic shell of the Canny edge detector applies a Gaussian filter to reduce any noise, determines the intensity gradient of the image, and removes weak edges not connected to strong edges. It should be noted that depending on the ambient light conditions in which the image was taken, the difference between the background and the edge of the droplet can start to become indistinguishable, making it difficult to apply an edge detection algorithm. In cases like this, the resulting edge image will have noticeable discontinuities breaking what should be the single edge around the drop. To circumvent this issue, a standard morphological opening is applied. The opening is a dilation followed by an erosion of pixel blobs within the image to connect broken portions of the edge but to stay within the true size of the drop. With a solid edge representing the true size of the drop, the enclosed area needs to be filled to create the blob of interest. In cases where the outer edge of the image is jagged, a median filter is applied for smoothing. Along with this, any background blobs that could not be thresholded out, the largest blob in the image is determined and all other blobs are removed. The images capturing the process are shown below.

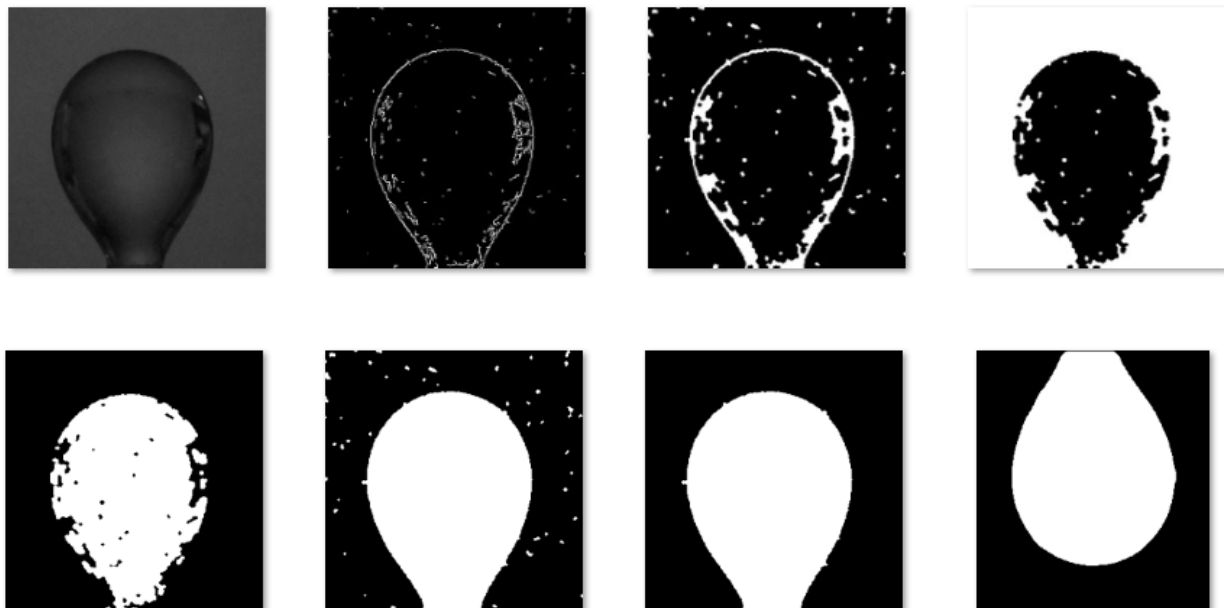


Figure 15: Images showing the process of edge detection, blob detection, and median filtering. Rotating the final image for orientation purposes.

From here, the theoretical mass of the drop can be calculated. Though there are several ways to calculate a volume of a three-dimensional body through a two-dimensional contour, the method that has been implemented is as follows:

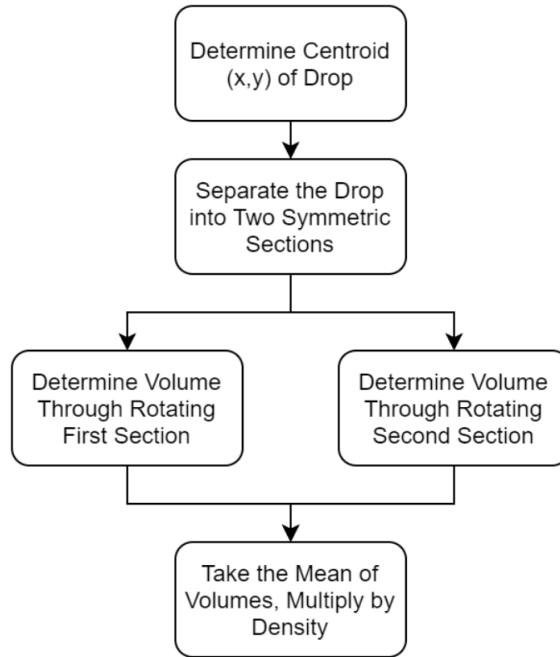


Figure 16: Flow chart for finding the mean of a single imaged droplet

The axis of symmetry in this particular application is in the direction of the gravitational force since the surface tension holding the drop from falling forms a meniscus at the nozzle which is unique to the rest of the body. The centroid, otherwise known as the center of mass, is used to determine where the axis of vertical symmetry will be. The volumetric contribution of each slice of the drop is done by rotating the radius of each disk around the axis of symmetry, as seen in the figure below.

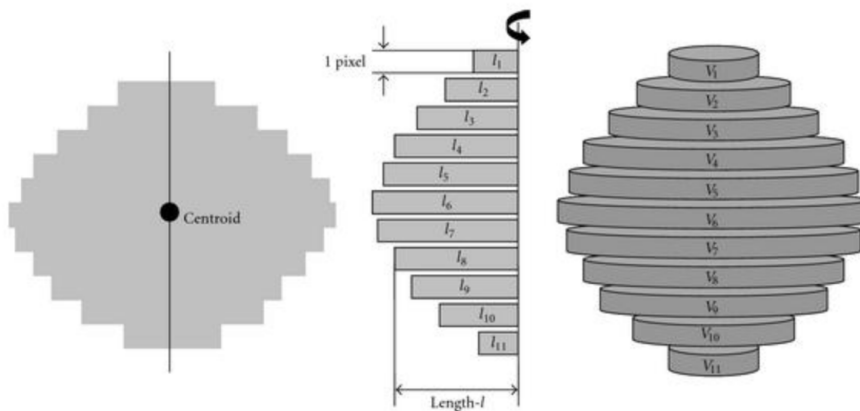


Figure 17: Volume Approximation of Single Droplet Side [13]



The total volume of the drop is then approximated by taking the mean of the volume calculated by the two sections individually. These volumes should be close to equal since it is assumed that there will be three-dimensional symmetry, and therefore, a single contour should capture this. Furthermore, this method helps to reduce any fluctuations in the blob's uniformity deriving from the thresholding method previously described.

Under circumstances in which the focal length and the distance away from an object is known, the angle (micro-radian) in which a single pixel on the imaging array subtends can be quickly calculated when knowing the pixel pitch of the sensor. Due to the imaging scheme that has been implemented, the designed focal length of the system is unknown and thus, a proper micro-radian value cannot be reported or used to determine the size of the drop. To get around this issue, a reference image of known length is placed at the focal plane of the camera. A high resolution image is taken and the number of pixels that cover the physical distance are counted. This measurement is known as the calibration factor. With this, the length per pixel can then be used to determine a radius of each disk. The disk is then rotated to find its area, then multiplied by the density of water and height of a single pixel to obtain mass. The mathematics is as such, and the calibration factor is the same for both relationships.

$$Area = \pi[(nP_{pixels})(Calibration_{Factor})]^2 \quad (7)$$

$$Mass = Area(Density)(Pixel)(Calibration_{Factor}) \quad (8)$$

Environment and Process Control

In order to heat, cool, and maintain the temperature of the solution throughout synthesis, we designed a joint heating, cooling and mixing control system. This system consists of a magnetic stirrer (the speed of which is tunable), three Peltier heating and cooling elements, a heating film, and a thermocouple to provide temperature feedback. The heating and cooling are controlled with a PID control system. A simple schematic of the set-up is seen below.

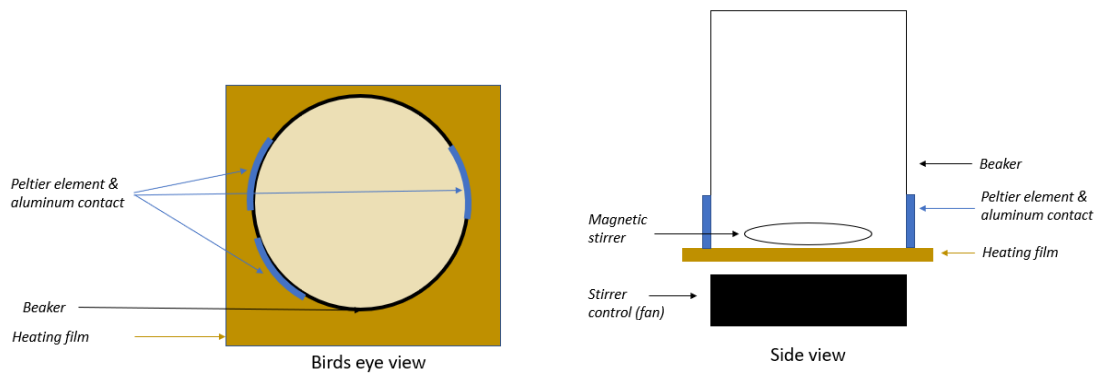


Figure 18: Schematic of Beaker and Fan Setup

Peltier's in this system are unevenly spaced around the beaker to allow a straight path through the beaker for the optical characterization beam.

This system is required to heat 300mL of the solution to 100 °C from room temperature, and to cool it to 25 °C from 100 °C within 20 minutes. This spec was deemed necessary after experimental testing was done in Dr. Soleymani's lab, using the standard synthesis procedure. The procedure was completed once with the regular ice cooling, and once with no assisted cooling. The temperature change was measured while cooling with ice, and the water was found to drop from 100 °C to approximately 25 °C over the 15 minute mixing period. This allowed us to define the "cool" temperature in our system as 25 °C. Dynamic light scattering measurements were taken using both the ice cooled and ambiently cooled solutions. While the peak size of the nanoparticle solution did not change within error, there was significant growth of the secondary nanoparticle size (>100 nm) in the solution that was not actively cooled.

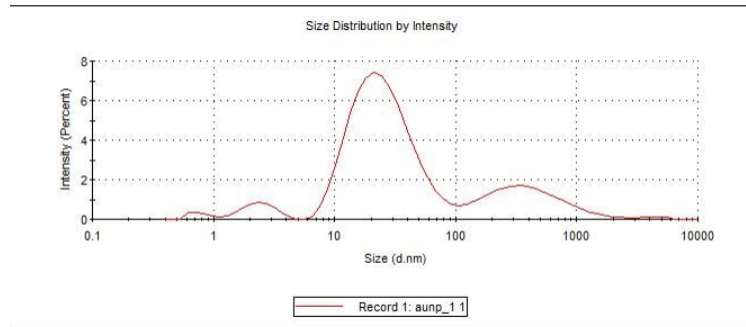


Figure 19: Ice Cooling

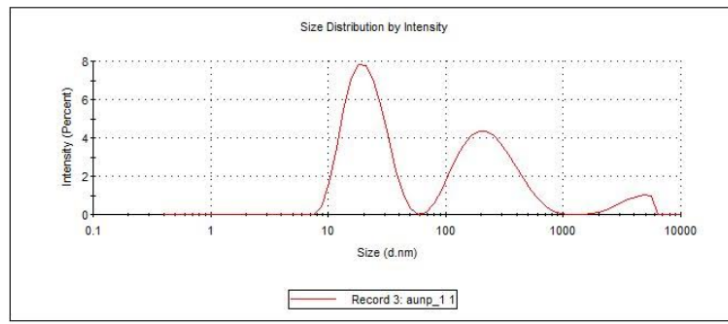


Figure 20: Ambient cooling

This meant that in order to achieve the quality of nanoparticle solution achieved in the lab, active cooling is necessary.

The total heat power required to heat and cool the systems are described as follows.

$$Q_{req,heat} = Q_{water} + Q_{environmental,loss} \quad (9)$$

$$Q_{req,heat} = \frac{mc_p \Delta T}{t} + Q_{environmental,loss}$$

$$Q_{req,heat} = 52.25 + Q_{environmental,loss}$$

Each Peltier is capable of pumping a maximum of 30 W [8] at approximately 2 A and can reach temperatures up to 125 °C. After some testing, it was determined that the environmental heat losses were too large to heat the water with the Peltier's alone. In order to supplement the heating, a Kapton heating film was added to the design, to sit underneath the beaker. This film can also be controlled by the Peliter PID control system and is capable of generating up to 72 W of heat at 24 V and 3 A supply [9]. This gives us a total heating load of 162 W, although much of this will be lost to the environment and in thermal resistance through the beaker. As a result, in the heating system, we need to minimize our environmental losses. This is a challenge since the body of the beaker cannot be insulated due to optics and cooling requirements. In order to minimize heat loss from the water, we added a lid to the beaker than is lifted off of the beaker



using a solenoid latch when the system requires cooling. We also minimize the thermal resistance from the Peltier to the beaker, a design decision discussed further below.

For cooling, environmental losses from the water work in our favour, while we cool the water in addition to the heating film that the beaker sits on:

$$Q_{req,cool} = Q_{water,cool} + Q_{film,cool} - Q_{environmental,loss} \quad (10)$$

$$Q_{req,cool} = \frac{mc_p \Delta T}{t} + \frac{mc_{p,film} \Delta T}{t} - Q_e$$

$$Q_{req,cool} = 76.5 \text{ W} + 1.2 \text{ W} - Q_e$$

Our goal for cooling is to maximize the heat pumping from the Peltier's, which are able to pump a maximum of 30 W each at approximately 2 A (achievable by our h-bridge [10]). This pumping will be limited by our thermal resistance, described in more detail below, so we need to maximize our environmental losses from the water itself. We do this by the addition of a cooling fan and by not insulating the beaker. We also include large heat sinks with fans on the Peltier elements, to remove heat from the hot side of the Peltier as quickly as possible, so their ability to cool is not impeded.

The additional heat pumping required to cool the heating film is only 1.6% of our total cooling load, making the addition of a heating film to improve our heating time a low-cost inclusion.

Since module demo, the heating film used in this system was changed to one with a smaller area (7.6 cm x 7.6 cm, compared to 10 cm x 10 cm previously). The film used during the first iteration of this heating design had a maximum wattage of 96 W, leading to a watt density of 0.96 W/ cm². During operation, the area of the film not in contact with the beaker experienced damage due to an inability to effectively transfer heat away from the film. Additionally, since a large area of the film wasn't contacting the beaker, significant heat was lost to the environment. The new, smaller film, has a lower maximum wattage (72 W at the max power of 24 V), but has a higher watt density of 1.2 W/cm². Since nearly the entire of the film is covered by the beaker, this higher watt density actually means *more* heat will be transferred to the beaker than in the larger film case. Additionally, the smaller film means no heat damage is done to the system components that surround the beaker.

In order to ensure that the corners of the film which do *not* contact the beaker can contribute to the water heating, and do not experience heat damage due to the lack of heat sink, a thin layer of aluminum foil was added to the surface of the film, connected with thermal tape. The addition of this aluminum reduces the thermal resistance experienced by the heating film, just as in the calculations for aluminum contacts, above. This facilitates the transfer of heat away from the surface of the film and allows the corners of the heating film to contribute the heating of the beaker through the aluminum contact.

The final change made to the heating system involves changing the thermal contact material used to hold the heat sink, Peltier and aluminum contact together. Previously, thermal



compound was used to hold these components together due to its high heat conductivity. At high temperatures, this compound would sometimes melt and cause the Peltier elements to slip from the centre of the heat sinks. In order to prevent this and ensure good heat transfer from the Peltier to the heat sink, the paste was replaced with a 0.15 mm thick thermal tape, with a thermal conductivity of 1.5 W/ mK. From its datasheet, we find that this tape is rated to hold up to 500 g of weight at high temperatures, and so is sufficient for holding our low mass Peltier element and contact. Additionally, this heat transfer tape actually has a *higher* thermal conductivity than the paste found in the capstone room, which has a thermal conductivity of 0.66 W/ mK. The thermal resistance from the thermal tape is then found to be lower than that of the thermal paste. This, coupled with its mechanical strength, make it the best choice for use.

The resistance of the thermal tape:

$$R = \frac{t}{k_{film}A} = 0.15 \text{ mm} / (1.5 * 0.03 * 0.032) = 0.1 \text{ W/K}$$

Compared to from the thermal paste:

$$R = \frac{t}{k_{film}A} = 0.1 \text{ mm} / (0.66 * 0.03 * 0.032) = 0.16 \text{ W/K}$$

Components and Design

A magnetic stirrer is a necessary part of this system in order to:

- Mix chemical components in the synthesis reaction
- Improve heat transfer in the system

Without the mixing provided by the stirrer, the heat transfer to the water from the Peltier elements and the heating film is primarily through natural convection. For water, this is typically corresponding to a heat transfer coefficient in the range of 100- 1200 W/m²K. With the introduction of stirring in the beaker, we can instead model the heat transfer in the system as forced convection.

In the case of a stirred mixture, the Reynolds number is defined as:

$$Re = \frac{\rho ND^2}{\mu} [11], (11)$$

Where ρ is the density of the fluid, N is the rotational speed of the stirrer, D is the diameter of the agitator, and μ is the viscosity of the fluid. In our system, with an RPM of 1200 (125.7 rad/s) and a stir bar of diameter 2.7 cm. This yields a Reynolds number of 140 285. This is flow in the turbulent regime. For forced convection in the turbulent regime, we can use this value and the Nusselt number to determine the heat transfer coefficient to water. The Nusselt number is empirically defined as:



$$Nu = \frac{hL}{k} = 0.37Re_l^{0.8}Pr^{(\frac{1}{3})} [6] (12)$$

And the Prandtl number is:

$$Pr = \frac{\mu c_p}{k} = 4.3247 (13)$$

This yields a Nusselt number of 790.3. Assuming that the fluid travels a distance equal to the circumference of the beaker (diameter of 7.7 cm), we find the heat transfer coefficient of the water in the beaker to be:

$$h = 2069.2 \frac{W}{m^2 K} (14)$$

This is a significant increase in heat transfer coefficient over just natural convection.

With this heat transfer coefficient, we can define the total thermal resistance of the heat flowing from the Peltier to the water. The average thickness of the beaker is 3 mm, and the Peltier element is 30 mm by 30 mm in area. 32 mm is the arc length of the beaker corresponding to this Peltier element. The resistance when the beaker is contacted to the Peltier directly is defined as:

$$R = \frac{1}{h_i A} + \frac{t}{k_{beaker} A} + \frac{t}{k_{air} A} [6] (15)$$

$$R = \frac{1}{2069.2 * (0.03 * 0.032)} + \frac{0.003 m}{1.005 * (0.03 * 0.032)} + \frac{0.003 m}{0.0262 * (0.03 * 0.02)}$$

$$R = 191.343 W/K$$

The thermal resistance from air is due to the fact that on either side of the centre of the Peltier, the element is separated from the curved surface of the beaker by approximately 3 mm of space. This means that for a set ΔT between the Peltier element and the water, the heat pumped is equal to:

$$Q = \frac{\Delta T}{191.343} (16)$$

This is a significant thermal resistance. In order to mitigate this, curved aluminum contacts were designed to be placed between the Peltier and the beaker. These contacts change the heat resistance to:

$$R = \frac{1}{h_i A} + \frac{t}{k_{beaker} A} + \frac{t}{k_{aluminum} A}$$

$$R = \frac{1}{2069.2 * (0.03 * 0.032)} + \frac{0.003}{1.005 * (0.03 * 0.032)} + \frac{0.006}{205 * 0.03 * 0.032}$$

$$R = 3.52 W/K$$

So, for a given ΔT between the Peltier element and the water,

$$Q = \frac{\Delta T}{3.52}$$

Which is a significant increase in the heat pumped for a given temperature, from the design with no aluminum contacts.



These aluminum contacts were milled in the JHE machine shop from the following design:

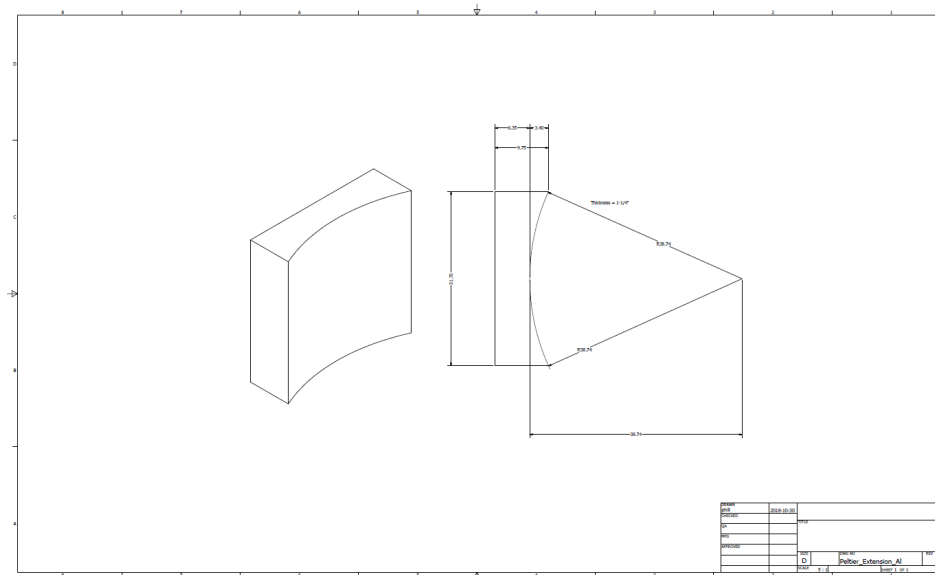


Figure 21: Aluminum Contact to Beaker

The Peltier, heat sink, fan and aluminum contact units are held in place around the beaker in order to achieve good contact. They are held in 3D printed heat sink holders, seen below:

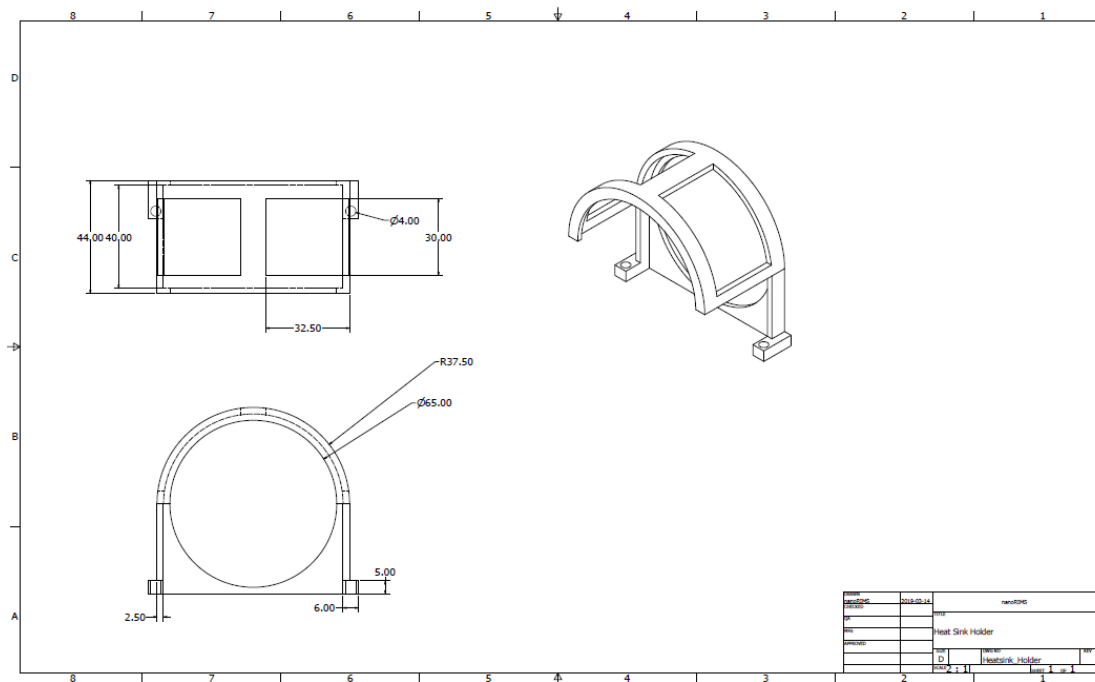


Figure 22: Heat Sink Holder



These holders are made with a number of spaces and holes in order to minimize material and not inhibit the performance of the heat sink.

Thermocouple Interpretation

In order to receive feedback to control the system and ensure that the nanoparticle synthesis procedure is being correctly followed, we need to be able to accurately read the temperature of the water bath. This is done by the integration of a digitized thermocouple into our system. The chosen thermocouple was selected because of its high temperature limit, measuring accurately from -55 to 125 °C, which contains our required range of 25-100 °C measurements. The thermocouple is waterproof and has a rated accuracy of ± 0.5 °C, which is necessary to meet our specified accuracy of measurement.

The thermocouple is digitized and returns a data array containing sensor information. The temperature measurement is contained in the first two elements of this array, containing the most significant bit in one element, and the rest of the temperature measurement in the next. The sensor has a nine-bit resolution, so the most significant bit must be bitwise shifted left 8 bits. It is then combined with the rest of the temperature measurement using a bitwise OR operation, to generate a reading in the form of a 16-bit integer. Since we have a nine-bit resolution sensor but a 16-bit integer, we then zero the last 7 bits of the 16-bit integer. Finally, this measurement can be converted to temperature in Celsius through the following conversion:

$$\text{Temp in celsius} = \frac{\text{adjusted measurement}}{16} \quad (17)$$

Heating / Cooling Control System

The timing of the heating and cooling system is controlled by the master Raspberry Pi, which communicates which set temperature needs to be set to the Arduino by sending an “h” for heating or a “c” for cooling. The Arduino is responsible for the PID temperature control system (described below), and also controls the opening of the lid by undoing the solenoid latch. The Arduino also returns a temperature reading to the Pi for a dual purpose; first, it informs the timing of the procedure. Second, it allows the touchscreen interface to store and then display temperature information about the conditions during the procedure. This system is summarized in the flowchart below.

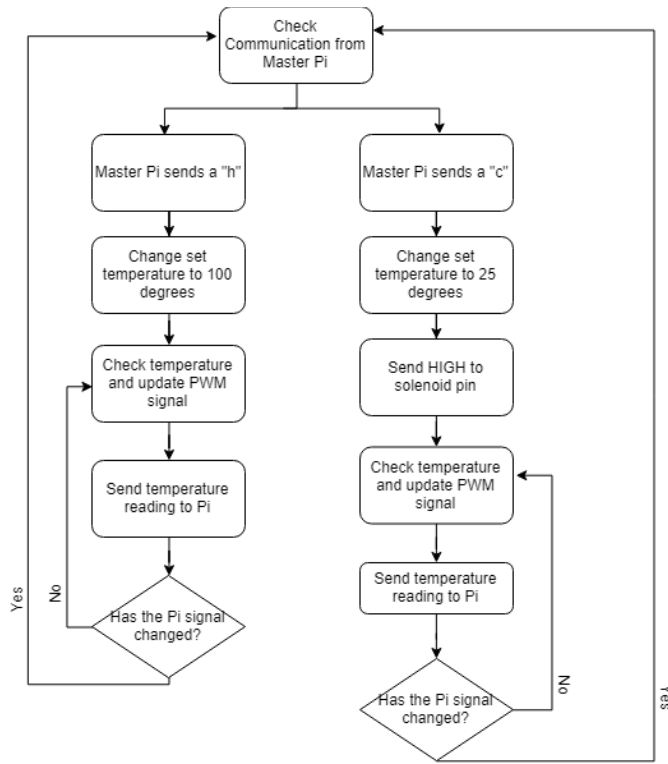


Figure 23: Heating and Cooling Communication with the Master Pi

The heating and cooling of the entire system is controlled using a PID system, which uses proportional, integral, and derivative error terms to maintain the temperature around a given set point. This PID system controls the pulse width and direction of the signal sent to the Peltier's and the heating film using an Arduino and h-bridge motor controllers. The output of the PID system is defined as:

$$u(t) = P + I + D = k_p e(t) + k_i \int_0^t e(t) dt + \frac{k_d}{dt} e(t) \quad (18)$$

Where k_p , k_i , k_d are the gain coefficients for proportional, integral and derivative control; respectively. The error term is calculated as the difference between the set temperature and the reading from the thermocouple. A simple block diagram of the system is seen below.

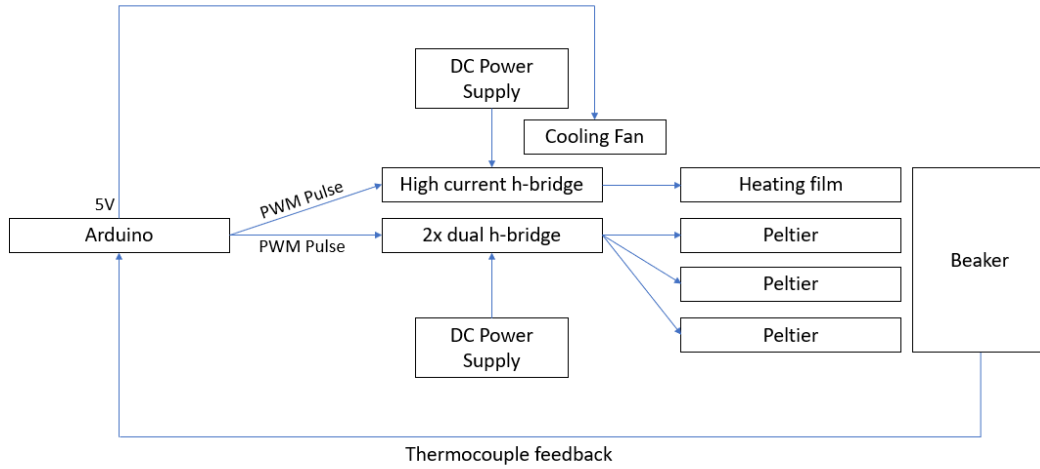


Figure 24: Block Diagram of System Setup

H-bridge motor drivers were used for controlling the peltier elements because they can easily switch the polarity of the PWM signal being supplied. Peltier elements heat when run forward, and cool when run backwards. Our PID system takes advantage of this fact to accurately control the water temperature by turning the first input high and the second input low when heating is needed; and turning the second input high and first input low when cooling is needed. This method also means that the heating film can be controlled with the same PID controller, by only connecting controls to the first input pin of the h-bridge. With this system, the film is ON when heating is needed and automatically OFF when cooling is required (input 1 is low).

Two cooling fans are necessary to cool the h-bridges, which generate a significant amount of heat when outputting close to 2 A for each Peltier. Each h-bridge used to control the Peltiers is also equipped with a heat sink. The h-bridge controlling the heating film is designed to tolerate up to 15 A of current, and each mosfet has a resistance of $3.5 \text{ m}\Omega$. Running the four mosfets required to power the heating film would generate a total of 0.25 W of heat, which can be sufficiently cooled using a heating fan, so a heat sink was not installed.

The gain constants, k_p , k_i , k_d , were tuned using the Ziegler-Nichols method [12], which uses the following approach:

Control Type	K_p	K_i	K_d
P	$0.5K_u$	-	-
PI	$0.45K_u$	$1.2K_p/T_u$	-
PID	$0.6K_u$	$2.0K_p/T_u$	$K_p T_u/8$

This method involves altering K_p until consistent oscillation around the set point is achieved. From this K_p value and subsequent oscillations, with a period T_u and a constant K_u are obtained. These values are used to tune the system into a PI controller then to a PID controller. Since we are heating water, we have a slowly responding system. At a k_p of 100, oscillations around the



set temperature occur with a period of approximately 60 seconds. Resulting in the following tuning:

Control Type	K_p	K_i	K_d
P	100	-	-
PI	90	1.8	-
PID	120	4	900

Optical Characterization

The optical characterization of the synthesized gold nanoparticles will utilize the specific absorption spectra of nanoparticles to identify their size. Each size of nanoparticle has a characteristic wavelength of peak absorption, with a linear relationship, seen in the Figure 21.

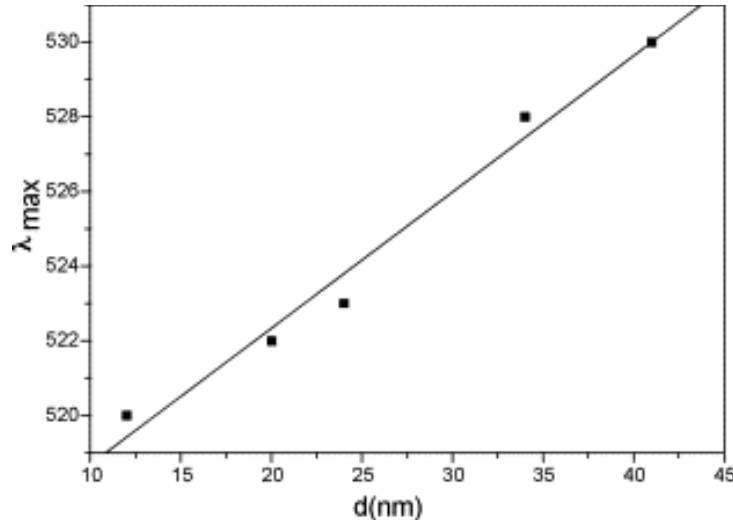


Figure 25: Relationship between the wavelength of max absorption and the diameter of gold nanoparticle [4].

The optical system of nanoRIMS has been designed to measure the 400-600 nm wavelength range in order to obtain the highest spatial resolution using the implemented linear CCD. With a broadband optical source placed at the focal point of a collimating lens, light passes through the beaker to a transmissive diffraction grating. The broadband light is consequently broken into its individual components which can then be measured. The optical system shown as such:

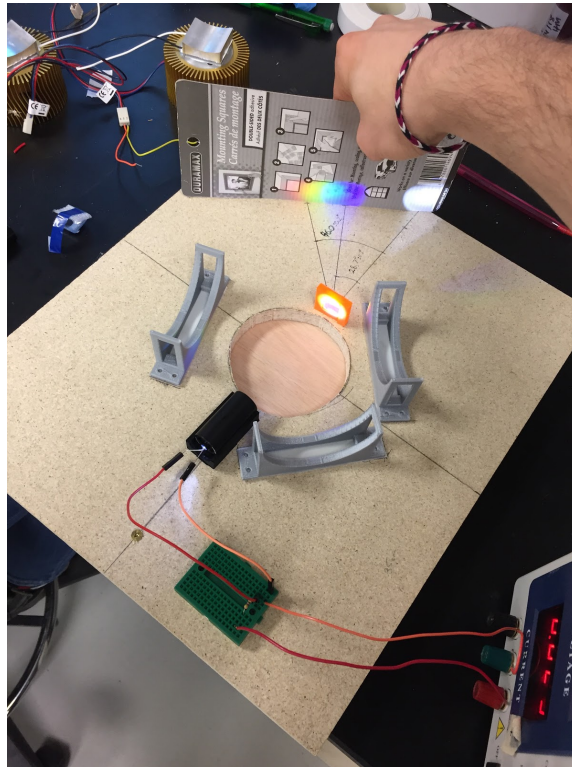


Figure 26: Mounted optical system

As can be seen, the diffraction of a single wavelength depends on the value of the wavelength itself. This relationship is defined as such,

$$a(\sin(\theta_m) - \sin(\theta_i)) = m\lambda \quad (19)$$

Where a , θ_m , θ_i , and m are the number of mm/line, the angle of diffraction for the m^{th} mode, the angle of incidence, and m is the mode number, respectively. For the purposes of the design, the first order mode of diffraction will be captured. To maximize the wavelength resolution on the linear CCD in the desired range, θ_m in the previously defined equation can be solved for at the extremes of the wavelength range. Doing this, 400 nm and 600 nm light will be diffracted 28.68° and 46.05° , respectively.

It must also be taken into account that light drops off in intensity following the inverse square law. Therefore, all portions of the sensor should be placed as close to equidistant from the diffraction grating as possible. Since this cannot be perfectly achieved due to the sensor geometry, the outer extremes of the sensor will be placed at these equal distances. An illustration of the design is shown in figure Y below.

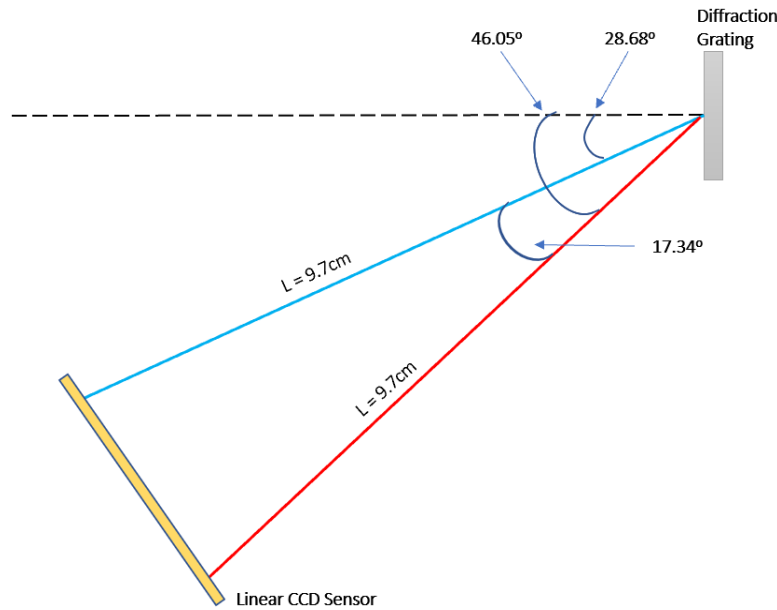


Figure 27: Geometry of the Optical Design

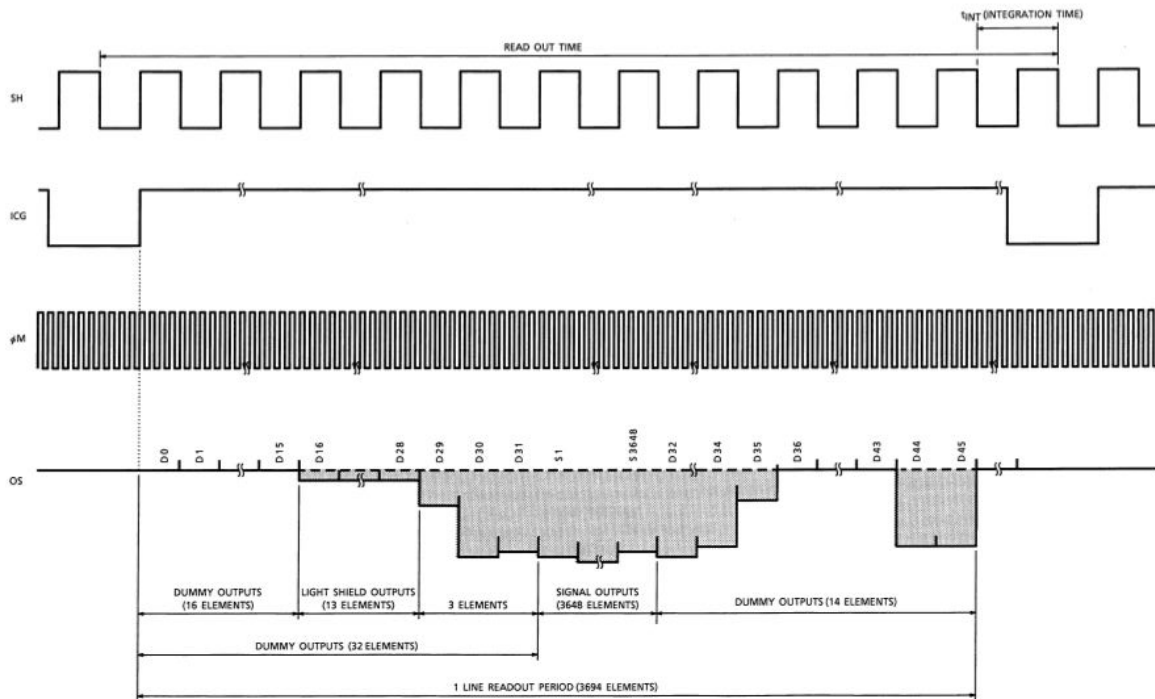
Since the geometry of the system is constrained based on the equidistant requirement, the law of cosines is used to determine the optimal distance in which the wavelength range will cover the entire sensor array. Knowing that the size of the active region of the sensor array is 2.92 cm, the equidistant length to the diffraction grating is calculated through the following.

$$L_E = \sqrt{\frac{L}{1 - \cos(\theta)}} \quad (20)$$

Where L is the length of the sensor array, and θ is the internal angle between the minimum and maximum diffracted rays. When calculating, the length becomes 9.7 cm, as depicted in figure 20. This geometry is used to create the “optical enclosure” component of the system described in Assembly Instructions, above.

The sensor that will be responsible for reading the intensity measurements of the light after the diffraction grating is the TCD1304DG. This is a 3694 x 1 linear charge coupled device (CCD). The datasheet provides optimal power ratings and timing diagrams that explain how the CCD must be driven in order to provide accurate measurements. We are using the CCD in electronic shutter mode, which allows us to control the exposure and optimize the image quality for our spectrophotometry. The CCD follows the timing diagram below:

TIMING CHART (Use electronic shutter function)

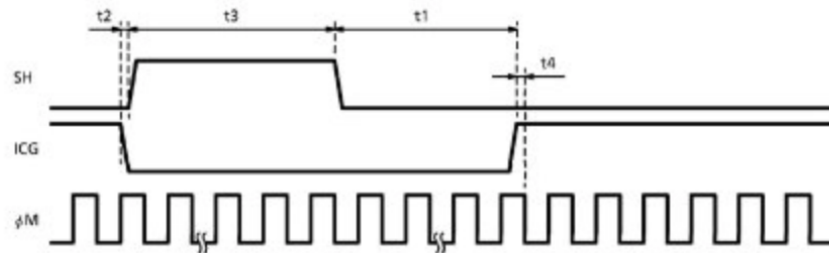


TCD1304DG-7

Figure 28: Timing Diagrams

There is also a separate timing requirement diagram and chart. This specifies the minimum delays required for the different clock signals, as the CCD would not work if all of the signals arrived at the exact same time:

TIMING REQUIREMENTS



CHARACTERISTIC	SYMBOL	MIN.	TYP.	MAX.	UNIT
ICG Pulse DELAY	t1	1000	5000	—	ns
Pulse Timing of ICG and SH	t2	100	500	1000	ns
SH Pulse Width	t3	1000	—	—	ns
Pulse Timing of ICG and ϕ M	t4	0	20	*	ns

* : You keep ϕ M "High" Level.

(Note) : If you use electronic shutter function. t_{INT} (MIN.) = $10\mu s$

Figure 29: Timing Diagrams

These timing diagrams outline the three driving clock signals required for the CCD to work. They are:

- fM: this is the master clock signal, which can run from 0.8 to 4 MHz
- SH: the shift gate that controls the pixels
- ICG: the integration clear gate that signals the start and end of a full measurement of all 3694 pixels

This results in an output signal OS, which is an analog voltage consisting of the 3648 pixel measurements back to back. The timing diagrams illustrate some of the important features of the CCD:

- There are 4 clock pulses per shift gate pulse, so the data rate is capped at 1/4th of the fM clock speed
- The minimum integration time per pixel is 10 microseconds
- Pixels only get bumped to the shift registers when ICG is high. When the SH period is lower than the ICG period, the SH period dictates the integration time per pixel

As for the delays, we can come to the following conclusions:

- Once ICG goes high to signal the measurement has begun, SH must go high with a delay of between 100 and 1000 nanoseconds (t2)



- Once high, SH must remain high for a minimum of 1000 nanoseconds, and there is no maximum time (t3)
- After SH goes low, ICG must go high with a delay of at least 1000 nanoseconds (t1)
- Finally, ICG should go high when fM is high with a typical delay of 20 nanoseconds (t4)

It does not take long to notice that the speeds required far exceed the maximum clock speed of a typical Arduino. Additionally, while a Raspberry Pi is in fact capable of achieving the necessary clock speeds, the Raspberry Pi does not have an onboard analog-to-digital converter (ADC), which would require a separate integrated circuit with its own timing requirements. This would be nigh impossible to implement in a language like Python using loops, and as a result, a Raspberry Pi would not be an ideal choice. Instead, the device used to drive the CCD is an STM32F411VET6 ARM microcontroller. The specifications for the microcontroller are provided in Appendix A, with the only information relevant for the mathematical modelling is that the base clock of the microcontroller is 100 MHz, with phase-locked loops allowing for frequency multiplication and division in integer multiples of the base clock. The STM32F4 also boasts an onboard 12-bit ADC with 15 channels, an SPI controller, 10 Timers clocked by the master clock, and direct memory access (DMA) to shift values from peripherals to memory and vice versa. As we will see, the STM32F4 easily meets the timing requirements of the CCD. Since the CCD will be connected to the Raspberry Pi through SPI (Serial Peripheral Interface), and SPI is capable of delivering data to the Raspberry Pi at a rate of 16 Megabits per second (Mbps), the CCD will be driven at its maximum speed of 4 MHz. This sets the data rate to 1 MHz:

$$4 \text{ Master clock cycles per pixel measurement} \rightarrow \text{Data rate} = 0.25 * fM = 1 \text{ MHz} \quad (21)$$

This means the maximum conversion time for the onboard ADC is 1 microsecond:

$$\text{Data rate} = 1 \text{ MHz}, 1 \text{ pixel sample time} = (1 \text{ MHz})^{-1} = 1 \mu\text{s} \quad (22)$$

What this means is that the onboard ADC must be able to sample faster than 1 microsecond, otherwise pixel data will be missed. Fortunately, the onboard ADC is driven at 30 MHz and is capable of 2.4 million samples per second (Msps). This is derived from the fact that each bit of the 12 bit ADC takes one clock cycle to be sampled:

$$30 \text{ MHz ADC clock} = (30 \text{ MHz})^{-1} \rightarrow 33.33 \text{ ns per pulse} \rightarrow 1 \text{ bit per pulse, 12 bits total} = 12 * (33.33 \text{ ns}) = 400 \text{ ns or } 0.40 \mu\text{s per ACD sample}$$

With the ADC being occupied for 0.4 microseconds per sample, this leaves 0.6 microseconds to take the measurement. This provides a sampling time of:

$$0.60 \mu\text{s} / 300 \text{ ns} = 18 \text{ ADC clock cycles}$$



Any sample taking 18 clock cycles or less will be able to measure the signal accurately. The ADC can only sample for a certain predetermined number of clock cycles, and in our case, the closest value to our desired number of cycles is 15 (the next being 28, too slow for our requirements). Thus, we can see the ADC will have no trouble sampling the output signal at the maximum speed the CCD can provide.

After confirming that the onboard ADC is capable of sampling fast enough for our application, we must determine the period required for each of the timers controlling the CCD. Each of the timers on the STM32F4 is tied to a group of multi-functional GPIO pins that can be configured to run at speeds up to 100 MHz. In our case, we will be using the general purpose timers TIM3 for the master clock, TIM4 for the ADC, TIM2 for the SH clock, and TIM5 for the ICG pulse. TIM3 and TIM4 are 16-bit, which is perfect as they are driving signals that only call for very short periods. TIM2 and TIM5 are 32-bit on the other hand, as they are driving the signals responsible for the integration times, and having a large range of integration times is necessary in order to ensure the CCD can be set to the required integration time once the device is fully integrated. As a result Keeping the pulses on separate timers gives us more control over the speeds for each individual GPIO pin. Starting with the master clock, we would like to drive the master clock at 4 MHz. TIM 3 is served by the APB1 peripheral clock, which by default is set to 100 MHz. This does not require any prescaling, as the timer period will be quite short, so the prescaler is left as 1. As an aside, if you are using a 16-bit timer, the maximum timer period would be $2^{16} - 1 = 65535$. If your required period exceeds this value, the base clock must be prescaled down to allow for the required period. The required period can be derived as such:

$$\text{Required Period} = (\text{AP B1 Frequency} / \text{Desired Master Clock Frequency}) - 1$$

$$\text{Required Period} = (100 \text{ MHz} / 4 \text{ MHz}) - 1 = 24$$

As this will be a clock cycle, we also want a duty cycle of 50%. This will require setting the pulse period to 50% of the timer period:

$$\text{Required Pulse for 50\% duty cycle} = \text{AP B1 Frequency} / (2 * \text{Desired Master Clock Frequency})$$

$$\text{Required Pulse for 50\% duty cycle} = 100 \text{ MHz} / (2 * 4 \text{ MHz}) = 12.5, \text{ truncated to } 12$$

This will provide the 50% duty cycle 4 MHz master clock. For the ADC on TIM4, we want a timer clock that samples at 1/4th of the master clock frequency (as each pixel takes 1/4th the master clock to be read out). This requires a period of:

$$\text{Required ADC Period} = (4 * \text{AP B1 Frequency} / \text{Master Clock Frequency}) - 1 = 99$$



For the ADC, we would like to produce a wave with a 25% duty cycle, so the pulse period will be:

$$\text{Required ADC Pulse} = (\text{APB1 Frequency} / 2 * \text{Master Clock Frequency}) - 1 = 24$$

As for TIM2 and TIM5, we would like to have the clocks equal to one another to more easily meet the timing requirements established above. As a result, the prescaler for TIM2 and TIM5 are set to the period of TIM3 (24, on the master clock), which will ensure that TIM2 and TIM5 have equal clocks. As the ICG period on TIM5 and the SH period on TIM2 can have a wide range of values, it would be more productive to determine the minimum values in order for the CCD to operate properly, and then any period values higher than that will be acceptable. The maximum resolution in time is determined by the master clock frequency. As we are running at the maximum frequency of 4 MHz, and it takes 4 cycles to read one pixel, the minimum SH pulse must be:

$$\text{Minimum SH Pulse} = 4 \text{ cycles} / 4 \text{ MHz} = 1 \mu\text{s}$$

The ICG pulse must be at least 1000 ns longer than the SH pulse, meaning that the minimum ICG pulse would appear to be 2 microseconds. According to the datasheet, the lowest integration time attainable is 10 microseconds, so the lowest possible period for TIM2 controlling the SH pulses and thus the integration time is:

$$\text{Minimum SH Period} = 10 \mu\text{s} * 4 \text{ MHz} = 40$$

Additionally, the total readout time is given by the data rate at 1/4th the master clock (1 MHz) and the total number of pixels to read, including the extra dummy pixels at both edges of the CCD (these supposedly provide a light shielding effect and make the data easier to read).

$$\text{Total Readout Time} = 3964 \text{ pixels} / 1 \text{ MHz} = 3.7 \text{ ms}$$

And since our clock is 4 MHz, we can use this total readout time to determine the minimum period of TIM5 controlling the ICG pulse:

$$\text{Minimum ICG Period} = 3.7 \text{ ms} * 4 \text{ MHz} = 14776$$

However, there is an extra requirement that the ICG pulses must coincide with the SH pulses, so we must use periods for TIM5 that are multiples of the TIM2 period to ensure that this occurs.

We can also calculate the required buffer size on the raspberry pi to receive all of this data. The SPI controller on the raspberry pi insists on being the Master in a Master-Slave configuration, and it also insists on the data being in an 8 bit format. This could present a problem, as the 12



bit ADC requires we store the pixel values as 16 bit words. This can be solved by sending each 16-bit word 8 bits at a time. However, the STM32F4 processor follows a little-endian format, so a 16-bit number will get mixed up like so:

Imagine a 16 bit number stored as hexadecimal like so: 0x1122

This is transmitted as two 8-bit numbers: 0x22 and 0x11

This will get recombined in the raspberry pi's memory as: 0x2211

This is easy enough to fix, as we can treat the two 8 bit numbers as 16-bit numbers, multiply the most significant number by 256, and add the two numbers together. This is demonstrated in an example using the numbers above:

0x11 becomes 0x0011 and 0x22 becomes 0x0022 in memory

$$0x0011 * 0x0100 + 0x0022 = 0x1100 + 0x0022 = 0x1122$$

Thus reconstructing our original 16-bit digit on the raspberry pi side. With our 16 MHz SPI transfer speed, the minimum transfer time for a full read of the CCD should be ~ 3.7 milliseconds:

$$\text{SPI Readout Time} = (16 \text{ bits} * 3694 \text{ pixels}) / 16 \text{ MHz} = 3.694 \text{ ms}$$

This will allow us to achieve a theoretical maximum of 270 integrations of the CCD per second. And, as we need to transmit two 8 bit words per pixel, we should have a receiving buffer of 7388 8 bit words on the raspberry pi.

As for the general flow of the program, the clocks will activate the CCD, which will start outputting analog data on the OS line. This will get read in by the ADC, and then the full ADC register will get dumped into memory using the direct memory access streams on board. Then, the direct memory access will transfer the register values to the SPI transmission buffer, where they will be sent to the raspberry pi on request. There will also be 3 interrupts that control the CCD system, and while there is no math involved in how they are implemented, a brief description of their function will be provided.

The three interrupts are:

- DMA2_Stream0_IRQHandler: This interrupt will trigger when the ADC has finished reading the CCD, transferring the contents of the ADC register into memory and then transferring the memory contents to the SPI transmission register
- DMA1_Stream4_IRQHandler: This interrupt will trigger when data is received from the SPI controller and will dump the contents of the 12 byte message sent from the raspberry pi into memory, which contains the new ICG and SH periods, as well as the number of integrations to take



- TIM5_IRQHandler: This interrupt triggers on the rising edge of the ICG pulse, which signals when the CCD is starting to output and turns on TIM4, starting the ADC as well as DMA2. This ensures that the CCD output is synced with the ADC so that data collection does not occur part way through the CCD output, which would result in missing data.

This concludes the math modelling for the CCD sensor, as the current driving circuit does not require any additional components outside of the +5 V source from the STM32F4, and the analog output from the CCD is clean enough that filtering is unnecessary at this time. Integration and optimization will involve conditioning the 0.6 to 2.7 V output from the CCD to cover the entire full scale range of the ADC, which is 0 to 3.3 V. This can be accomplished with a differential rail to rail op-amp circuit, which will be discussed in a future report.

With the optical infrastructure in place, the final spectrum to determine the nanoparticle diameter distribution can be determined. The flow chart shown below illustrates the steps needed in order to obtain the spectrum.

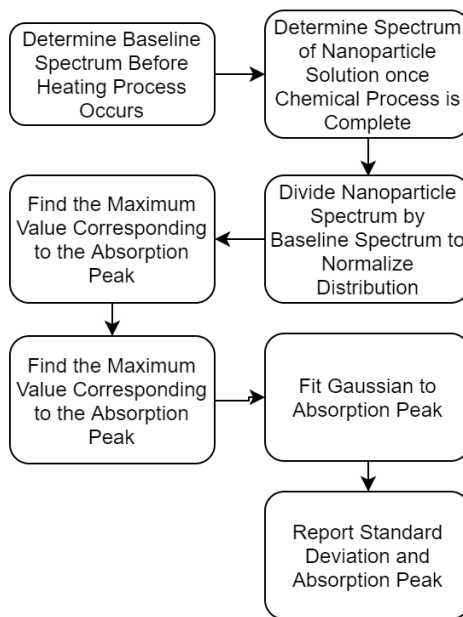


Figure 30: Flow Diagram to Obtain Final Optical Spectrum for Nanoparticle Solution

Fan Control and Load Cell

The fan consists of 4 pins: a +12 V supply, a ground wire, a tachometer output, and a PWM input that controls the fan. The tachometer consists of a Hall sensor internal to the fan that registers a magnetic pulse each time the fan completes a half rotation, as there are two magnetics space 180 degrees apart inside of the fan. As a result, we can determine the RPM of the fan like so:



$$Fan RPM = (Tachometer Output Frequency / 2) * 60 \quad (23)$$

The output frequency is measured on one of the analog pins on the Arduino, which measures the time between a transition from High to Low to High on the pin, signifying one complete period. As this would be an unreliable measurement if only measured once, due to the possibility for the measurement to start at different points in time for the High pulse, multiple measurements are collected and averaged together to provide a more reliable measurement. The fan circuit is quite simple, consisting of a unity gain op-amp follower after the tachometer output, which simply serves to optimize the impedance of the fan to the Arduino. This was added after prior testing determined the resistance of the fan on its own was too high for the Arduino, as incoming measurements were attenuated significantly. As the maximum RPM of the fan is 6800 (which provides a maximum tachometer output frequency of 226.66 Hz), the op amp has no risk of saturating and causing slewing.

The most important aspect of the fan from a mathematical perspective is the PID control and tuning. As we are using the fan as a base for the magnetic stirrer, we must control the fan to within +/- 15 RPM, and the best control system for this task is a PID controller. For this task, the Ziegler-Nichols method was chosen, as it provides optimal disturbance rejection, while the overshoot provided is acceptable as it will happen at the beginning of the reaction when the stirrer RPM plays less important a role in the reaction. While the Ziegler-Nichols method was described above in the Heating and Cooling section, it is restated here for convenience:

Control Type	K_p	K_i	K_d
P	$0.5K_u$	-	-
PI	$0.45K_u$	$1.2K_p/T_u$	-
PID	$0.6K_u$	$2.0K_p/T_u$	$K_p T_u/8$

The Ziegler-Nichols method involves using only proportional control and increasing the proportional gain until the system begins to oscillate around the set point. At this point, the ultimate gain K_u has been determined, and the ultimate period of oscillation measured is T_u . This is used to determine the I and D gain values to be used. For the fan system, K_u was determined to be 1.75, and the period of oscillation was 28 seconds. This was used to derive the gain values:

Control Type	K_p	K_i	K_d
PID	1.05	0.075	3.675



These gain values resulted in a successful PID control system, with testing outlined in the Performance section.

One of the issues proposed by this method of stirring the solution is whether the measured RPM of the fan is indicative of the RPM of the stir rod. This challenge required some research to determine if commercial high-quality magnetic stirrers have some sort of feedback mechanism with which they measure the RPM of the stir rod (also called a 'flea'). As it turns out, they do not, as the RPM of the stirrer is the same as the RPM of the fan, so long as the stir rod is still coupled to the magnetic moment of the magnets on the fan. An explanation of the physics behind this follows:

As the magnetic stir bar moves, it experiences two moments acting on it. One of these moments is from the magnets attached to the computer fan, and the other is from the friction of the mixture being stirred. If we first assume the fan is stationary, the flea will move until the magnetic moment has been minimized and the magnetic moments are aligned. Once the motor starts moving, the flea will attempt to follow the magnets attached to the motor in order to keep the moment minimized. This causes a drag or friction force to form, which increases in proportion to the speed of the flea. For the flea to follow the motor, the flea will have to reach an equilibrium where the magnetic moment is equal and opposite to the drag moment. Effectively, the flea will find an equilibrium position slightly offset from the equilibrium position at 0 RPM. There will be a permanent offset from the 0 RPM equilibrium position, but otherwise the flea will move at the same speed as the magnets on the fan.

Where issues come up is when the RPM exceeds a certain threshold, usually 2500+ RPM from testing and literature on the topic (well below our 1200 RPM speed). At these high speeds, it is simply not possible for the magnetic moment to balance out the drag moment, as the drag moment becomes too large due to the increased speed. This will cause the flea to move far enough from the equilibrium position that the flea will "decouple" from the magnets on the fan, and at that point, the outcome is the stir bar getting flung away from the magnets. It will not be possible to re-couple the stir bar with the fan magnets until the RPM is reduced to a sufficiently slow speed. The viscosity of the fluid will affect the RPM at which the flea will decouple from the magnetic moment of the fan magnets, as higher viscosity means more drag, but as we are dealing with liquids that have similar viscosity to water, this has proved a non-issue, so long as the RPM is kept below 2000.

As for the load cell used in measuring the weight of the beaker, the operating principle behind the load cell is straightforward. The load cell is an aluminum bar with 4 strain gauges. Each strain gauge consists of a wheatstone bridge, where three of the resistors

have a known value and one of the resistors (in this case, the one subjected to the strain) is unknown.

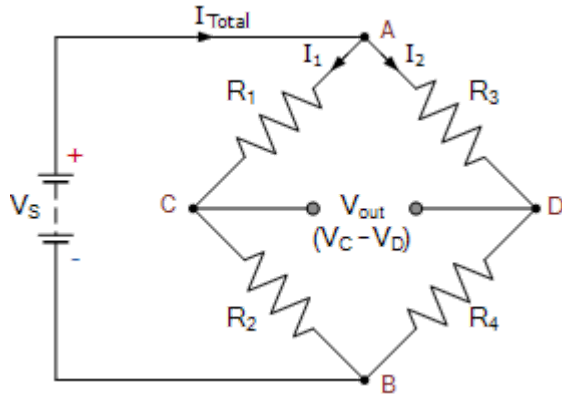


Figure 31: A typical wheatstone bridge formation

The concept is that as a resistor is subjected to a strain, its resistance changes in a predictable manner. If we can measure the unknown resistance, we can relate the resistance back to the strain the resistor was subjected to, and thus measure the weight of the object causing the strain. The relationship between the strain of the strain gauge and the change in resistance is:

$$\Delta R/R = K * \epsilon \quad (24)$$

Where R is the initial resistance, delta R is the change caused by contraction or stretching of the resistor, K is the proportional constant known as the gauge factor, and epsilon is the strain. So long as the strain applied is within the proportional limit, which is 0-3 kg for our load cell, the response of the gauge will be linear. This makes it a simple question of figuring out the proportional constant of the load cell and determining how the voltage output of the load cell converts to a strain. Unfortunately, the actual resistor values are not listed on the data sheet, and the recommended method of using the load cell is to place an object of a known weight onto the load cell, and then calculate the proportional constant required to give that weight. As the proportional constant is a constant, this should not change across the entire 0-3 kg range. This method was used to find the calibration factor of the load cell, and it is shown in the Performance section that the load cell is accurate to within 1 gram (the 100% spec), so while the mathematical modelling is lacking, the method does work.

Beaker Lid Design

After Module Demo and moving towards Integration Demo, there was a clear need for an extra module that could fulfill the following requirements:

- Ensure pump outlets are set directly above the beaker.
- Provide a rigid structure for image processing equipment and WPM pump.
- Minimize pump tubing and image processing equipment from steam exposure.
- Prevent spilling of fluids from beaker caused by splashing during pumping.



- Allow for the thermocouple to sit in the beaker.
- Trap steam during heating phase to reduce heating losses.
- Unseal beaker at the start of cooling phase to increase evaporative cooling.

To meet these requirements, it was decided the overall beaker lid system would be broken down into 3 modules: (1) the beaker lid, (2) the latch, and (3) the seal.

The beaker lid would provide the housing for the pump and image processing equipment, and the sealing device. The latch would seal the lid to the beaker and be electronically controlled to release at the start of cooling process. Lastly, the seal would provide protection to the tubing and image processing equipment prior to the release of the latch and during the heating process. To reduce actuation, it was decided the user would be the one to latch the lid after placing the beaker in the reactor (this would be done by physically lowering the lid).

Beaker Lid

The beaker lid's design was further broken down into three parts that were joined together vertically to perform the above requirements.

The first part designed was the 'Lip' that sits directly on top of the beaker when the lid is engaged. Due to the asymmetric shape of the beaker caused by the spout, measurements of the top of the beaker were conducted and found the following values:

Dimension	Value (mm)
Beaker Top Outer Diameter	84.6
Beaker Wall Thickness	2.6
Spout Tip from Inner Wall	13.0
Spout Tip from Beaker Top	9.0
Spout Tip from Centre	

The distance of the spout tip from the centre was determined using the following equation:

$$R = \text{Outer Radius} - \text{Wall Thickness} + \text{Spout Tip from In. Wall} = 52.7 \text{ mm (25)}$$

Using these values, the lip was designed to enclose the beaker's top with the final designed lip shown below:

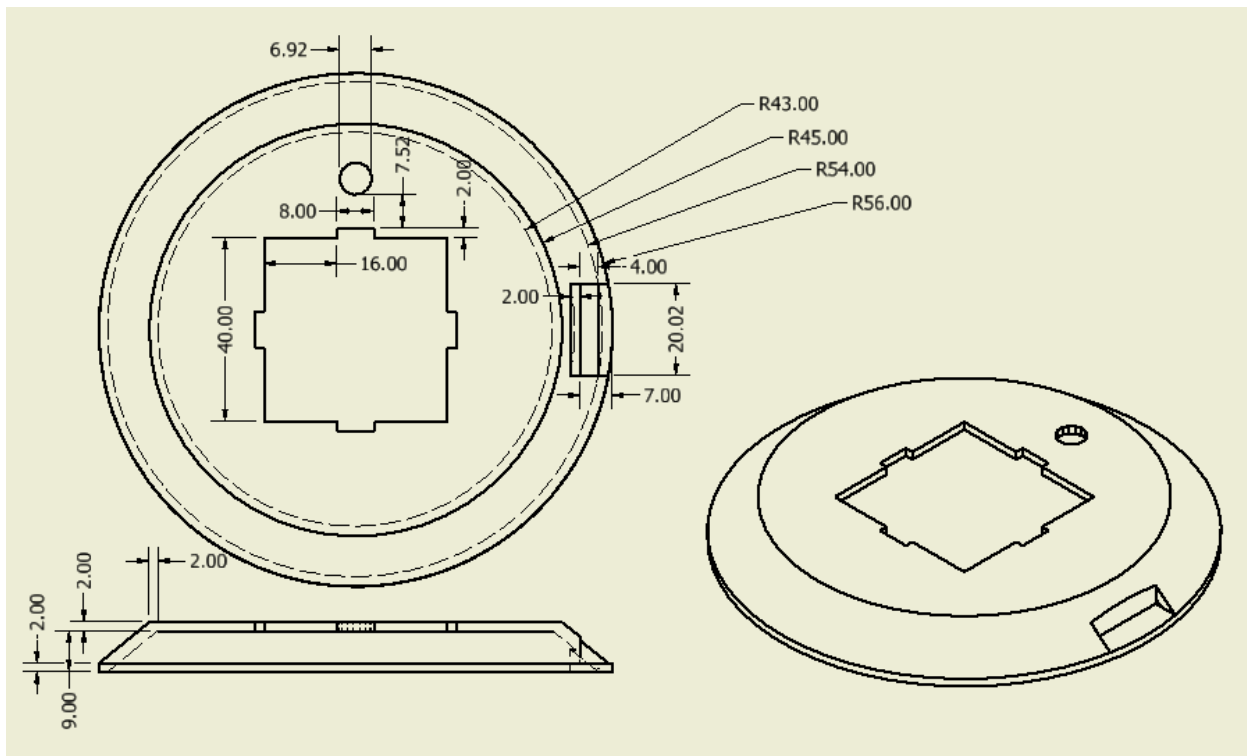


Figure 32: Engineering Drawing of the Beaker Lid Lip.

In the part, there are two concentric circles of diameters approximately equal to the outer beaker wall (86 mm) and spout tip (108.0 mm). The inner circle is a bit larger than the measurement to give some tolerance due to beaker dimension variation. Between the two is a vertical displacement of 9.0 mm to match the shape of the beaker. The lip was printed with a 2 mm thickness to give some structural rigidity (~3 layers of 3D printing).

A thermocouple hole was sized to the current thermocouple's largest diameter (6.92 mm) and placed off centre but on the flat part of the lip to ensure it would go straight into the beaker.

A 40 mm x 40 mm square hole was cut into the centre of the beaker lip to allow for the liquids to be pumped in from above. The 4 cm dimension was chosen to encompass the original focal length of the image processing equipment (~ 2 - 3 cm). Camera would be flush with the wall, and the pipette tip would sit somewhere in the middle of the lid. Four 2 mm x 8 mm rectangles were cut out of this square to guide the part above (Beaker Lid Bottom) and give it 4 possible orientations.

The latch hole cut into the side of the lip's dimension is determined by the latch system discussed in its respective section.

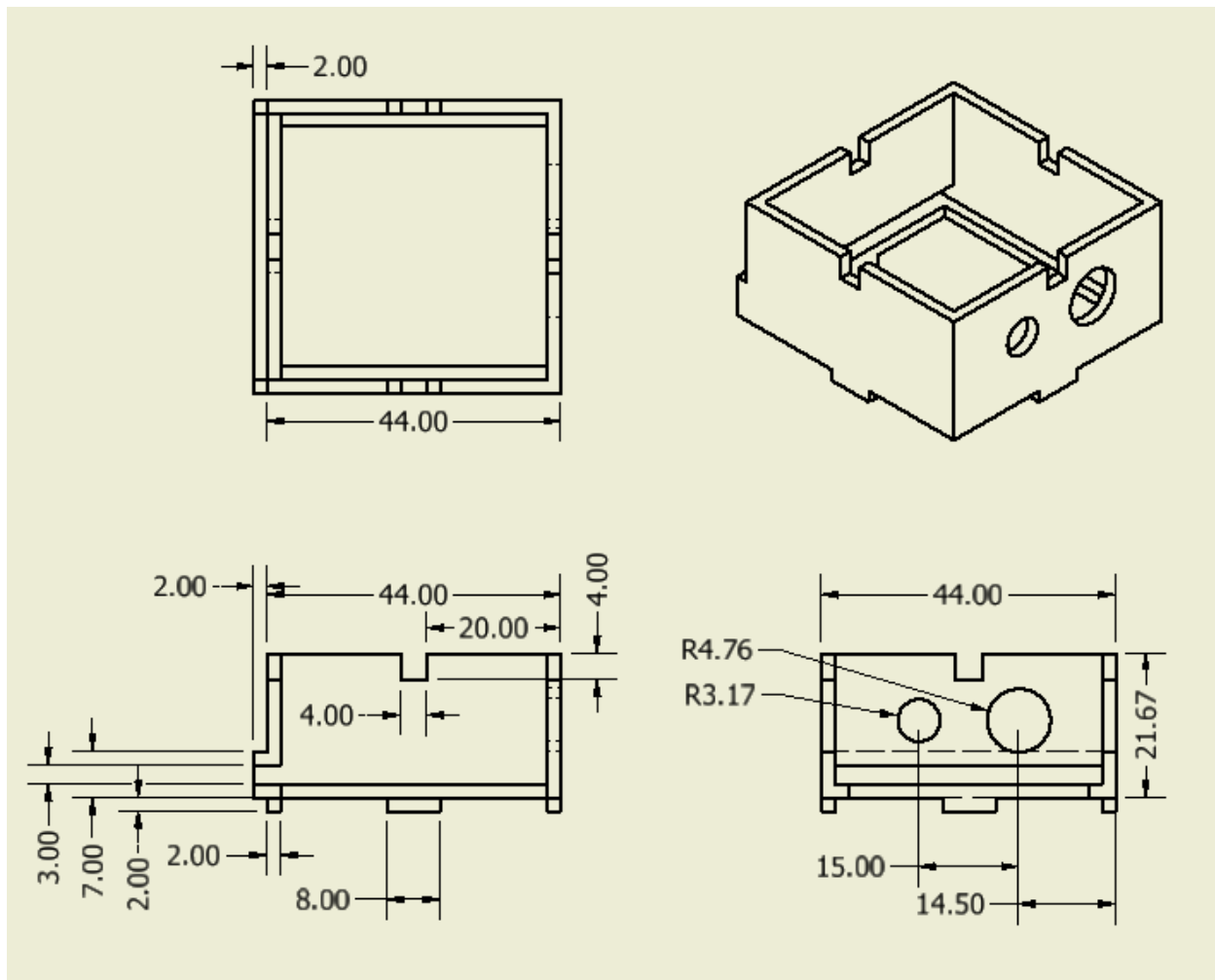


Figure 33: Engineering Drawing for the Beaker Lid Bottom.

In the above figure, the Beaker Lid Bottom is depicted. The base shape for this part is given by the 40 mm x 40 mm square shell with a 2 mm wall thickness as discussed in the Beaker Lid Lip section. The guides into the Lip were added to the bottom of the piece and extended 2 mm down to match the thickness of the Lip.

On one side, two holes are cut out to fit the tubing for the WP11 and WP10 pumps ($\frac{3}{8}$ " and $\frac{1}{4}$ " outer diameter, respectively).

To prevent the seal from blocking the pump outlets should its retraction be obstructed, the hole for the sealing plate was placed on the opposite side of the tube holes and just below the lowest point of either tube. It was given a width of 40 mm to match the cavity and a thickness of 3 mm in case the sealing plate required a layer of insulation. This layer would protect it from the steam/heat or increase sealing capability, a cut silicone baking mat was the most likely candidate. The seal hole extended 2 mm from the outer wall to help guide the seal and prevent catching when the plate is fully retracted.

Not shown in the drawing is the LED hole drilled after 3D printing to provide optimal illumination (intensity and angle). This hole was drilled at the centre of the side directly below the camera (in the Beaker Lid Top) with a 35 deg angle from the vertical. This allowed for the light to illuminate the wall directly behind the droplet, doing so increased edge detection in the image processing.

The height of the piece was designed to be just enough for the sealing plate, two holes, and ~2 mm of space. Like the Lip, holes sized at 2 mm x 2 mm were cut from all 4 sides to provide guides and 4 possible orientations for the part above (Beaker Lid Top).

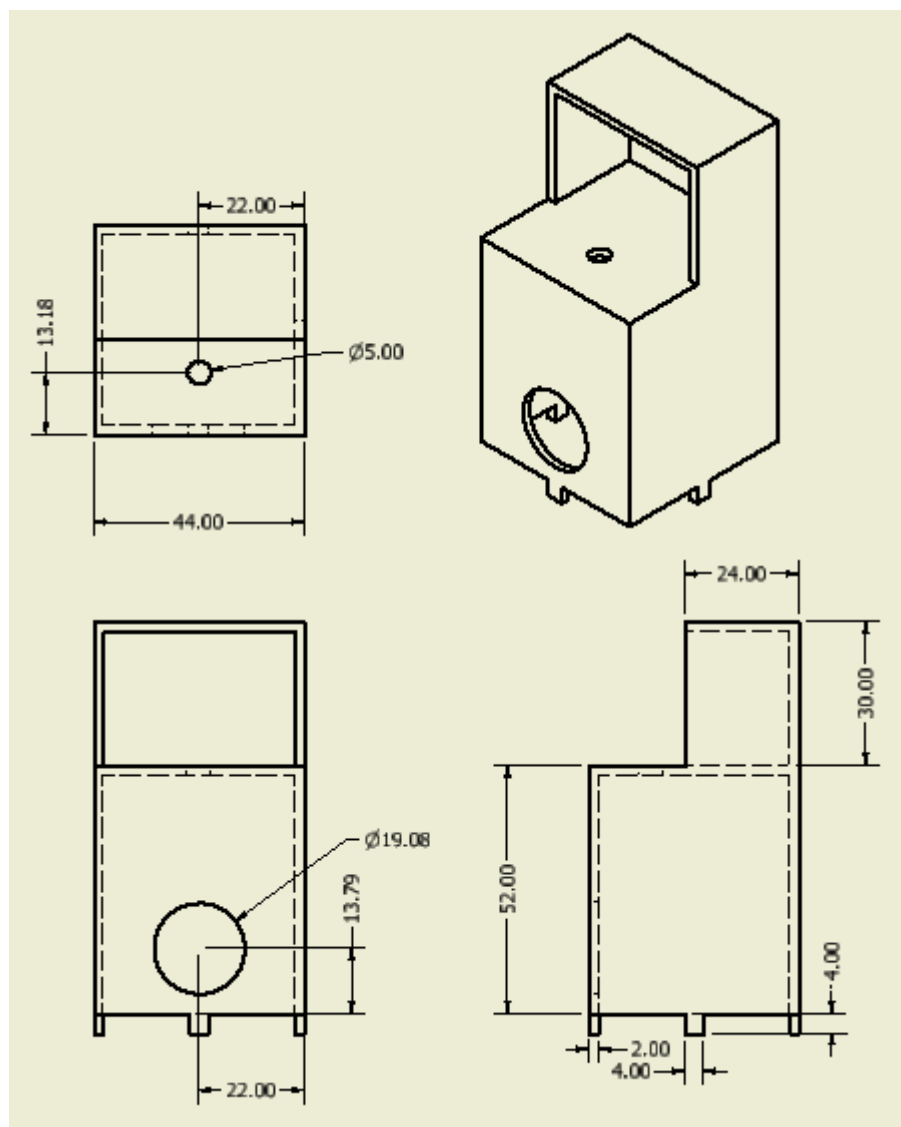


Figure 34: Engineering Drawings for the Beaker Lid Top.

The above figure depicts the final piece for the beaker lid, the Beaker Lid Top. This particular piece is designed to hold the image processing equipment (Raspberry PiCamera, pipette tip), the WPM pump, and the AuCl_3 reservoir.

To match the parts below, the main cavity was given a 40 mm x 40 mm square cross-section and 2 mm wall thickness. The vertical height of this cavity was set to give ~5 mm of space from the bottom of the camera, which is set to point directly at the tip of the pipette.

The 5 mm hole for the pipette is set at the top of the main cavity, 13.18 mm from the wall the camera is set on. This was determined to be the focal length after modification to the PiCamera's adjustable lens to reduce the horizontal space usage of the image processing equipment. The camera's centre sits 13.79 mm from the bottom of the piece and was set after measuring the depth the pipette sits inside its hole. The 5 mm dimension was set such that the pipette (OD = ~7mm) could be pressure fit into its hole allowing for consistent tip placement during image processing.

Above the main cavity is a shelf 3 cm high to elevate the pump and AuCl_3 reservoir. This is done to relieve stresses induced on the pipette by the tubing and allow for the reservoir to sit atop the beaker lid. After the part was printed, a hole was drilled into the top of the shelf to secure the pump using a screw and nut.

Latch

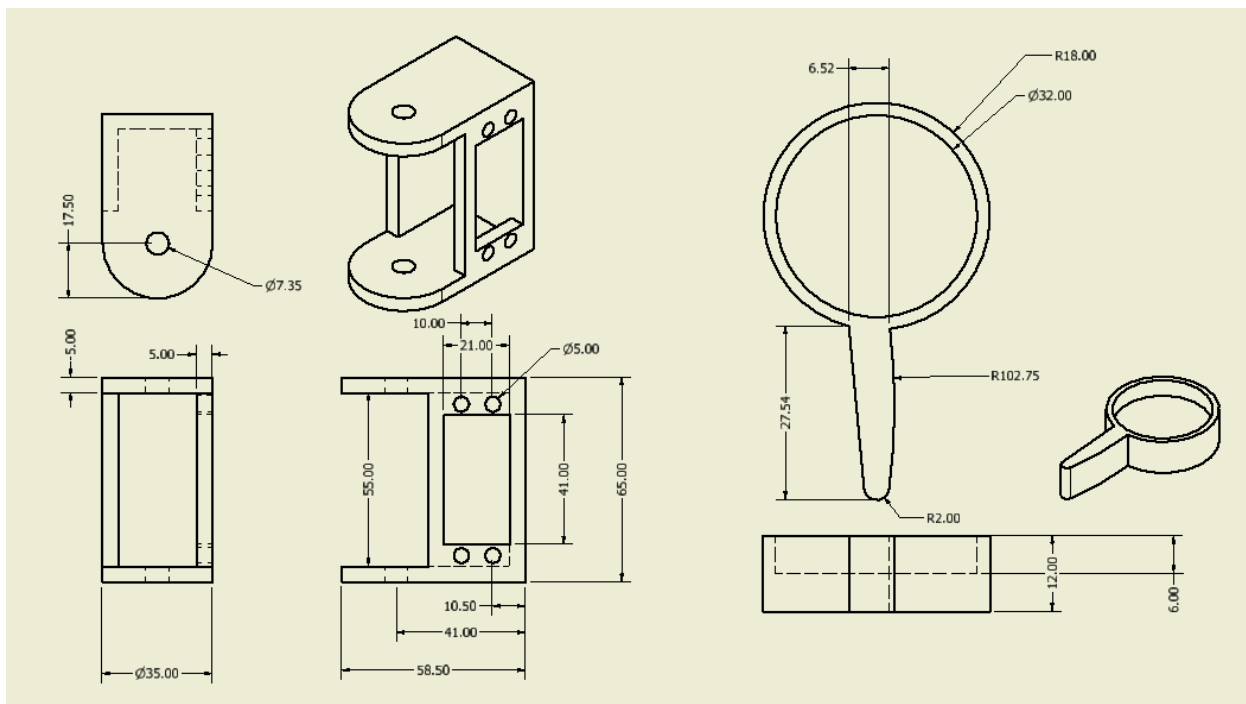


Figure 35: The Engineering Drawings for the 2 parts of the Latch (excluding the MG 996R servo motor). In order from left to right, the servo motor's base and latch arm.



Shown above are the drawings for the servo motor latching system. The latching system was required to be electronically controlled to release the lid when the cooling process began. The user will be required to ensure the lid is latched and engage the system before the synthesis process begins.

After previous work with a lever arm attached to the back wall of the reactor proved to produce errors when rotating the beaker lid. To solve this issue, the lid was constrained to move in a purely vertical manner. This was done by adding $\frac{1}{4}$ " thread rods as rails into the reactor plate and guides into the beaker lid (see Figure 1).

To provide a restoring force and lift the beaker lid from the beaker, a spring attached to an elevated position and beaker lid was the chosen mechanism. This is due to the availability and ease of modelling of springs.

To provide the latching mechanism and resist the spring force, a servo motor was chosen due to their relatively high stall torques and accurate positioning. The accurate positioning will be used to move the latch between the 'latched' and 'unlatched' modes. As springs tend to have k 's in the 100's of N/m, a strong servo motor was desired. The MG996R servo motor has a stall torque of 0.925 Nm at 4.8 V (~ 10 greater than the common SG90) and was chosen due to its availability and relative cheap price (<\$ 10).

To minimize moments produced in the couple between the spring and latch arm, it would be optimal to have them apply their forces at the same point. Since this is physically impossible, they were placed as close as possible without interfering. To prevent horizontal forces on the rails from the beaker lid, the spring was oriented vertically and between the two rails. To minimize the torque required by the motor to resist the spring, it was placed 1 mm away from the edge of the beaker lid. Summing the length of the motor arm, gap, and distance of spring from beaker lid edge gives us the required lever arm length for the latch.

$$l_{arm} = l_{motor} + l_{gap} + l_{spring} = (0.613 + 0.1 + 1.0) = 1.713 \text{ cm}$$

Using the lever arm length, the maximum force the servo motor can apply is calculated using the following equation:

$$\tau = Fl \rightarrow F_{max} = \tau_{max}/l_{arm} = (0.925 \text{ Nm})/(0.01713 \text{ m}) = 54.0 \text{ N}$$

Thus, the spring can only apply a force of 54.0N before the servo motor cannot resist and latch the lid in place.

To calculate the maximum spring constant able to be used in the system, the following equation was used:

$$F_s(x) = kx \text{ [N]}$$

Where x and k are the displacement from equilibrium in 'm' and spring constant in 'N/m', respectively. Since the lid should displace enough to allow for the user to place a beaker into the

cavity when retracted, this corresponds to a distance of 11 - 13 cm. Thus, the maximum spring constant is calculated to be:

$$k = F/x = (54.0 \text{ N})/(0.13 \text{ m}) = 415 \text{ N/m}$$

To determine the spring constants available, one of each spring type in the Performance Tool 200 Piece Spring Assortment had a known weight (52 g) applied and its extension distance measured. The spring constants were then determined using the following formula:

$$k = F_g/x = mg/x = (0.052 \text{ kg})(9.81 \text{ m/s}^2)/x = 0.51 \text{ N/mm}$$

The lowest spring constant found has a measured extension of 1.47 mm, corresponding to a k of 347.0 N/m. This value is well below the maximum and was used for the restoring force. If one wanted to use a stronger spring, either a stronger servo motor or lower extension length is required.

Seal

The sealing system was designed to fit atop the beaker lid and create a protective barrier between the beaker's contents/steam and the equipment enclosed by the lid.

Given the design of the lid, linear actuation of the seal is required. However, to provide 4 cm of linear motion directly from an actuator would require to have the actuator at least 4 cm away from the lid or a complex mechanical design. In order to simplify the design and reduce costs, a servo-motor (SG 90, <\$ 1/ea) was used with a conversion from rotational to linear motion, as shown below. An added bonus to this system is that servo-motors have their own feedback in the form of a potentiometer. This allows for them to determine and set their positions without the use of an external sensor. The one limitation is that servo-motors cannot rotate more than 180 deg.

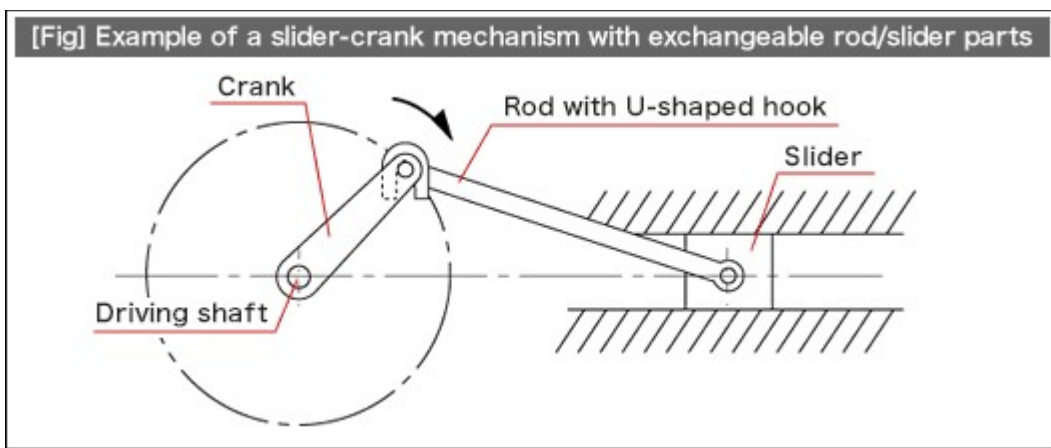
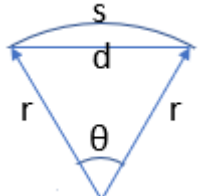


Figure 36: A summary of the concept used to convert rotational motion to linear motion. Extracted from [13].



As one can see in the above figure, there are some points in the servo-motor's rotation where much of its movement is perpendicular to the linear motion. Thus, it would be best to limit its rotation to a certain range and extend the crank.

Given a range of rotation of 60 deg and a required linear actuation of 4 cm, we can determine the the crank length using the following diagram and formula (from cosine law):



$$d^2 = 2r^2(1 - \cos(\theta)) \text{ or } r = d/\sqrt{2(1 - \cos(\theta))} \quad (25)$$

As a range of rotation of 60 deg would make an equilateral triangle, thus requiring a 4 cm crank. One can reduce the crank length with increasing range of rotation but with quickly diminishing returns (the reciprocal of the square root of cosine). To save 0.5 cm, the range of motion was set to 70 deg instead ($r = 3.49$ cm).

Using this information, a crank was manufactured to the desired length and a simple servo-motor code was written for the Arduino where 'sealing' was to set the rotation to a calibrated angle (where the seal was just touching the inner wall of the lid), and 'unsealing' was rotating in the opposite direction 70 deg. The code for this can be found in the Appendix.

GUI

There is no significant mathematical modelling required for the GUI.

Optimization Demo Performance

The metrics defined for the optimization demo report are: time needed to complete the process, reliability of characterization, accuracy of size produced and standard deviation of the distribution. The testing plans for each of these metrics are defined in the "Integration Demo Performance and Testing Plans" section of this report. The results of testing are reported here. The optimization specifications were met in the integration demo stage of this project, and their performance documented in that section.



Time Taken to Complete Process

Table: Time to Complete Process Results

Run Number	Time to Complete Process (h:m:s)
1	
2	
3	

Reliability of Characterization

Table: Reliability of Characterization

Run Number	TEM Size Measurement (nm)	nanoRIMS size measurement (nm)	Percent difference (%)	DLS Distribution measurement (nm)	nanoRIMS distribution measurement (nm)	Percent difference (%)
1						
2						
3						



Accuracy of Size Produced

Table: Accuracy of Size Produced

Run Number	TEM Peak Size Measurement (nm)
1	
2	
3	

Standard Deviation of Distribution

Table: Standard Deviation of Nanoparticle Distribution

Run Number	DLS Standard Deviation Measurement
1	
2	
3	

Integration Demo Performance and Testing Plans

The metrics defined for integration demo report are: time needed to complete the process, reliability of characterization, accuracy of size produced and standard deviation of the nano-particle size distribution. The testing plans and performance for each of these metrics are documented in this section.



Time Taken to Complete Process

The time taken to complete the process is defined as the time required for the nanoRIMS systems to both synthesize and characterize gold nanoparticles after the user turns on the system. This was measured using a timer for three runs of the reactor system, starting when the system is turned on and ending when a characterization result is received by the user.

Table: Time to Complete Process Results

Run Number	Time to Complete Process (h:m:s)
1	1:56:30

While longer than an ideal synthesis process, this reaction time is well within our 100% spec of making nanoparticles within 6 hours.

Reliability of Characterization

The reliability of the nanoRIMS characterization system is determined by how often the characterization result of the system agrees with the results found using traditional measurement methods: transmission electron microscope (TEM) size measurements and dynamic light scattering (DLS) size distribution measurements. Each batch of nanoparticles synthesized during nanoRIMS testing is characterized using both TEM and DLS measurements, performed by well trained graduate students in Dr. Soleymani's lab.

The nanoRIMS characterization system generates an absorption spectrum by following the process outlined in *Optical Characterization* above. The peak size of the nanoparticles is determined from this near gaussian spectrum by converting the pixel reading from the CCD to a wavelength of peak absorption by the expression:

$$\text{wavelength} = \text{pixel} * 0.0541 \text{ nm/pixel} + 400 \text{ nm} \quad (26)$$

In this expression, 0.0541 nm/pixel is the factor converting a pixel number on the CCD to a wavelength reading, since the sensor has 3964 pixels and is calibrated to cover 200 nm of light (400- 600 nm). The 400 nm offset is added because on this sensor, the '0' pixel corresponds to the beginning of our wavelength range, at 400 nm. This wavelength measurement is then converted to a nanoparticle diameter using the relationship described in the *Optical Characterization* section, above. This calculation is done to find the peak size of the nanoparticle distribution, and will be compared to the TEM size measurement.

In order to find the distribution of the nanoparticle solution, the full width half maximum of the absorption peak is found by locating the pixel positions where the half maximum point occurs. The full width is the difference between these two pixel points. The standard deviation can then be found from the full width half maximum definition:

$$FWHM = 2\sqrt{2\ln 2}\sigma \quad (27)$$

Where sigma is the standard deviation of the gaussian. This is converted from a pixel measurement to a wavelength measurement through the same method described above.

When running through the process of determining the Gaussian distribution of absorption, spectrums of water, the gold nanoparticle solution, and the dark current of the sensor were taken. The images below illustrate the results for each of these cases.

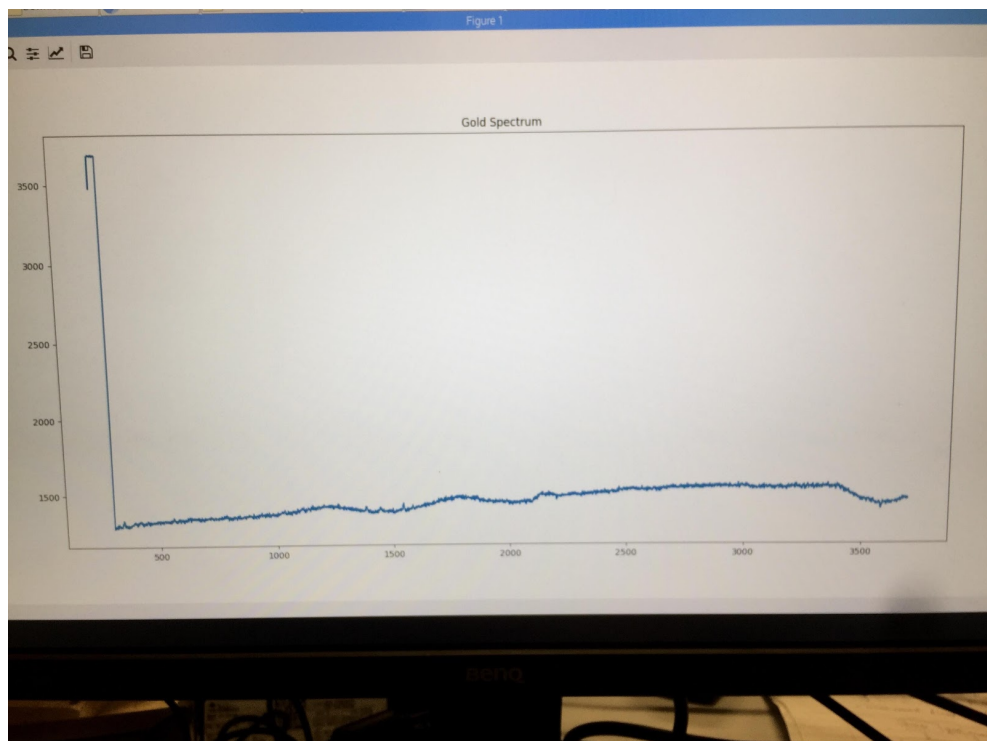


Figure 37: Gold Optical Spectrum of Run 1 Nanoparticles.

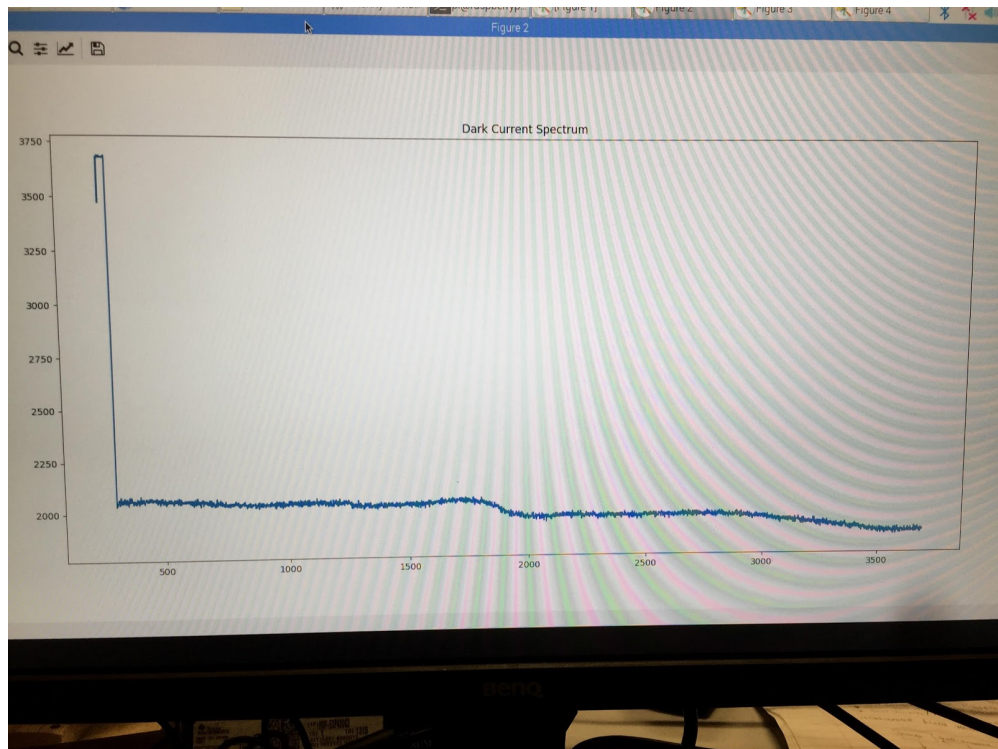


Figure 38: Dark Current Sensor Noise.

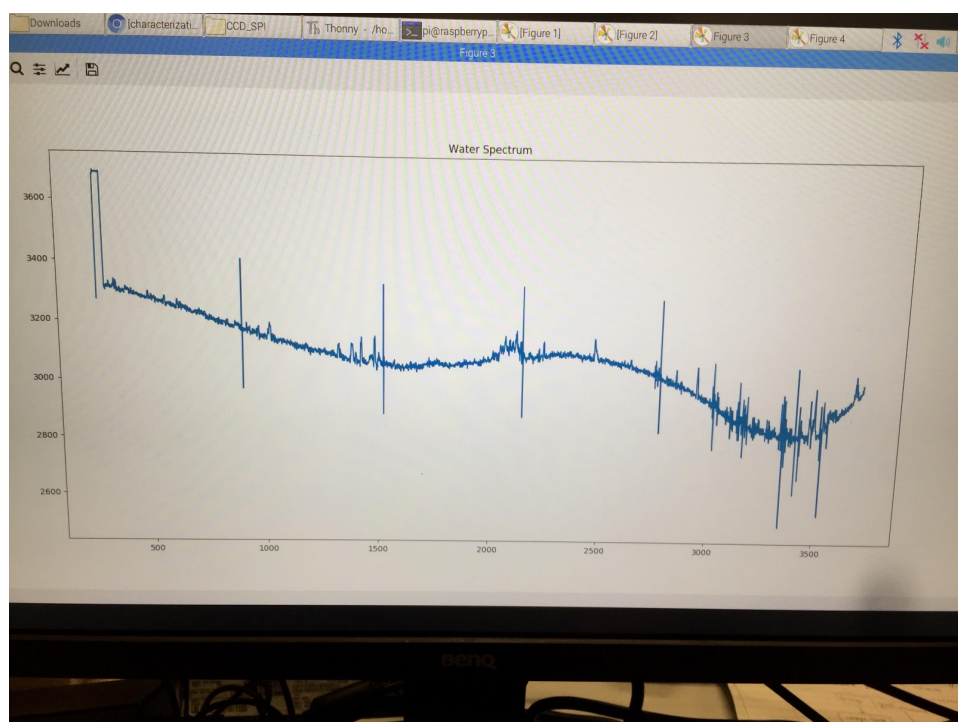


Figure 39: Water Baseline Spectrum

With the spectrums above, a normalized distribution of the absorption can be determined by subtracting the dark current from the gold nanoparticle spectrum and normalizing by the baseline.

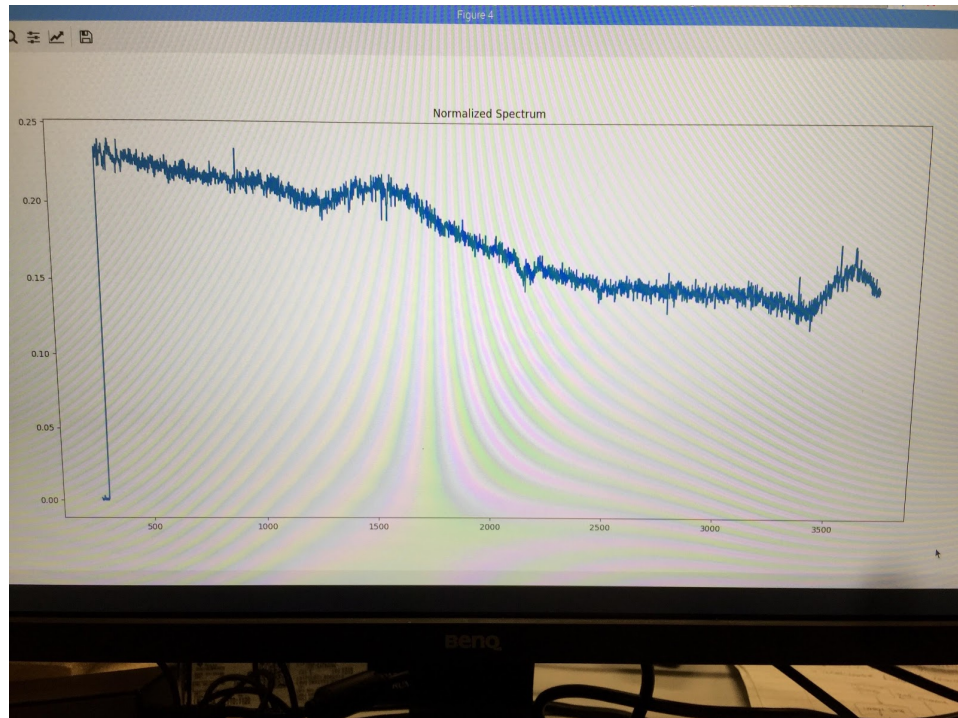


Figure 40: Normalized Spectrum. The spectrum is Absorption vs. Pixel Index

When reading from the left to the right side of the data, it can be seen that optical absorption decreases as a function of increasing pixel index (decrease in wavelength). When the spectrum reaches the 1317 to 1678 pixel range, the amount of absorbed light increases from the general linearly decreasing trend. In reference to measurements that were completed by Raham and compared to the research standard Nanoparticles provided by Sigma-Aldrich, the experimental fit for ~13 nm sized particles has a peak absorption at 517 nm [16]. When approximating the peak absorption of the distribution we have acquired, our expected absorption lies at 517.3 nm.

The properties of this absorption distribution are shown in “Run Number 1” below.

Table: Reliability of Characterization

Run Number	TEM Size Measurement (nm)	nanoRIMS size measurement (nm)	Percent difference (%)	DLS Distribution measurement (nm)	nanoRIMS distribution measurement (nm)	Percent difference (%)
1	12.8	13.9	8.6%	10	9.95	0.5%



Accuracy of Size Produced

The aim of nanoRIMS is to produce nanoparticles with high quality and consistency, and an important part of that is ensuring that the size of nanoparticles produced matches well with the desired size. In this demo, the goal is to produce 12 nm gold nanoparticles. To test if this size of nanoparticle is being produced, the synthesized nanoparticles will be measured using both TEM and DLS measurement systems in order to accurately determine their peak size.

Table: Accuracy of Size Produced

Run Number	TEM Peak Size Measurement (nm)
1	12.8 +/- 0.4

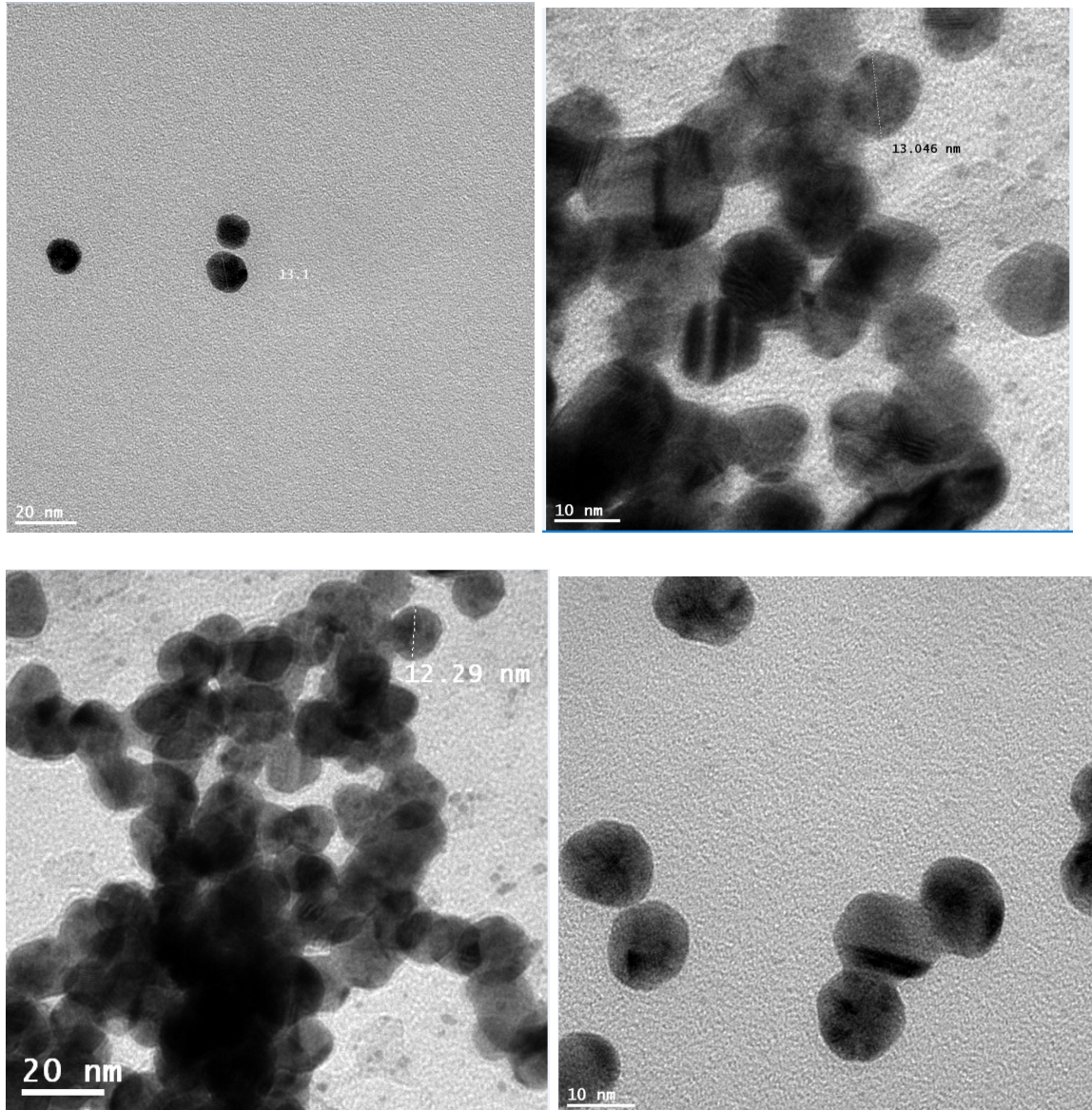


Figure 41: TEM Measurements of Nanoparticles

The TEM size measurement is the average of three size measurements taken on a transmission electron microscope, shown above. The size of the indicated nanoparticle is labelled in [nm] on the image. The scale bars shown in the TEM images verify the consistency of the measurement and size.

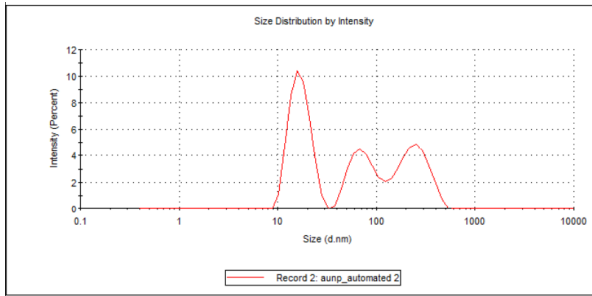
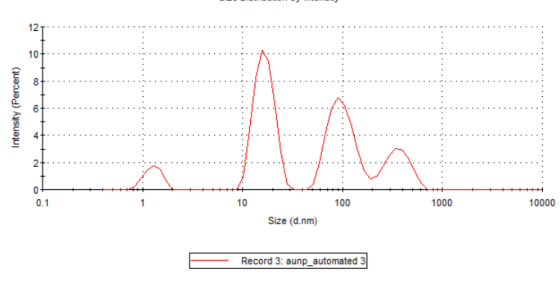
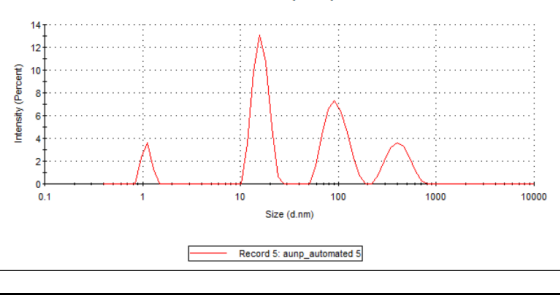
Standard Deviation of Distribution

The peak size of the nanoparticles produced is an important metric to determine the quality of the solution, but we also have to consider the distribution of sizes present in the solution. While



there will always be a size distribution of nanoparticles, a smaller spread means a higher quality nanoparticle solution. This spread is best quantified by the standard deviation of the nanoparticle distribution, which is typically gaussian in nature. The standard deviation of the size spread is measured using a dynamic light scattering measurement in order to accurately determine the distribution of nanoparticle sizes present in the solution.

Table: Standard Deviation of Nanoparticle Distribution

Run Number	DLS Standard Deviation Measurement
1	 A line graph titled "Size Distribution by Intensity". The y-axis is labeled "Intensity (Percent)" and ranges from 0 to 12. The x-axis is labeled "Size (d.nm)" on a logarithmic scale with major ticks at 0.1, 1, 10, 100, 1000, and 10000. A red line shows a primary peak at approximately 15 nm and a secondary peak at approximately 150 nm. A legend at the bottom right indicates the plot corresponds to "Record 2: aupn_automated 2".
2	 A line graph titled "Size Distribution by Intensity". The axes and data series are identical to the first plot, showing a primary peak at ~15 nm and a secondary peak at ~150 nm. The legend indicates it corresponds to "Record 3: aupn_automated 3".
3	 A line graph titled "Size Distribution by Intensity". The axes and data series are identical to the first plot, showing a primary peak at ~15 nm and a secondary peak at ~150 nm. The legend indicates it corresponds to "Record 5: aupn_automated 5".

The average distribution on all of these DLS plots is 10 nm +/- 2 nm. This is well within the required specification of a 40 nm distribution in the synthesized nanoparticles.

Module Demo Performance

Fluid Transport

For the tests in the following two sections, a pumping rig and imaging rig were designed, manufactured, and assembled. Drawings for the two can be found in Figures 33 and 34, respectively.

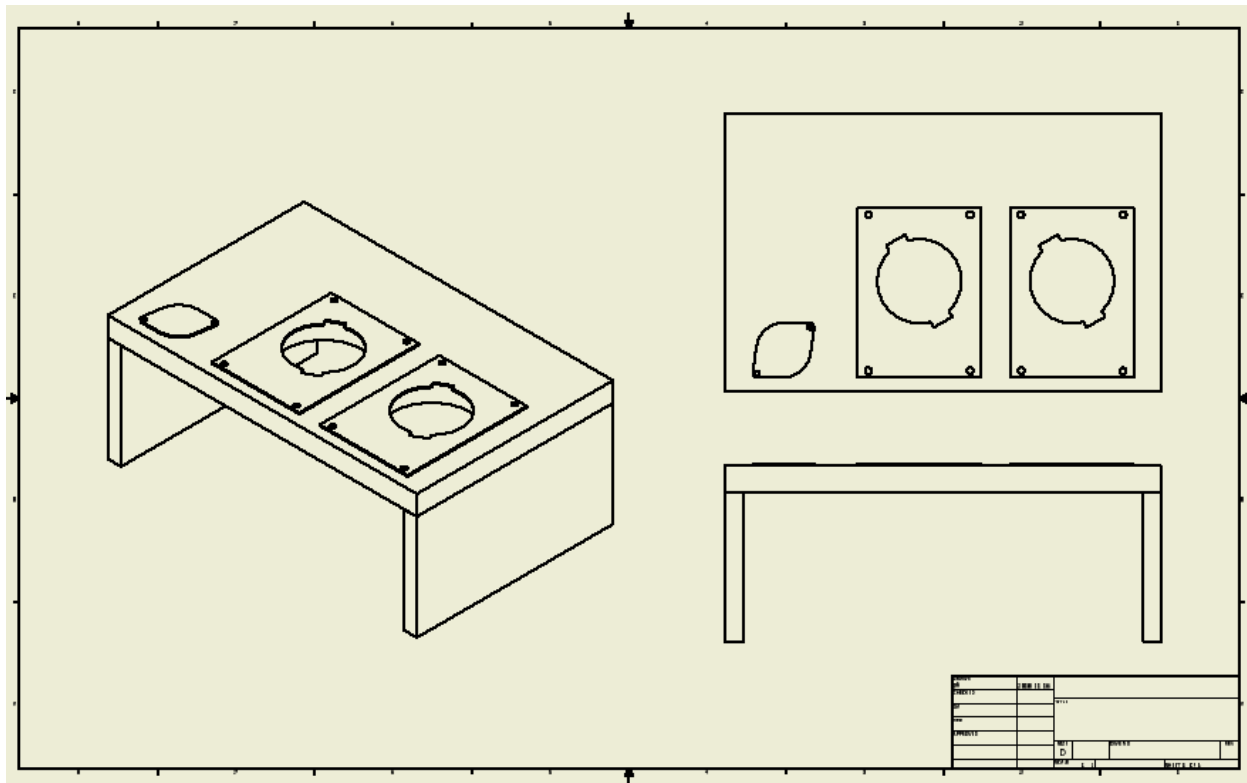


Figure 42: Drawing of the Pumping Rig used for testing.

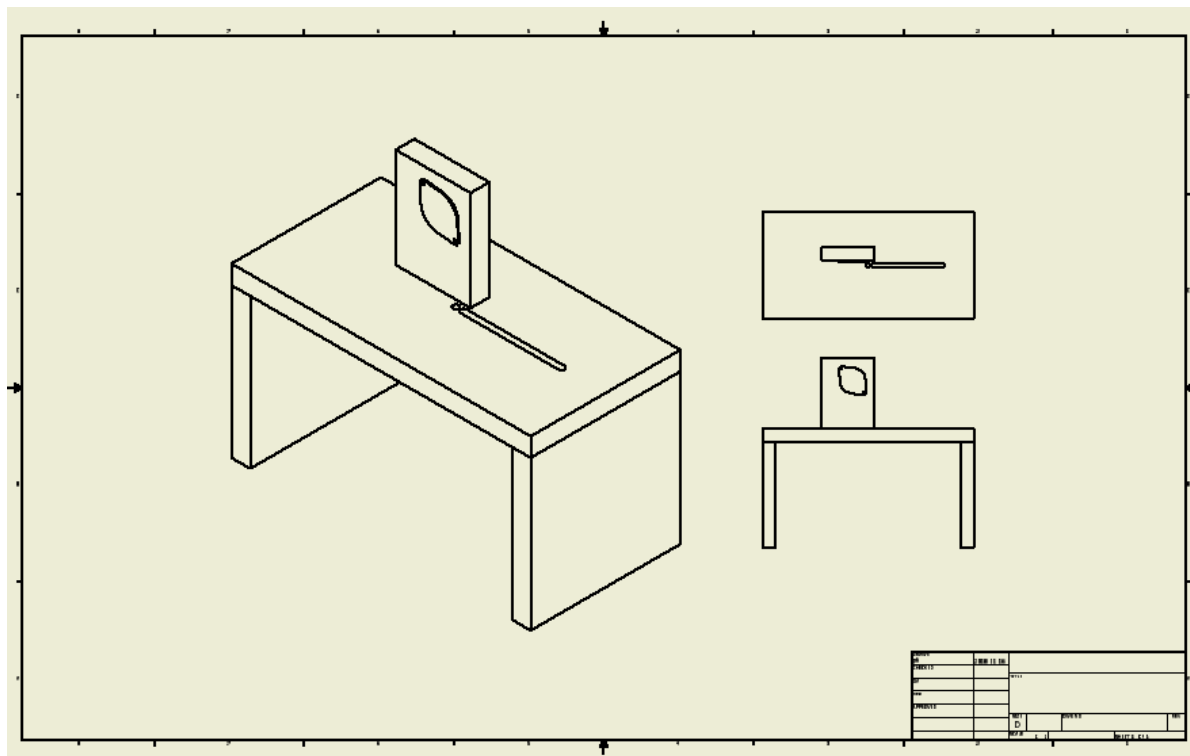


Figure 43: Drawing of Imaging Test Rig used for testing.

With the pumps and reservoirs set in the pumping rig, the fluid transport system was tested with the following procedure:

- 1) Turn on attached DC Power Supply, set to 12 V and maximum current output
- 2) Ensure tubing is empty, purge the lines by calling `purge.py`
- 3) Using a milligram scale (resolution of 0.1 mg), place the beaker inside and tare the measurement
- 4) Place beaker at outlet and prime tubing by calling the appropriate `prime_(pump model)` function
- 5) Begin fluid dispensing by calling `(pump model)_(volume to dispense)`, wait for pump to come to a stop
- 6) Take beaker and place on milligram scale, measure mass of water dispensed
- 7) Divide measured mass by density and compare to expected value with relative error
- 8) Repeat 3 times total to confirm repeatability

Note: Pump models are WP10 and WP11. Volumes to dispense are 30 mL and 300 mL.



The results of the tests are shown in Table below:

Table: Test Results for Dispensed Volumes >10 mL

Pump Model	Vol. to Disp. (mL)	Actual Vol. (mL)	Error (%)
WP10	300	301	0.33
WP10	300	300	0.00
WP10	300	299	-0.33
WP11	30.0	30.0	0.00
WP11	30.0	29.8	-0.67
WP11	30.0	29.8	-0.67

Image Processing

With the ultimate goal of determining the volume of a droplet of fluid, a testing plan must be developed to quantify the success of the algorithm. The following testing plan will be used to quantify the success of the system.

- 1) Using a microgram scale, the scale is zeroed to the weight of the containment object used to capture a droplet of fluid. The object that has been traditionally used is a small glass beaker.
- 2) Monitoring the size of the droplet using the Raspberry Pi Camera, the drop is made as large as possible before the surface tension is insufficient to keep the droplet from falling.
- 3) An image of the drop is taken using a low exposure and conditions that highlight the edges of the drop.
- 4) Without disturbing the drop, the small glass beaker is placed below the drop. The drop is forced to fall into the beaker and the weight is measured using the microgram scale.
- 5) From here, the image processing algorithm is used to determine the expected mass of the drop.

In the optimization of the system, the imaged droplet will need to be one that is at its breaking point from the nozzle. This will provide the most accurate results when comparing it to the true



amount of fluid that has been released. For testing, the outlined method proves the proof of concept. The results below capture the different tests that have been completing proving the implemented method. For each test, the measured mass, the calculated expected mass, and the associated error are presented. All tests were done in succession to each other. As per the DOS, the error must be within 3% of the measured value.

Calibration Trial	Measured (grams)	Calculated (grams)	Error (%)
1	0.0137	0.0136	1.01
2	0.0146	0.0145	1.00
3	0.0172	0.0169	1.96
4	0.0174	0.0173	0.58
5	0.0167	0.0167	0.00
6	0.0166	0.0170	0.02
7	0.0168	0.0166	0.01
8	0.0172	0.0169	0.02

As seen, the results show a high degree of reliability and success. It might be kept in mind that environmental conditions play a key factor in the overall measurement, which is the largest source of error contributing to the imaging.

Sensor Alignment

In order to properly determine the mounting location of the linear CCD sensor, the geometry derived in the *Optical Characterization* will be utilized. As defined, the left and right sides of the sensor will be placed at an equidistant condition for the 400 nm and 600 nm optical path lengths. Two laser pointers with separate emission spectra of 405 nm and 532 nm will be used to acquire a defined alignment of the sensor to the diffraction grating. To confirm this alignment, an optical filtering method will be used. With a *Thorlabs* Sputtered 500 nm Edge Pass Filter, a *Schott* VG9 Bandpass Filter, a *Schott* BG3 6 Bandpass Filter, and a *Thorlabs* 543.5 nm Line Filter, the alignment can be finely tuned.

When using the Sputtered 500 nm Edge Pass Filter, the 400 nm sensor position can effectively be calibrated. The spectrum for the used filter is shown below.

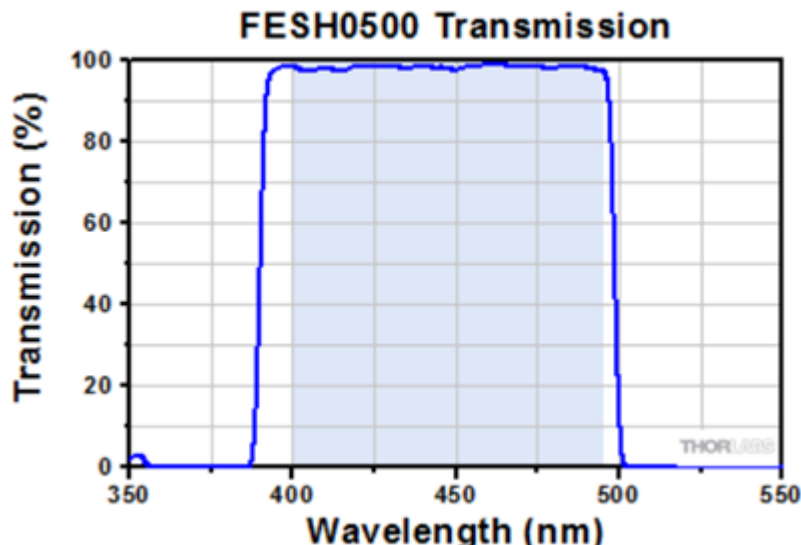


Figure 44: Graphical representation of the transmission as a function of the incident wavelength. Shaded region illustrates the transmission region of the filter.

Using the band intrinsic to the filter, the 400 nm to 500 nm region covered by the sensor will be confirmed. To again confirm the location of the 400 nm location on the sensor, the Schott VG9 Bandpass filter can be utilized. There is a convenient minimum of the internal transmittance associated to the filter at the 400 nm location. The internal transmittance versus the incident wavelength is shown below. The internal transmittance of an optical filter refers to the energy loss through absorption, whereas the total transmittance refers to the total energy loss through all possible interactions.

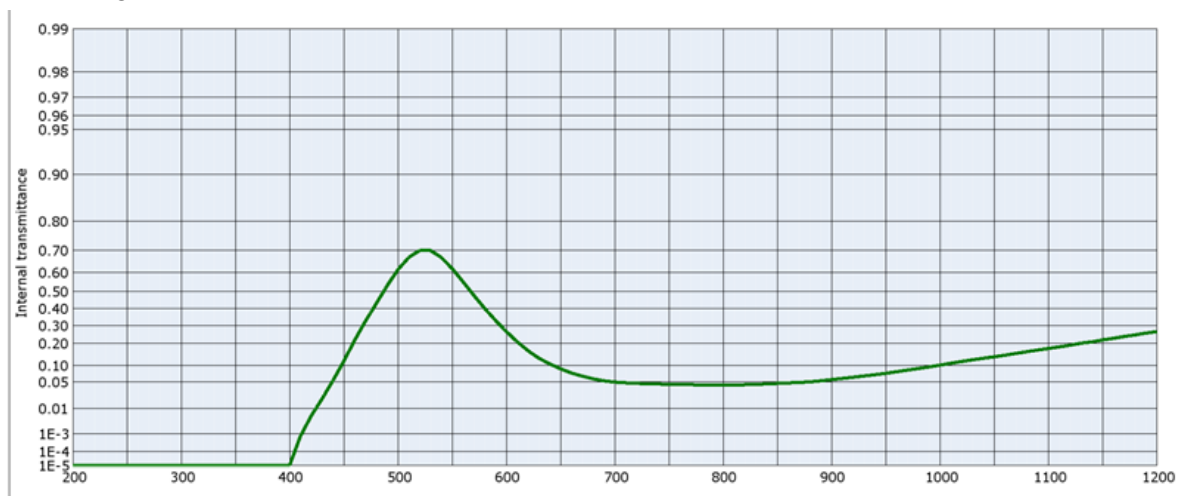


Figure 45: Schott VG9 Bandpass Filter. Internal Transmittance vs. Incident Wavelength

With this information, the 400 nm location of the sensor can be confidently stated, and due to the physical geometry of the sensor, the 600 nm position will subsequently be placed in the desired location. To confirm the location of the 600 nm pixel areas on the sensor, the *Schott* BG3 Bandpass filter will be used. The spectrum of the filter is a non-zero internal transmittance across the wavelength region of interest with a sharp drop off near 600 nm's. The spectrum is shown below.

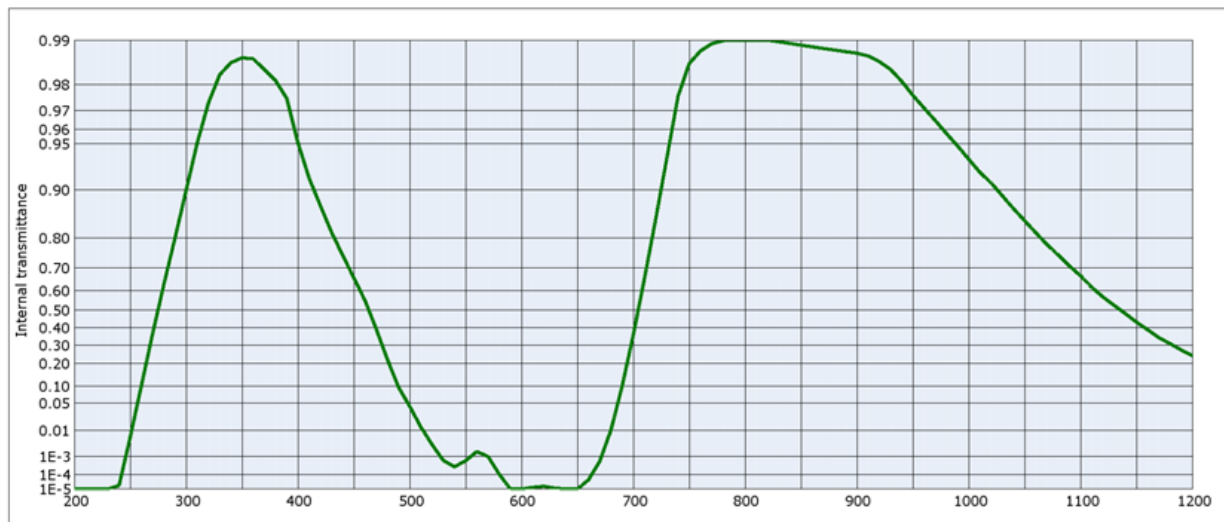


Figure 46: Schott BG3 Bandpass Filter. Internal Transmittance vs. Incident Wavelength

With all of this, the sensor should be confidently aligned to the desired location following the geometrical restrictions previously defined. Therefore, the spectrum incident into the sensor should identically match any defined filter response within the 400 nm to 600 nm wavelength range. Along with this, it would be useful to test the spatial resolution of the sensor when using a narrow band laser line filter. With the *Thorlabs* 543.5 nm laser line filter, the transmittance peak and the full-width half-maximum reported in the supplied data sheets of the filter can be used to confirm the spatial resolution of the sensor for an individual wavelength. The transmission of the filter as a function of wavelength is shown below.

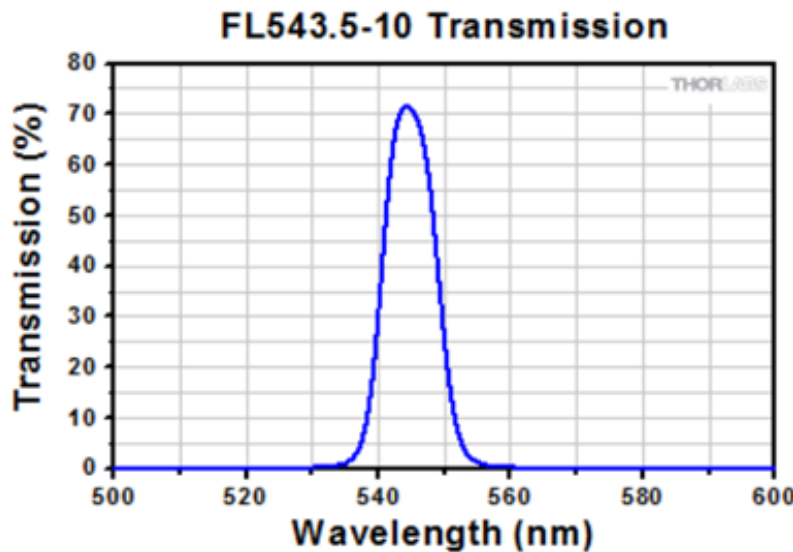


Figure 47: Thorlabs Narrow Band 543.5 nm Laser Line Filter.

The peak of the transmittance will be measured and the spread of the maximum intensity will be quantified.

Optical Testing Plan

With all of the optical elements mounted into the system, the spectrum of light incident onto the sensor can be determined. The sensor has been mounted onto a 2D optical stage thus enabling slight changes in sensor location.

With the final spectrum acquired, the maximum intensity of the distribution can be determined. When using a 543.5 nm Laser Line Filter, the expected pixel value of the maximum intensity on the linear CCD sensor was determined. The spectrum shown below was gathered by exposing the sensor with the laser line filter light with a baseline division, as previously mentioned.

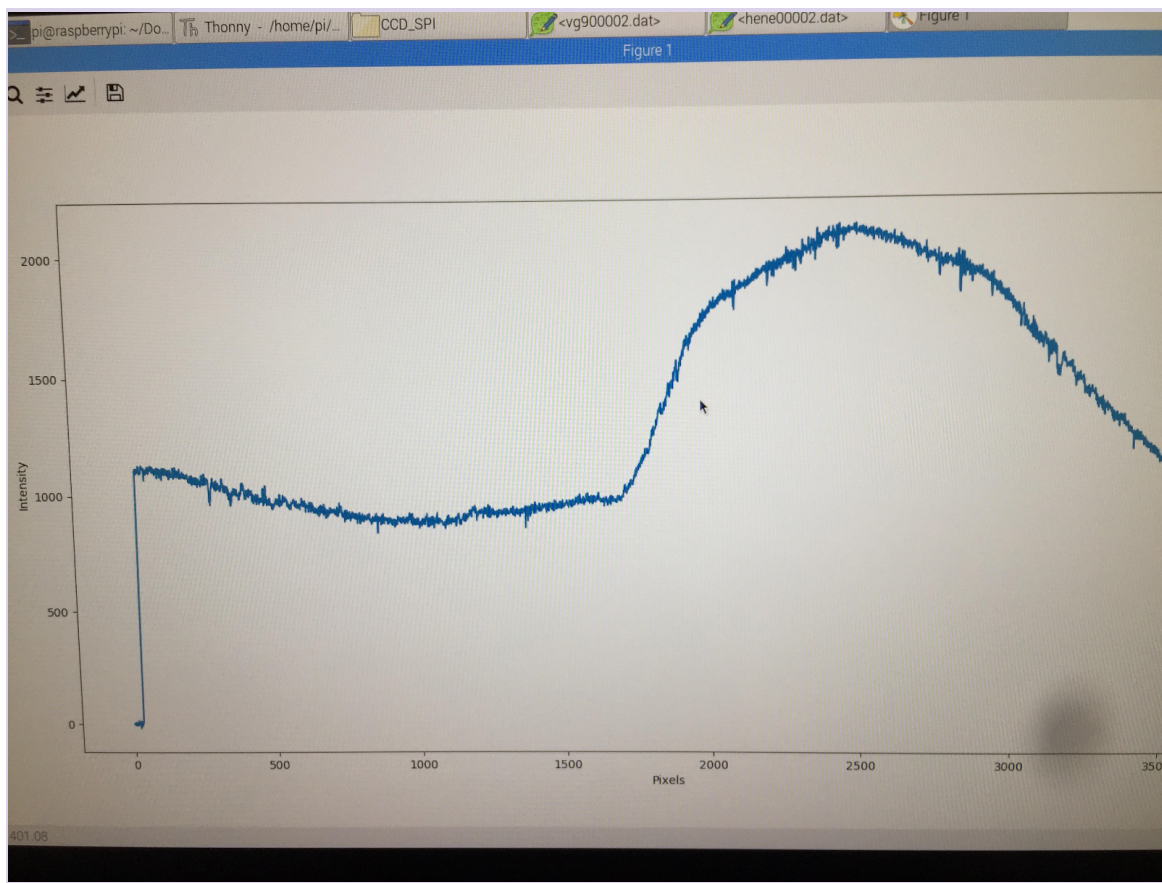


Figure 48: Spectrum read by the linear CCD sensor using the 543.2 Laser Line Filter

When referring to figure 39, it can be seen that the width of the spectrum is significantly larger than the expected result. This is primarily due to the dispersion following the diffraction grating. This dispersion will be able to be reduced with a manufactured slit behind the grating.

When calculating the location peak of the distribution, the pixel index corresponding to the 543.2 nm transmission was determined to be 2462 out of the 3694 possible pixels. With perfect alignment, the wavelength corresponding to a particular pixel value is as such:

$$\lambda = \frac{170}{3694}(pixel_{max}) + 430$$

Where 170 nm is the difference between the minimum and maximum emitted wavelengths of the broadband LED source and 430 nm is the minimum wavelength emission. With the distribution provided above, the pixel value corresponding to the peak intensity is 2462.

$$\lambda = \frac{170}{3694}(2462) + 430 = 543.30\text{nm}$$

Along with these measurements, we can perform a final test to confirm how well each pixel corresponds to its optimized wavelength. The plots below illustrate the pixel location of 405 nm and 532 nm. As referenced, the emission was from two independent 5 mW laser pointers.



Figure 49: Spectrum read by the linear CCD sensor using the 405 nm laser pointer. The right most side of the spectrum corresponds to the 405 nm. Left most side illustrates a sensor readout error.

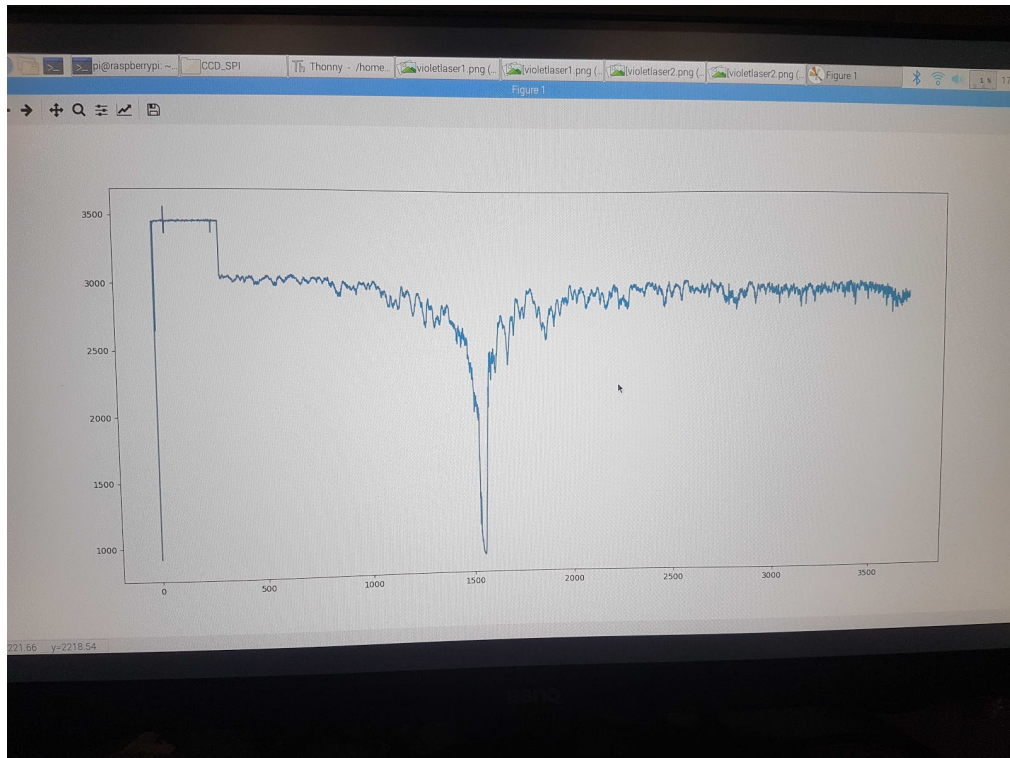


Figure 50: Spectrum read by the linear CCD sensor using the 532 nm laser pointer. Sharp dip in the middle of the spectrum is the expected location.

Therefore, the sensor can be aligned within 0.20 nm of an expected wavelength, thus meeting the module demo specifications. The limiting factor for further confidence in this value is to tighten the broadening previously discussed.

Environment and Process Control

In order to test the performance of the environment control module we need to determine the following specifications:

- How accurately can we hold the temperature of 300 mL of water?
- How quickly can we cool 300 mL from 100 °C to 25 °C?
- How quickly can we heat 300 mL from 25 °C to 100 °C?

Before any of these performance factors can be measured using the thermocouple in our system, we first need to validate that the thermocouple can measure temperature to within ± 0.5 °C of the actual water temperature. The temperature of the water is verified using an IR digital temperature reader. For each temperature, three measurements will be taken with the IR



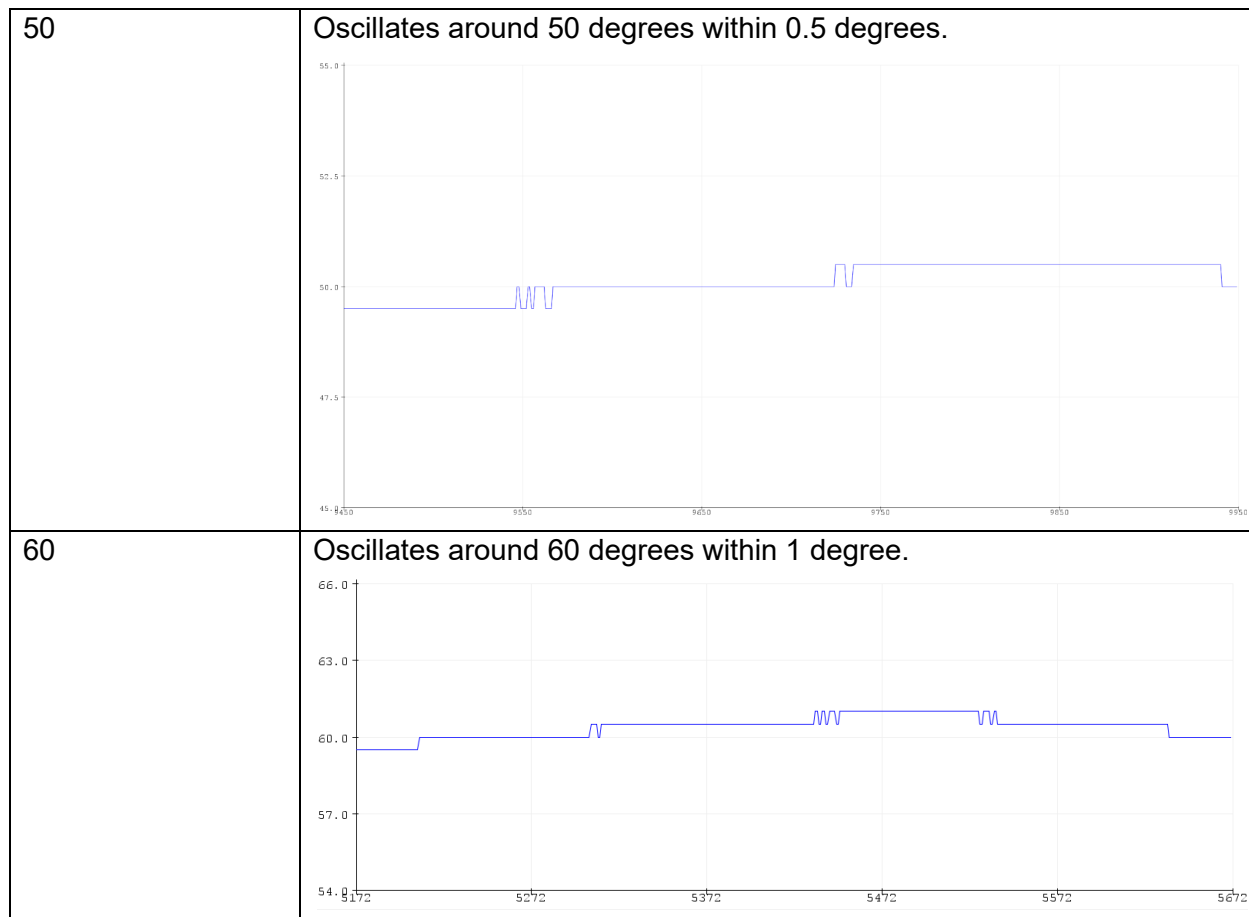
sensor and the average taken. The standard deviation of these measurements is taken as the error.

The following results are found:

Thermocouple Temperature (°C)	IR Sensor Temperature (°C)
30	30 +/- 0.2
40	40.1 +/- 0.1
50	50 +/- 0.1
60	60 +/- 0.2

Next, the ability of the PID system to hold the 300 mL of water to a set temperature is tested. The system is set to a range of temperatures, and the temperature measured with the thermocouple over a period of 5 minutes, to ensure that there is enough time to observe any changes in the water temperature that might occur.

Set Temperature (°C)	Temperature behaviour
30	Oscillates around 30 degrees within 0.5 degrees. A line graph titled "COM3 (Arduino/Genuino Uno)" showing temperature over time. The y-axis ranges from 25.0 to 35.0 degrees Celsius with increments of 2.5. The x-axis shows time in minutes from 16:04 to 23:04. The temperature starts at approximately 29.5°C, steps up to 30.0°C at 17:04, remains flat until 19:04, then steps up again to 30.5°C. From 20:04 to 22:04, the temperature remains constant at 30.5°C before showing small oscillations between 30.0°C and 30.5°C. A zoomed-in view of the 20:04 to 22:04 period shows the oscillations more clearly.
40	Oscillates around 40 degrees within 0.5 degrees. A line graph titled "COM3 (Arduino/Genuino Uno)" showing temperature over time. The y-axis ranges from 35.0 to 45.0 degrees Celsius with increments of 2.5. The x-axis shows time in minutes from 16:06 to 23:06. The temperature starts at approximately 39.5°C, steps up to 40.0°C at 17:06, remains flat until 19:06, then steps up again to 40.5°C. From 20:06 to 22:06, the temperature remains constant at 40.5°C before showing small oscillations between 40.0°C and 40.5°C. A zoomed-in view of the 20:06 to 22:06 period shows the oscillations more clearly.



Finally, the time it takes to heat and cool the system between 100° and 25° is measured. A timer is set when the set point temperature is changed, and the temperature from the thermocouple is observed until the set point is met, at which point the timer is stopped. The average delay in stopping the timer is within 15 seconds, which is set as the error in the measurement.

Set Temperature (°C)	Time required
25 from 100	29 min 10 sec +/- 15sec
100 from 25	38 min 51 s +/- 15 sec

In order to test the performance of the fan module, the tachometer output read by the Arduino must be verified using an external method. In this case, as the tachometer outputs a near ideal square wave, an oscilloscope was used to measure the frequency of the tachometer and the resulting value was compared with the output from the Arduino. As we require a set speed of 1200 RPM as per the standard of the Turkevich method used by Dr. Soleymani, the set point used in the test was 1200 RPM. The result from the oscilloscope is displayed below:

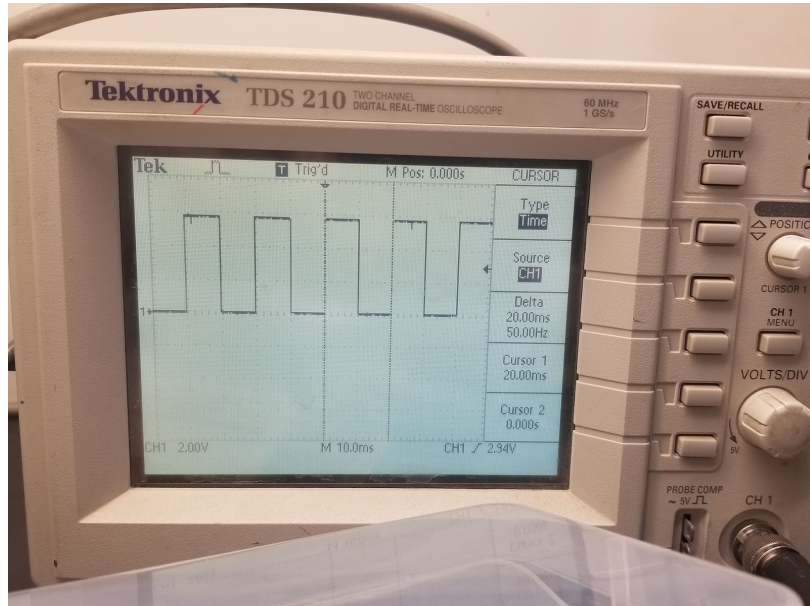


Figure 51: Signal from Oscilloscope

Following the formula from the mathematical modelling above, we can see that the RPM of the fan according to the Tachometer is:

$$RPM = (\text{Tachometer frequency}) / 2 * 60 = (50/2) * 60 = 1200 \text{ RPM}$$

The highest error possible would be $\frac{1}{2}$ the tick size on the oscilloscope, which in this case is 1 millisecond. This would be a 5% maximum error, resulting in a potential variation of ± 60 RPM from the measured value on the oscilloscope. While it cannot be demonstrated in a static image, the actual oscilloscope reading was extremely stable and did not move about the set point, and the measurements from the Arduino were taken every 5 seconds without averaging as a comparison point:

Arduino Measurement #	Measured RPM
1	1202
2	1199
3	1200
4	1200
5	1201

These measurements show excellent agreement with the set point of 1200 RPM. The next steps will involve re-tuning the PID once the complete device has been assembled, as the

potential changes in process factors will mean that the old PID gain values may no longer apply. This will involve once again using the Ziegler-Nichols method to find the optimal gain values, as well as taking multiple measurements of the RPM at multiple set points while stirring the liquid to ensure that the system functions as intended.

The load cell testing was fairly simple due to the nature of the load cell as a weight measuring instrument. To test the load cell, a second scale with an resolution of 1 gram was used to weigh an object, thus providing a reference point for the load cell. In this case, a drill battery was used, which was measured to weigh 374 +/- 1 gram.



Figure 52: Load Cell with drill battery

The result from the load cell was recorded and is displayed below in Figure 34:

```
Reading: 0.37486 kg calibration_factor: 1317775.50
```

Figure 53: Load Cell results from Arduino

It is clear that the load cell is reporting 0.374 kg or 374 grams, with a fluctuation of less than 2⁻² grams. Unfortunately, due to the resolution of the test scale, this accuracy cannot be verified. However, the scale is shown to be accurate to within 1 gram, which hits the 100% specification and meets our requirements. The load cell was also tested with the beaker of gold nanoparticles, weighing 67 grams, and it was able to detect this



as well. Future testing will involve re-calculating the calibration factor of the load cell once it has been mounted in the complete device, as the zero weight of the load cell will change when the switch to acrylic components is made.

GUI Testing

The GUI was tested using the fan in order to get a live data stream, as well as the ability to modify the fan RPM on demand. Additionally, a second thread running alongside the main thread waits for the user to enter a USB into the Pi. Upon inserting the USB, the CCD characterization files are automatically transferred to the media drive. The testing procedure involved hooking up the Arduino controlling the fan to the Raspberry Pi and testing the fan's response to external disturbances to ensure the PID response was accurately modelled in real time. The RPM + and RPM - buttons should increase or decrease, respectively, the RPM set point of the fan by 50. This was tested using the touchscreen and the fan accurately reached the desired set points according to user input. There is also an option for the user to select the size of nanoparticles they would like to produce, as well as start and stop buttons for the user to control when the procedure starts and stops. Finally, there is an input textbox allowing the user to enter the initial volume of one of the reservoirs so that fluid tracking can take place.

Future development will involve creating a central menu for the GUI that looks much nicer than the current implementation, as well as combining all of the serial data streams to collect all required information for the nanoparticle synthesis procedure (temperature, fan speed, load cell reading, CCD spectra, etc). We would also like to expand the fluid reservoir tracking to include all 3 reservoirs, as a single reservoir was used for a proof of concept.

EHS Code Considerations

Electrical Safety

Throughout this portion of the capstone project, we are using a number of DC power supplies and electrical components, some at high currents (up to 3 A). Electrical safety is covered in section 17.0 of the McMaster EOHSS Lab Safety Handbook [7]. As outlined in this report, precautions are taking when working with electronics. All equipment is properly grounded, and wires and cords are checked for frying before use. All wires must also be dry before plugged into circuits. This is of special note in our case because our project involves the pumping and heating of liquids, extra caution is taken to ensure that all of the circuit components are dry before turned on or plugged in.



Working with Chemicals

Our project involves working with a number of chemicals: gold chloride, trisodium citrate, and gold nanoparticles. The safety hazards associated with all these chemicals are summarized in the MSDS section, below. For all of these chemicals, general handling precautions are taken. All chemicals are only handled when wearing gloves, and are stored in clearly labelled containers. Waste, including paper towels used to clean up any spills, are stored in labelled containers used only for the purpose of waste. These bins will be taken to Dr. Soleymani lab to be correctly disposed of.

First aid steps to be taken if necessary are outlined in the MSDS section of our report.

Power Supply Safety

The power supply we are using to provide DC power to the entirety of the device is an EVGA 400 Watt Advanced Technology eXtended (ATX) power supply. The power supply takes 120 VAC at up to 10A. The device converts this AC input into 5 DC signals, described in the table below:

DC Output	+3.3 V	+5 V	+12 V	+5 Vusb	-12 V
Max Output	24 A	15 A	34 A	3 A	0.3 A
Max Power	79 W	75 W	408 W	15 W	3.6 W
Total Allowable Output	430 W @ 50C				

The device offers a single +12 V rail, which offers the best power output and stability when providing power to our 12 V components. Additionally, all of the ratings above are rated at continuous power, not peak power. This provides better device longevity and stability, and allows us to base our calculations off of the numbers above as opposed to unsustainable and unstable peak wattages. Also, testing has shown that the ATX meets the 80+ bronze standard, which means voltage ripple is maintained at <2.5% at load, and the efficiency is 80% or higher, typically hovering around 90% which is more than enough overhead for the circuit.

As for additional safety features, the power supply features Over Voltage Protection (OVP), Over Power Protection (OPP), and Short Circuit Protection (SCP). To elaborate, OVP will shut down or clamp the output voltage using an internal control circuit should the voltage output



exceed the set rail voltages by a set amount. This will prevent any of the devices connected to the power supply from getting damaged by excessive voltage applied to the devices. This is typically handled by either diverting the extra voltage to an internal capacitor, or simply shutting off the device entirely when the threshold is met. Moving on, OPP shuts down the power supply if the power delivered to the attached circuit exceeds a set point above the maximum power ratings listed above. On a smaller power supply such as the EVGA 400 W, this is typically achieved by using a monitoring circuit attached to a PWM controller. The circuit monitors the total current pulled by the power supply at all times, and if the current exceeds the pre-programmed set point, the device is shut down. Finally, SCP is typically achieved using a few transistors connected in such a way that the power supply will shut down if any of the outputs are suddenly short circuited (suddenly connected to ground). The most likely cause of a short circuit would be one of the components in the circuit burning out. In this case, the SCP would prevent further damage to other components in the circuit.

All of these protections would make the device extremely safe to use in any of our use cases for nanoRIMS. However, to err on the side of caution, there are also additional automotive fuses attached to each of the rails drawing more than 5 A. In this case, that only consists of the 12 V rail, although it will be an optimization goal to add fuses to the 5 V and 3.3 V lines as well. The 12 V line will not be pulling more than 12 - 13 amps on one line at any one time in the process (assuming peak current), and so a 15 amp fuse has been attached to the line. This is likely above the set OPP threshold in the device for a single line, but should the OPP circuit fail, the fuse will blow and prevent further damage to the internal circuitry of nanoRIMS. With these multiple layers of protection, it is extremely unlikely that there is any scenario where nanoRIMS could fail in such a way that it presents a hazard to those operating or handling the device.

MSDS Considerations

MSDS sheets for each of the chemicals dealt with are included with the submission of this report. A summary of hazards and first aid responses is provided here.

Chemical	Hazards	Safety measures	Response
Gold Chloride	Skin and eye irritant if contacted. Irritant if ingested or inhaled.	Always use gloves when handling AuCl ₃ .	In case of contact with skin, wash hands with soap and water. In case of contact with eyes, rinse thoroughly with water. If ingested, do not induce vomiting but seek medical attention.



Sodium citrate dihydrate	Mild skin and eye irritant if contacted. Mild irritant if ingested or inhaled.	Always use gloves when handling sodium citrate dihydrate.	In case of contact with skin, wash hands with soap and water. In case of contact with eyes, rinse thoroughly with water. If ingested, do not induce vomiting but seek medical attention.
Gold nanoparticles	Harmful if swallowed, irritant if contacted with the skin	Always use gloves when handling gold nanoparticles.	If nanoparticles contact the skin, wash thoroughly with water for at least 15 minutes. If the solution contacts the eyes, flush with water for at least 15 minutes. If the solution is ingested, rinse your mouth with water and contact a doctor.



References

- [1] Thermo-Fisher, "Laboratory Bottles," [Online]. Available: <https://www.thermofisher.com/ca/en/home/life-science/lab-plasticware-supplies/reusable-plasticware/laboratory-bottles.html>. [Accessed 16 November 2018].
- [2] CDF Corporation, "Polyethylene Chemical Resistance Chart," [Online]. Available: http://www.cdf1.com/technical%20bulletins/Polyethylene_Chemical_Resistance_Chart.pdf. [Accessed 16 November 2018].
- [3] Gen. Eng. & Biotech. News, "Basic Considerations for Laboratory Water," [Online]. Available: <https://www.genengnews.com/magazine/basic-considerations-for-laboratory-water/> [Accessed 16 November 2018].
- [4] Blue-White Industries Ltd., "Diaphragm Pumps Vs Peristaltic Pumps. What's the best choice for you?" [Online]. Available: <https://www.blue-white.com/diaphragm-pumps-vs-peristaltic-pumps-whats-best-choice/>. [Accessed 16 November 2018].
- [5] Gentek Windows, "Vinyl Chemical Compatibilities," [Online]. Available: http://www.gentekwindows.ca/Links/Chemical_Compatibility.htm. [Accessed 16 November 2018].
- [6] Y. A. Cengel, J. M. Cimbala, and R. H. Turner, *Fundamentals of Thermal Fluid Sciences*. S.L.: McGraw-Hill Education / Asia, 2017.
- [7] Blue-White Industries Ltd., "Peristaltic Pump Wear Factors," [Online]. Available: <https://www.blue-white.com/peristaltic-pump-wear-factors/>. [Accessed 16 November 2018].
- [8] Marlow, "Technical Data Sheet for XLT2422," [Online]. Available: https://cdn2.hubspot.net/hubfs/547732/Data_Sheets/XLT2422.pdf. [Accessed November 2018].
- [9] Omega, "Polyimide Insulated Flexible Heaters," 2018. [Online]. Available: <https://www.omega.com/pptst/KHRA-KHLVA-KHA-SERIES.html>. [Accessed December 2018].
- [10] "Tutorial- L298N Dual Motor Controller," 2018. [Online]. Available: <https://hackerstore.nl/PDFs/Tutorial298.pdf>. [Accessed October 2018].
- [11] A. Ebrahimi, M. Bandari and M. Parvari, "Effect of Mixer Rotational Speed on Heat Transfer Coefficient in Preparation of Nickel Perovskite From Laboratory to Bench Scale," *Iranian Journal of Chemical Engineering*, vol. 6, no. 3, 2009.
- [12] "PID Theory Explained," National Instruments, 29 March 2011. [Online]. Available: <http://www.ni.com/white-paper/3782/en/>. [Accessed 10 April 2018].



- [13] C. Layosa, "Rotary to Linear Motion", November 2017. [Online]. Available: <http://blog.misumiusa.com/rotary-to-linear-motion/>. [Accessed: January 18 2019]
- [14] "An Optical Approach for the Determination of Droplet Volumes for Nanodispensing," 2009. [Online]. Journal of Analytical Methods in Chemistry. Available: <https://www.hindawi.com/journals/jamc/2009/198732/> . [Accessed October 17th, 2018]
- [15] McMaster University, "Laboratory Safety Handbook," July 2008. [Online]. Available: <http://www.workingatmcmaster.ca/med/document/Lab-Safety-Handbook-1-36.pdf>. [Accessed November 2018].